STATIC AND DYNAMIC RESPONSE OF MONOPILES FOR OFFSHORE WIND TURBINES

by

Vonmarie Martínez-Chaluisant

A thesis submitted in partial fulfillment of the requirements for the degree of

Master of Science

(Civil and Environmental Engineering)

at the

UNIVERSITY OF WISCONSIN-MADISON

2011

STATIC AND DYNAMIC RESPONSE OF MONOPILES FOR OFFSHORE WIND TURBINES

Approved

_____

Dante O. Fratta, Associate Professor

12/12/2011

"*Wind power isn't the silver bullet that will solve all our energy challenges – there isn't one. But it is a key part of a comprehensive strategy to move us from an economy that runs on fossil fuels to one that relies on more homegrown fuels and clean energy.*"

-President Barak Obama, April 2010

Abstract

Current design recommendations for monopile foundations for offshore wind turbines were designed and tested for offshore oil and gas structures. Large-diameter (3.5 to 7 m) monopiles, like the ones used for offshore wind turbines do not follow the same elastic deformation relationships as those developed for small-diameter (0.5 to 1.5 m) monopiles, like the ones used for offshore oil and gas industry. Design recommendations and other publications differ by up to 90% in the prediction of displacement and rotation influence factors used in the design of rigid monopiles. Furthermore, offshore wind turbine structures are sensitive to rotations and dynamic changes in the pile-soil system. Accurate prediction of rotation is a major design problem.

A numerical analysis is presented for the study of static loading of monopiles for offshore wind turbines. Different foundation geometries and loading conditions were studied and used to develop a functional form of design equations. Studied variables include (i) pile diameter, (ii) pile length to diameter ratio, (iii) load eccentricity to pile diameter ratio, and (iv) soil stiffness distribution profile.

An experimental study of the dynamic response of model offshore wind turbines founded on monopiles is presented. These dynamic experiments were analyzed by comparing the physical model test results of natural frequency to an analytical solution, and two methods were compared for the damping calculation. Studied parameters include (i) soil condition, (ii) pile foundation material, (iii) rotor and nacelle mass, and (iv) loading

condition. The response to free vibration and its decay was monitored using a vertical array of MEMS accelerometers, and the collected data were processed using auto-power spectra to assess the natural frequency of the structures.

Physical model results were compared to closed-form approximations using Rayleigh's energy method. Good prediction of natural frequency was achieved for turbines founded in rock and stiff sandy soil conditions, however, the natural frequency of turbines founded in soft clay was overpredicted by up to 40%. Damping results were achieved in all cases using the logarithmic decrement method. Relative pile-soil stiffness effect on damping was also studied. For a given impulse loading, damping ratios slightly increase as the pile becomes more rigid. These results highlight the importance of structure-sediment interaction in the evaluation of the dynamic performance of offshore wind turbines.

Acknowledgments

I couldn't say thank you enough to all the people who supported me during my stay in Madison, WI. Thanks to my advisor James A. Schneider for his research and professional guidance, and for giving me the opportunity to work at Fugro; and Dante O. Fratta, for his support and guidance through my research and life decisions. Especial thanks to Dante and his family, for their kindness and hospitality during familiar events.

I will also like to thank my family in Puerto Rico, for believing in me. My parents, Yvonne Chaluisant and José F. Martínez, my sisters, Jacqueline and Jennifer, for doing all they could at the distance. My friends in Madison for being my family, my Geo-friends: Ozlem Bozyurt, Crystal Smith, Andrés Tascón, Marcos Montoro, Andrew Keene, Paul Lang, Ayse Ozdogan and Gizem Bozkurt; and my Puerto Rican friends: Sonia Cortés, Gretchen González, and Yashira Zayas.

Thanks to professors Tuncer Edil and James Tinjum, for being part of my defense committee. This acknowledgment is also extended to those professors at the University of Puerto Rico-Mayaguez that inspired me: Luis Suárez, Hiram González, and Sergio González.

Finally, I would like to recognize Kelly Burton and the Graduate Engineering Research Scholars, for the financial support provided.

Table of Contents

Abstract i

Acknowledgments iii

Table of Contents iv

List of Figures vii

List of Tables xiv

1. Introduction 1

1.1. Analysis of Monopile Foundation Response 3

1.2. Dynamic Response of Monopile Foundations 5

1.3. Analysis Techniques 6

1.3.1. Numerical Analysis 6

1.3.2. Empirical Analysis 7

1.4. Hypotheses 8

1.5. Outline of Thesis 9

2. Literature Review 10

2.1. Offshore Wind Energy 10

2.2. Loading Conditions 11

2.3. Substructure and Foundation Options 12

2.4. Verification Agencies, Design Codes and Standards 14

2.4.1. Stiffness Coefficients 14

2.4.2. Influence Factors 17

2.5. Soil Behavior 39

2.5.1. Material Damping and Cyclic Response 40

2.5.2. Constitutive Models 43

2.6. Dynamic Response 45

2.7. Other Factors Influencing Monopile Response 47

3. Finite Element Analysis of Flexible and Rigid Piles in Elastic Soil 49

3.1. Introduction 49

3.2. Overview of Plaxis 3D Foundations 50

3.3. Validation Studies 52

3.4. Analysis of Lateral Deformations 56

3.4.1. Homogeneous Stiffness with Depth 56

3.4.2. Stiffness Increasing with Depth 63

3.5. Development of Functional Form for Design Equations 70

3.5.1. Homogeneous Stiffness with Depth 72

3.5.2. Stiffness Increasing with Depth 78

3.6. Discussion 84

4. Experimental Studies 90

4.1. Introduction 90

4.2. Equipment 91

4.3. Methods 93

4.3.1. Rayleigh's Energy Method 95

4.3.2. Half Power Bandwidth Method 96

4.3.3. Logarithmic Decrement Method 97

4.3.4. Frequency Response Function 98

4.4. Results 99

4.4.1. Natural Frequency 99

4.4.2. Damping 106

4.5. Influence of Pile-Soil Relative Stiffness on Dynamic Response 111

5. Summary and Conclusions 113

Bibliography 115

Appendix A Literature Review Additional Graphs 119

Appendix B Natural Frequency and Damping Results 121

List of Figures

Figure 1.1 Spring model for lateral resistance of pile-soil interaction 4

Figure 1.2 Uncoupled springs with dashpots, and inertia at the surface (after Zaaijer, 2005) 5

Figure 2.1 Offshore wind resource in 50 nautical miles from the U.S. coastline for annual average wind speed sites above 7.0 m/s at 90 m elevation (Musial & Ram, 2010)..... 11

Figure 2.2 Foundations for different water depths (after Musial et al., 2006) 13

Figure 2.3 Six degrees of freedom for a rigid block 15

Figure 2.4 Soil stiffness profiles 16

Figure 2.5 Earth pressure distribution around the pile (a) prior and (b) after lateral loading (after Reese et al., 1974)..... 18

Figure 2.6 Poulos (1971) model and influence factors fitting 24

Figure 2.7 Influence factors presented by Randolph (1981) and Poulos (1971) for pure horizontal load 26

Figure 2.8 Influence factors presented by Randolph (1981) and Poulos (1971) for combined loading..... 27

Figure 2.9 Influence factors presented by Randolph (1981) and Poulos (1971) for pure moment load..... 28

Figure 2.10 Influence factors presented by Scott (1981) and Poulos (1971) for pure horizontal load 31

Figure 2.11 Influence factors presented by Scott (1981) and Poulos (1971) for combined loading..... 32

Figure 2.12 Influence factors presented by Scott (1981) and Poulos (1971) for pure moment load 33

Figure 2.13 Influence factors presented by DNV/Risø (2001) and Poulos (1971) for pure horizontal load 34

Figure 2.14 Influence factors presented by DNV/Risø (2001) and Poulos (1971)) for combined loading 35

Figure 2.15 Influence factors presented by DNV/Risø (2001) and Poulos (1971) for pure moment load..... 36

Figure 2.16 Influence factors presented by DNV/Risø (2001) and Randolph (1981) for linearly increasing stiffness with depth 38

Figure 2.17 Load vs settlement plate test (Burland & Lord, 1969)..... 39

Figure 2.18 Hysteresis loops of a soil-structure interaction system (Gerolymos & Gazetas, 2006) 42

Figure 2.19 Hyberbolic stress-strain relation for a drained triaxial test (Plaxis 3D Foundation Material Models Manual, 2011) 44

Figure 2.20 Frequency measurement of a Vestas V90 3.0 MW wind turbine in operational mode (Ibsen, 2008) 46

Figure 3.1 Plaxis 3D Foundation model (a) deformed mesh and (b) displacements 49

Figure 3.2 Influence factor for (a) displacement and (b) rotation of combined loading in homogeneous stiffness distribution with L/D=60 54

Figure 3.3 Influence factors for (a) displacement and (b) rotations of combined loading in linearly increasing stiffness distribution with L/D=60 55

Figure 3.4 Variations in pile (a) displacement and (b) rotation influence factors with stiffness ratio in homogeneous soils for L/D=15 59

Figure 3.5 Variations in pile (a) displacement and (b) rotation influence factors with stiffness ratio in homogeneous soils for L/D=4..... 60

Figure 3.6 Variations in pile (a) displacement and (b) rotation influence factors with stiffness ratio in homogeneous soils for L/D=10 61

Figure 3.7 Comparison between Plaxis and Randolph (1981) for (a) displacement and 62

Figure 3.8 Displacement influence factors for piles with (a) D=1 m and (b) D=6 m, and L/D=4 65

Figure 3.9 Rotation influence factors for piles with (a) D=1 m and (b) D=6 m, and L/D=4 66

Figure 3.10 Displacement influence factors for piles with (a) D=1 m and (b) D=6 m, and L/D=10..... 67

Figure 3.11 Rotation influence factors for piles with (a) D=1 m and (b) D=6 m, and L/D=10 68

Figure 3.12 Comparison between Plaxis and Randolph (1981) for (a) displacement and (b) rotation influence factors 69

Figure 3.13 Displacement influence factors for piles with (a) D=1 m and (b) D=6 m, and L/D=4..... 73

Figure 3.14 Rotational influence factors for piles with (a) D=1 m and (b) D=6 m, and L/D=4 74

Figure 3.15 Influence factors for (a) displacement and (b) rotation of piles with L/D=10..... 75

Figure 3.16 Influence factors for (a) displacement and (b) rotation of piles with L/D=15..... 76

Figure 3.17 Comparison between the two models and Randolph (1981) for (a) displacement and (b) rotation influence factors..... 77

Figure 3.18 Displacement influence factors for piles with (a) D=1 m and (b) D=6 m, and L/D=4 79

Figure 3.19 Rotational influence factors for piles with (a) D=1 m and (b) D=6 m, and L/D=4 80

Figure 3.20 Displacement influence factors for piles with (a) D=1 m and (b) D=6 m, and L/D=10 81

Figure 3.21 Rotational influence factors for piles with (a) D=1 m and (b) D=6 m, and L/D=10 82

Figure 3.22 Comparison between the two models and Randolph (1981) for (a) displacement and (b) rotation influence factors 83

Figure 3.23 Proposed influence factors comparison for (a) displacements and (b) rotations for soils with homogeneous stiffness distribution with depth 86

Figure 3.24 Proposed influence factors comparison for (a) displacements and (b) rotations for soils with homogeneous stiffness distribution with depth 87

Figure 3.25 Proposed influence factors comparison for (a) displacements and (b) rotations for soils with linearly increasing stiffness distribution with depth 88

Figure 3.26 Proposed influence factors comparison for (a) displacements and (b) rotations for soils with linearly increasing stiffness distribution with depth 89

Figure 4.1 Diagram of test setup 92

Figure 4.2 Cantilevered horizontal beam 95

Figure 4.3 Rotated cantilever beam to have a structure with similar boundary conditions . 96

Figure 4.4 Graphical determination of half power bandwidth 97

Figure 4.5 Graphical determination of logarithmic decrement 98

Figure 4.6 Physical model failure in clay for the copper and PVC towers 99

Figure 4.7 Example of the frequency response spectra 100

Figure 4.8 Natural frequency comparison for the tower, tower and nacelle, and tower, nacelle and rotor 100

Figure 4.9 Comparison of measured and predicted natural frequency for turbines founded in monopiles in concrete 102

Figure 4.10 Comparison of measured and predicted natural frequency for turbines founded on monopiles in sand 103

Figure 4.11 Comparison of measured and predicted natural frequency for turbines founded on monopiles in soft clay 104

Figure 4.12 Pile flexibility effects on the determination of natural frequency 105

Figure 4.13 Bandwidth and logarithmic decrement method comparison 106

Figure 4.14 Damping ratio for variation in pile flexibility factor 110

Figure 4.15 Frequency response comparison by fitting the single degree of freedom system response to the data by using Equation 4.5 111

Appendix Figures

Figure A.1 Comparison between Scott (1981) and LPile 120

Figure B.1 Copper long tower with rotor and nacelle founded in concrete 121

Figure B.2 Copper long tower with nacelle founded in concrete 122

Figure B.3 Copper long tower founded in concrete 123

Figure B.4 Copper short tower with rotor and nacelle founded in concrete 124

Figure B.5 Copper short tower with nacelle founded in concrete 125

Figure B.6 Copper short tower founded in concrete 126

Figure B.7 PVC tower with rotor and nacelle founded in concrete 127

Figure B.8 PVC tower with nacelle founded in concrete 128

Figure B.9 PVC tower founded in concrete 129

Figure B.10 PVC tower with rotor and nacelle embedded 16D in sand 130

Figure B.11 PVC tower with nacelle embedded 16D in sand 131

Figure B.12 PVC tower embedded 16D in sand 132

Figure B.13 PVC tower with nacelle embedded 8D in sand 133

Figure B.14 PVC tower embedded 8D in sand 134

Figure B.15 PVC tower with rotor and nacelle embedded in concrete with a 90 mm clay layer 135

Figure B.16 Copper short tower with rotor and nacelle embedded in concrete with a 90 mm clay layer 136

Figure B.17 Copper long tower with rotor and nacelle embedded in concrete with a 90 mm clay layer 137

Figure B.18 Copper short tower with rotor and nacelle embedded in clay 138

Figure B.19 Copper short tower with nacelle embedded in clay 139

Figure B.20 Copper short tower embedded in clay 140

Figure B.21 PVC tower with rotor and nacelle embedded 16D in clay 141

Figure B.22 PVC tower with nacelle embedded 16D in clay 142

Figure B.23 PVC tower embedded 16D in clay 143

List of Tables

Table 2.1 Stiffness coefficients for use in Equation 2.1 (DNV/Risø, 2001) 17

Table 2.2 Influence factors for use in Equation 2.4 for flexible piles 21

Table 2.3 Influence factors for use in Equation 2.4 for rigid piles 21

Table 3.1 Validation studies with R=0.5 m and L=60 m 53

Table 3.2 Summary of analyses for homogeneous stiffness with depth 58

Table 3.3 Summary of analyses for linearly increasing stiffness with depth 64

Table 3.4 Influence factors for homogeneous stiffness with depth 72

Table 3.5 Influence factors for linearly increasing stiffness with depth 78

Table 4.1 Properties of model tower materials 91

Table 4.2 Properties of foundation materials 93

Table 4.3 Experimental tests 94

Table 4.4 Natural frequency results for each of the test performed 101

Table 4.5 Damping ratio results 109

1. Introduction

There is an increase in energy demand, as well as continued increase in world oil prices. Renewable energy gives us the opportunity of reducing the dependency of fossil fuel – coal, oil, and natural gas. In September 2010, the National Renewable Energy Laboratory (NREL) reported that if offshore wind resources are developed along the U.S. coastline and the Great Lakes, U.S. could produce 20% of its electricity from wind. From this 20%, 54 GW can be extracted from offshore wind farms (Musial & Ram, 2010). One of the advantages of developing offshore wind farms in the U.S. coastline is that large urban areas exist in those regions, where there is high energy demand and reduced land-based generation and transmission.

Shallow water (less than 30 m) exists along portions of the U.S. coastline, and projects are in the planning and permitting process in Northeast and Mid-Atlantic regions (Musial & Ram, 2010). Other sites are also being considered in the Great Lakes, Gulf of Mexico, and Pacific Coast. However, the sites along the Pacific Coast present greater challenges due to deeper waters (Musial & Ram, 2010).

Current methodologies for the design of monopiles for offshore wind turbines use the load transfer (p-y) curves method, which was originally developed and tested for small-diameter (D=0.32 m), long, slender and flexible piles in the oil and gas industry. Rigid monopiles, with length to diameter ratios (L/D) generally less than 12 and diameters from 3.5 to 7 m, are typically used for offshore wind turbines. Flexible piles, with L/D from 12 to

120 and D from 0.5 to 3 m, are typically used for offshore oil and gas structures. As lateral loads increase, diameter requirements also increase to prevent excessive rotation and displacement. Recent projects have applied a serviceability limit for rotations at the mudline of 0.5° (Achmus et al., 2009). For rotations that are this small, response is controlled more by nonlinear elasticity than plasticity deformations of the foundation soils.

When the diameter of the pile is increased and the embedded length is decreased, the behavior of the monopile foundation changes from flexible to rigid. The pile flexibility factor (K_R) is a dimensionless measure of the flexibility of the pile relative to the soil (Poulos, 1971), and is defined as

$$K_R = \frac{E_p I_p}{E_s L^4} \qquad \text{Equation 1.1}$$

where E_p is the pile Young's modulus, I_p is the pile moment of inertia, E_s is the soil Young's modulus, and L is the embedment pile length. Pile behavior can be divided based on their flexibility: (i) very flexible piles, with $K_R<10^{-5}$; (ii) flexible piles, with $K_R<10^{-2}$; (iii) stiff piles, with $K_R>10^{-2}$; and (iv) perfectly stiff piles, with $K_R>1$. Offshore wind turbine towers founded in rigid piles behave different than those founded in flexible piles, and the current design approach might not be appropriate. Current design practices need to be improved to be cost-effective and provide rigid piles with a safe, stable, and economical design.

Our numerical models and analysis suggests that large-diameter (3.5 to 7 m) monopiles do not follow the same elastic deformation relationships as those developed for small-diameter (0.5 to 1.5 m) monopiles. Also, Rayleigh's energy method tends to

underpredict the natural frequency of rigid monopiles for offshore wind turbines. Finally, for a given impulse loading, damping ratios slightly increase as the pile becomes more rigid.

1.1. Analysis of Monopile Foundation Response

There are three methodologies for estimating the displacements of laterally loaded piles: (i) finite element methods, which treat the soil as a continuum; (ii) integral equations, where a soil stiffness matrix is developed by discretizing the boundaries of the continuum; and (iii) load transfer function where a function is fit to pile load tests (e.g., Winkler model). These three methods are discussed in detail by Randolph (1977).

The load transfer function, commonly referred to as the p-y curve method, is the approach used by the American Petroleum Institute (API), and adopted by DNV/Risø (2001), to calculate lateral deflections for laterally loaded piles. The method analyzes the pile as an elastic beam that is loaded transversely and restrained by linear or non-linear springs. The springs are distributed along the pile length, as shown in Figure 1.1.

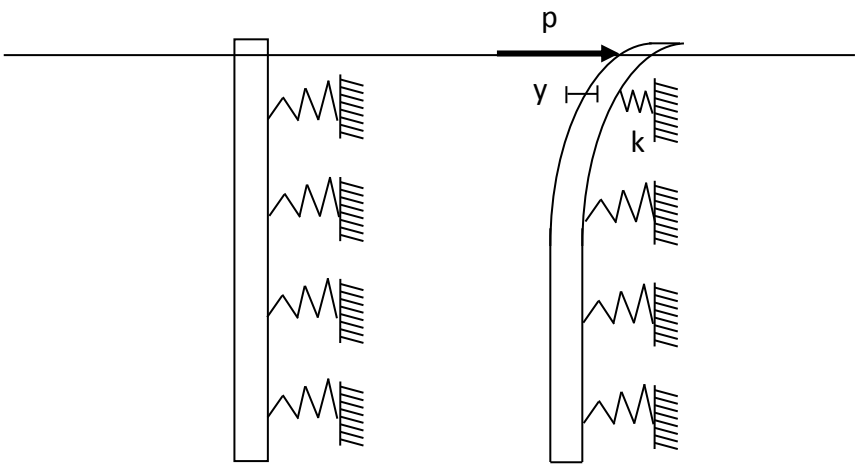

Figure 1.1 Spring model for lateral resistance of pile-soil interaction

The p-y curves method was initially developed by Reese and Matlock (1956) for the analysis of long, slender, and flexible piles. The method has been verified for flexible piles, where the deflections are restrained to the upper part of the pile. The length of the upper part of the pile that deflects under lateral loading is known as the effective, active or critical length (L_c) (Randolph, 1981). The length that does not deform does not contribute to the lateral loading response. Piles with embedded lengths larger than the critical length behave as infinitively long piles. When considering the response of monopile foundations, significant differences exist in the behavior of stout rigid monopiles and slender monopiles.

Zaaijer (2005) states that the soil-structure interaction can be expressed in a single stiffness matrix using two approaches. The first approach to obtain the stiffness matrix uses the Winkler's assumption. This assumption is based on the stress-strain relation where the lateral resistance is modeled with non-linear springs, as shown in Figure 1.1. The second approach uses uncoupled springs, dashpots, and inertia at the surface, as shown in Figure

1.2. Each spring is accompanied by an associated dashpot in parallel, that represents the soil 'viscous' resistance (later called damping). This model is used for gravity based foundations that are assumed to behave in a rigid fashion.

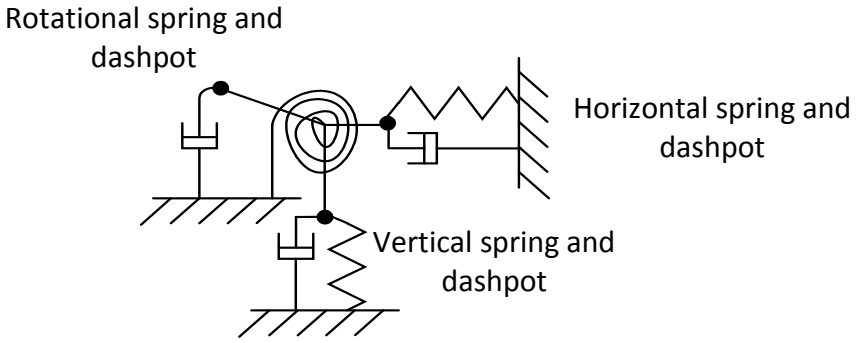

Figure 1.2 Uncoupled springs with dashpots, and inertia at the surface (after Zaaijer, 2005)

1.2. Dynamic Response of Monopile Foundations

The dynamic response of a system can be described by its natural frequency and damping characteristics. Zaaijer (2005) studied how to predict the natural frequency of foundation systems and how sensitive the natural frequency is to the input parameters. Zaaijer (2005) analyzed: (i) the parameter sensitivity to uncertainty, lifetime of the structure, and location; (ii) site variations; (iii) loading conditions; and (iv) different pile and gravity base foundation models.

1.3. Analysis Techniques

1.3.1. Numerical Analysis

In the finite element method, the real problem is approximated by discretizing the continuum in a number of elements that simulate the same mechanical behavior as the real soil and structure (Scott, 1981). Finite element modeling was selected to model the soil-structure interaction because it allows us to perform more accurate pile modeling, considers the soil as a continuum and the small rate of displacement using plastic calculation. Homogeneous and linearly increasing stiffness soil profiles were considered in the numerical analysis models. Small-diameter piles (D=1 m) were modeled using both stiffness profiles and compared to the solution presented by Randolph (1981) to validate our numerical models. Large-diameter piles (D=6 m) were modeled and compared to Randolph (1981) to evaluate where the prediction deviates from the behavior.

In this study, we compare current methodologies (e.g., DNV/Risø, 2001) to estimate lateral displacements and rotations with finite element models to identify where the current models are not appropriate. In an effort to fill this gap in the available methods, we developed a design approach with a moment-rotation relationship to predict rotation and displacement for rigid piles.

1.3.2. Empirical Analysis

Empirical analysis consisted on perform laboratory scale models to study the dynamic behavior of monopiles founded in sand, soft clay, sediment over rock, and rock. Dynamic behavior of a system is characterized by its natural frequency and damping (Zaaijer, 2005). The natural frequency was estimated using Rayleigh's method, explained in detail in a later chapter, and compared to the natural frequency measured in the laboratory experiments.

Damping was calculated using two methods: logarithmic decrement and half power bandwidth. The dynamic response of towers subjected to lateral loads with different soil, water level, and loading conditions are measured in this study to gain information on theoretical model performance, as well as methods for physical modeling of soil-structure interaction. Based on our study, water level does not have an impact on damping or natural frequency.

1.4. Hypotheses

The p-y curves method is based on limited tests performed on flexible piles. This method gained acceptance due to the low number of failures in piles designed using p-y curves (LeBlanc et al., 2009). At the moment, the p-y curves method is being used outside the range that it was developed for. Research proves that the method is not appropriate for rigid piles (LeBlanc et al., 2009) but an approach like the one presented in this thesis has not been developed. We evaluate three main hypotheses here in:

- Large-diameter (3.5 to 7 m) monopiles, like the ones used as foundations for offshore wind turbines, do not follow the same elastic deformation relationships as those developed for small-diameter (0.5 to 1.5 m) monopiles, like the ones used for offshore oil and gas structures.
- Soils do not behave as rigid materials, consequently the Rayleigh's energy method will tend to overpredict the natural frequency of rigid monopiles for offshore wind turbines.
- For a given impulse loading, damping ratios increase as the pile becomes more rigid.

1.5. Outline of Thesis

This thesis is composed of five chapters. This introduction (Chapter 1) demonstrates the importance of this research study for the offshore wind turbine industry and describes the analysis techniques used in the study and our hypotheses. Chapter 2 presents the challenges of design for offshore wind turbines, the current foundation options and methodologies to estimate displacement and rotations for monopile foundations. Also, describes the importance of studying the dynamic response of the structure.

Chapter 3 presents validation studies, numerical analysis results, and a developed functional form of the design equations to calculate displacement and rotations at the mudline. Chapter 4 presents the dynamic tests results, comparison methods, and pile to soil relative stiffness effects on dynamic response of monopile foundations. Chapter 5 presents a summary of the conclusions, and recommendations for future research work.

2. Literature Review

2.1. Offshore Wind Energy

Offshore winds tend to have higher and constant velocities, less turbulence, and are more uniform than onshore winds. One of the major oppositions for onshore wind turbines are the aesthetic concerns, offshore locations reduces or even eliminates this constraint. Larger capacity wind turbines can be installed offshore, increasing energy output for each wind farm location, but also increasing the forces that foundations are exposed to (Houlsby & Byrne, 2003).

Offshore wind resources in the United States have been quantified by region, water depth, and distance from the coast. Figure 2.1 shows a map of the U.S. with the offshore wind resource that totals more than 4000 GW. In September 2010, the National Renewable Energy Laboratory (NREL) reported that the offshore wind resource of 4000 GW is four times the capacity of current U.S. electrical grid (Musial & Ram, 2010). However, more studies are needed to evaluate public concerns and siting restrictions, as well as array effects. These constraints can reduce the available wind potential by 60% or more.

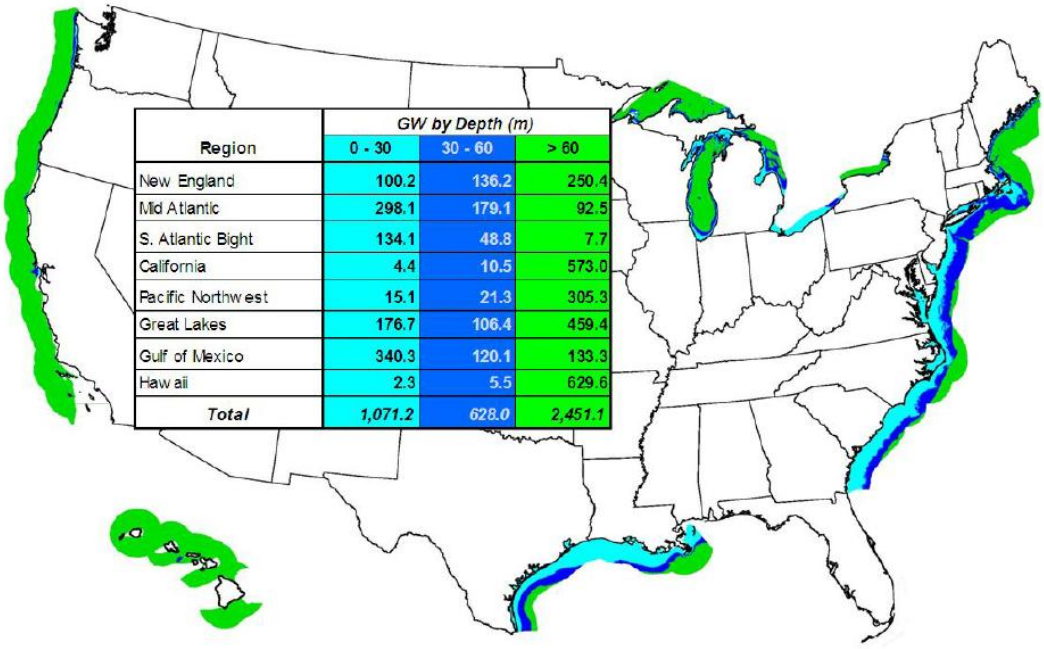

Region	GW by Depth (m)		
	0 - 30	30 - 60	> 60
New England	100.2	136.2	250.4
Mid Atlantic	298.1	179.1	92.5
S. Atlantic Bight	134.1	48.8	7.7
California	4.4	10.5	573.0
Pacific Northwest	15.1	21.3	305.3
Great Lakes	176.7	106.4	459.4
Gulf of Mexico	340.3	120.1	133.3
Hawaii	2.3	5.5	629.6
Total	*1,071.2*	*628.0*	*2,451.1*

Figure 2.1 Offshore wind resource in 50 nautical miles from the U.S. coastline for annual average wind speed sites above 7.0 m/s at 90 m elevation (Musial & Ram, 2010)

2.2. Loading Conditions

Even though foundation designs for offshore wind turbines are mostly guided by oil and gas industry experience, water depths and loading conditions are quite different. Offshore platforms for the oil and gas industry are designed to have minimum interaction with environmental loads, while offshore wind turbines are design to interact with them. Dynamic effects are more important for wind turbines because the design is constrained between the rotor (1P) and passing blade (3P) natural frequencies. In the oil and gas industry, platforms are design to avoid wave energy designing the structures with periods lower than 5 s or higher than 30 s (Schneider & Senders, 2010). Offshore wind turbine

superstructures are exposed to dynamic loads due to wind and waves during normal operation, a situation that is not encountered in onshore wind farms. Offshore wind turbine structures are more sensitive to dynamic changes in the system than the oil and gas platforms. These dynamic changes are the result of stiffness changes in the pile-foundation system.

Monopiles foundations for offshore wind turbines are exposed to large moments and horizontal loads, and small vertical loads in comparison with foundations for the oil and gas industry. The ratio between horizontal to vertical load (H/V) for offshore wind turbines is between 1.4 and 2.6, versus 0.25 in the oil and gas industry (e.g., Houlsby et al., 2005; Schneider & Senders, 2010). For a 3.5-MW turbine, the applied overturning moment during an extreme condition is estimated around 120 MN-m (Houlsby & Byrne, 2003), most of the overturning moment loading is the result of the horizontal wind load at hub height.

2.3. Substructure and Foundation Options

Foundation selection is mostly guided by water depth. In shallow waters, less than 30 m, the substructure options are adapted from onshore and offshore systems like gravity bases, monopiles, and suction buckets. For transitional water, between 30 and 60 m, the options are similar to oil and gas industry jacket foundations. For deeper waters, more than 60 m, a structure that extends to the seabed may not be cost effective, and the current preferred design is floating platforms. Figure 2.2 shows the foundations recommended for the

different water depths. Depending upon the substructure type and weight, foundation loads may act predominantly in a lateral direction, in tension, compression, or both (e.g., jacket or tripod).

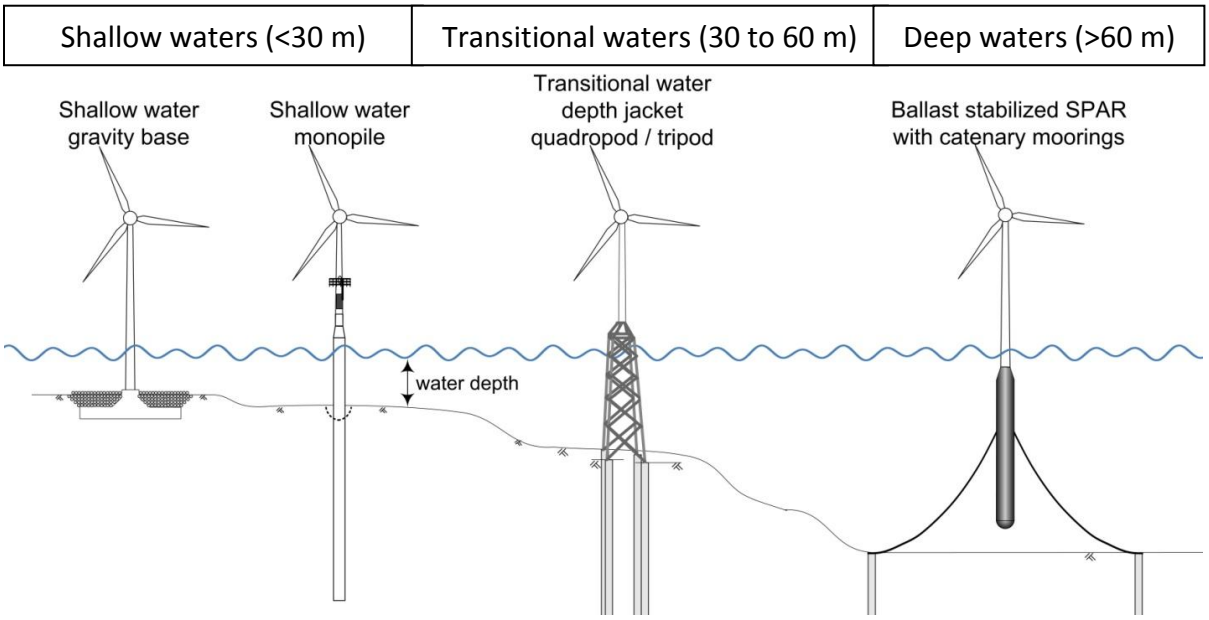

Figure 2.2 Foundations for different water depths (after Musial et al., 2006)

Each foundation option has its own challenges and different considerations are needed for each of them. This study is focused on monopiles because it is most likely the foundation selection for initial offshore wind turbine development in the United States. This assumption is based on the fact that monopile foundations have been used for other offshore wind farms at similar water depths, and have been proven to work.

2.4. Verification Agencies, Design Codes and Standards

There are several design standards and guidelines for the design of offshore wind turbines. Two commonly used design standards:

- Guidelines for the design of wind turbines (DNV/Risø, 2001);
- Design of offshore wind turbine structures (DNV, 2007).

For geotechnical aspects and foundation design, these guidelines have been based on recommendations in American Petroleum Institute Recommended Practice for Fixed Offshore Structures (API RP2A, 2000).

For calculating deformations, most recommendations use elastic stiffness coefficients or influence factors based on the analysis of flexible piles (e.g., DNV/Risø, 2001; Zaaijer, 2005). Since these factors tend to underestimate displacements and rotations for rigid piles, stiffness coefficients have been left out of verification agency design guidance DNV (2007). This section provides a review of the format of design equations and compares recommendations from design manuals (DNV/Risø, 2001) and results of previous research (e.g., Poulos, 1971; Randolph, 1981).

2.4.1. Stiffness Coefficients

It is common to present recommendations for assessment of the elastic response of foundations using a stiffness matrix (Randolph, 1981). A pile foundation element may have

six degrees of freedom, as shown in Figure 2.3, but for the design of offshore wind turbines, we are primarily concerned with two: lateral (or horizontal) translation and rocking.

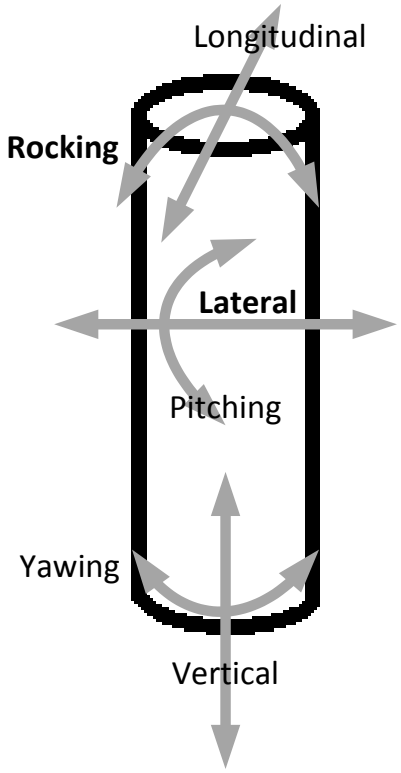

Figure 2.3 Six degrees of freedom for a rigid block

When considering only horizontal translation and rocking, the stiffness matrix will take a form similar to (e.g., Doherty & Deeks, 2003):

$$\begin{bmatrix} \frac{H}{GR^2} \\ \frac{M}{GR^3} \end{bmatrix} = \begin{bmatrix} K_H & K_{HM} \\ K_{MH} & K_M \end{bmatrix} \begin{bmatrix} \frac{u}{R} \\ \theta_M \end{bmatrix} \qquad \text{Equation 2.1}$$

where H is the horizontal load, M is the moment load, G is the shear modulus of the soil, R is the radius of the foundation element, u is the horizontal displacement, and θ_M is the

rotation angle due to moment loading (rocking). K_H and K_M are the elastic stiffness coefficients for horizontal movement due to pure horizontal load and rotation (rocking) due to pure moment loading, respectively. K_{HM} and K_{MH} are the elastic stiffness coefficients for horizontal movement due to moment loading and for rotation (rocking) due to horizontal loading, respectively. The values of K_{HM} and K_{MH} are equal as justified by the Maxwell-Betti reciprocal theorem (Cook, 2001).

Elastic stiffness coefficients recommended for offshore wind turbine foundations have been presented by DNV/Risø (2001) for the homogeneous case, as well as stiffness increasing linearly with depth. Table 2.1 shows the stiffness coefficients presented by DNV/Risø (2001) for flexible piles, where E_p is the pile Young's modulus, z is the depth, D is the pile diameter, G_s is the soil shear modulus, and G_m is the rate of change of shear modulus with depth. Figure 2.4 shows the soil stiffness profiles for three cases: (a) constant stiffness; (b) stiffness increasing linearly with depth and intercept at mudline of zero; and (c) stiffness increasing linearly with depth and intercept different than zero at the mudline.

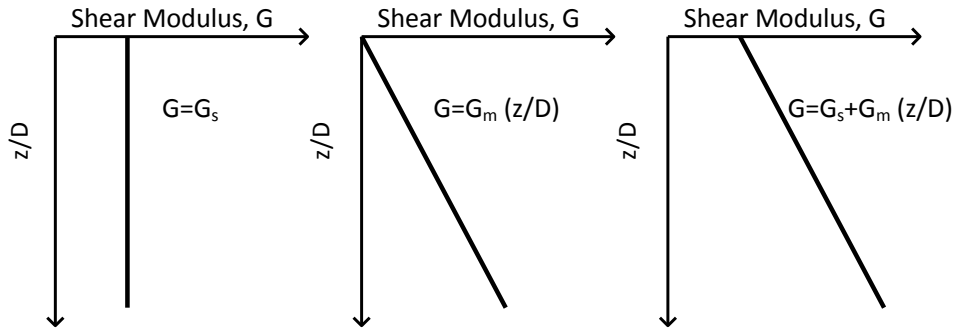

Figure 2.4 Soil stiffness profiles

Table 2.1 Stiffness coefficients for use in Equation 2.1 (DNV/Risø, 2001)

Reference / Shear Modulus Distribution	Horizontal $\frac{K_H}{DE_s}$	Rocking $\frac{K_M}{D^3E_s}$	Coupled $\frac{K_{HM}}{D^2E_s}$
Homogeneous $G = G_s$	$1.08\left(\frac{E_p}{G}\right)^{0.21}$	$0.16\left(\frac{E_p}{G}\right)^{0.75}$	$-0.22\left(\frac{E_p}{G}\right)^{0.50}$
Linear Increase with Depth $G = G_m \cdot (z/D)$	$0.6\left(\frac{E_p}{G}\right)^{0.35}$	$0.14\left(\frac{E_p}{G}\right)^{0.80}$	$-0.17\left(\frac{E_p}{G}\right)^{0.60}$

2.4.2. Influence Factors

Poulos (1971) presents a series of influence factors (I_{uH}, I_{uM}, $I_{\theta H}$, $I_{\theta M}$) to calculate displacements (u) and rotations (θ), due to horizontal (H) or moment (M) loading. Influence factors are coefficients for the inverse of the stiffness matrix, and are often expressed in equation, rather than matrix, format (e.g., Randolph, 1981). These equations allow for simple hand calculations of surface displacements or rotations for various assumptions related to changes in stiffness with depth along the length of a foundation.

Influence factors presented by Poulos (1971) decrease with increasing pile flexibility factor (K_R) and increasing length-to-diameter ratio (L/D). Influence factors vary slightly for stiff piles, and remain constant for perfectly stiff piles. In Poulos (1971) work, the soil is assumed to be elastic, homogeneous, and isotropic, as shown in Figure 2.4(a). The pile is assumed to be a vertical beam with constant flexibility (E_pI_p) and uniform stress distribution across the width of the pile, as shown in Figure 2.5(a). The uniform stress distribution was

found to be negligible for L/D=15, but displacements and rotations were found to be underestimated by about 25 to 30% for L/D=2 (Poulos, 1971). Figure 2.5(b) shows the estimated non-uniform distribution due to soil nonlinearities for laterally loaded piles. Poulos (1971) compares elastic theory with subgrade reaction theory using the same framework, influence factors that vary with the pile flexibility factor, and found that subgrade reaction theory overestimates the displacements and rotations. The error is higher for piles with $K_R=10^{-5}$, and as the L/D ratio decreases, the difference increases (Poulos, 1971).

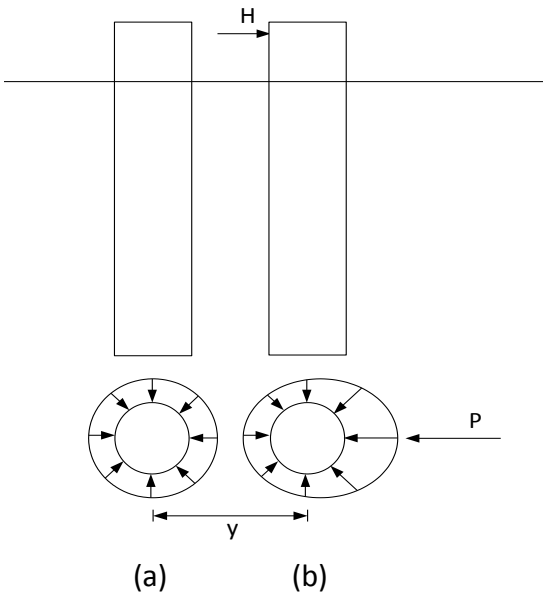

Figure 2.5 Earth pressure distribution around the pile (a) prior and (b) after lateral loading (after Reese et al., 1974)

Horizontal (I_{uH}), coupled ($I_{uM}=I_{\theta H}$), and rocking ($I_{\theta M}$) influence factors are related to stiffness coefficients as:

$$I_{uH} = \frac{K_M}{K_H K_M - K_{MH}^2}$$ Equation 2.2a

$$I_{uM} = I_{\theta H} = \frac{-K_{MH}}{K_H K_M - K_{MH}^2}$$ Equation 2.2b

$$I_{\theta M} = \frac{K_H}{K_H K_M - K_{MH}^2}$$ Equation 2.2c

To avoid considering changes in the stiffness coefficients due to Poisson's ratio (ν), the G* parameter was introduced by Randolph (1981) based on finite element analyses of soil variations.

$$G^* = G\left(1 + \frac{3}{4}\nu\right)$$ Equation 2.3

Incorporating influence factors to estimate translations or rotations results in equations of the following formats (Randolph, 1981):

$$\frac{u}{R} = I_{uH}\frac{H}{G^* R^2} + I_{uM}\frac{M}{G^* R^3}$$ Equation 2.4a

$$\theta = I_{\theta H}\frac{H}{G^* R^2} + I_{\theta M}\frac{M}{G^* R^3}$$ Equation 2.4b

Influence factors for the case of coupled horizontal translation and rocking have been presented in chart format for flexible and rigid piles for a homogeneous elastic soil by Poulos (1971) and Scott (1981), and have been presented in equation format for flexible piles for a homogeneous elastic soil and soil with stiffness increasing linearly with depth by Randolph (1981). Influence factors for flexible and rigid piles are compared in Table 2.2 and

Table 2.3, respectively. The following functional form was used to fit recommended trends from previous studies:

$$I_{xx} = a\left(\frac{E_p}{G^*}\right)^{-n} \qquad \text{Equation 2.5a}$$

$$I_{xx} = b\left(\frac{L}{R}\right)^{n^*} \qquad \text{Equation 2.5b}$$

where a, b, n, and n* are fitting coefficients. Equation 2.5a allows the evaluation of flexible piles, where the influence factor reduces as ratio of pile Young's modulus to soil shear modulus (E_p/G^*) increases. Equation 2.5b allows the evaluation of rigid piles, where influence factor is constant with changes in the ratio of pile to soil stiffness, and the behavior is mostly guided by the pile length to radius (L/R) ratio.

The main framework for this analysis was Randolph (1981), which normalized displacements using the radius, u/R. The influence factors presented by Randolph (1981) and Poulos (1971) are compared in Figure 2.7 to Figure 2.9. Poulos (1971) normalized the displacements using the embedment length, u/L. Randolph (1981) was looking at flexible pile behavior, and considered that normalizing by pile length will require a set of graphs for each pile length, then normalized by pile radius.

The different coefficients presented in the tables were obtained by fitting an algebraic expression to the different equations (e.g., Scott, 1981) and stiffness coefficients (e.g., DNV/Risø, 2001), compared to influence factors presented by Poulos (1971), and shown in Figure 2.10 to Figure 2.15. The scatter in the prediction of the influence factors

for rigid piles is one of the main drives of this study. Differences between the references studied are due to the theories and assumptions they used. We will compare and discuss each of them.

Table 2.2 Influence factors for use in Equation 2.4 for flexible piles

Reference / Shear Modulus Distribution	Horizontal I_{uH}	Rocking $I_{\theta M}$	Coupled $I_{uM}=I_{\theta H}$
DNV/Risø (2001) Homogeneous $G = G_s$	$1.52\left(\frac{E_p}{G^*}\right)^{-0.21}$	$15.76\left(\frac{E_p}{G^*}\right)^{-0.75}$	$2.61\left(\frac{E_p}{G^*}\right)^{-0.50}$
Randolph (1981) Homogeneous $G = G_s$	$0.25\left(\frac{E_p}{G^*}\right)^{-1/7}$	$0.80\left(\frac{E_p}{G^*}\right)^{-5/7}$	$0.27\left(\frac{E_p}{G^*}\right)^{-3/7}$
Scott (1981) Homogeneous $G = G_s$	$0.84\left(\frac{E_p}{G^*}\right)^{-0.25}$	$1.40\left(\frac{E_p}{G^*}\right)^{-0.75}$	$0.77\left(\frac{E_p}{G^*}\right)^{-0.50}$
Poulos (1971) Homogeneous $G = G_s$	$0.47\left(\frac{E_p}{G^*}\right)^{-0.20}$	$0.55\left(\frac{E_p}{G^*}\right)^{-0.69}$	$0.40\left(\frac{E_p}{G^*}\right)^{-0.45}$
Randolph (1981) Linear increase with depth $G = G_m \cdot (z/R)$	$0.54\left(\frac{E_p}{G_m^*}\right)^{-3/9}$	$1.13\left(\frac{E_p}{G_m^*}\right)^{-7/9}$	$0.60\left(\frac{E_p}{G_m^*}\right)^{-5/9}$
DNV/Risø (2001) Linear increase with depth $G = G_m \cdot (z/R)$	$2.54\left(\frac{E_p}{G_m^*}\right)^{-0.35}$	$10.89\left(\frac{E_p}{G_m^*}\right)^{-0.80}$	$3.09\left(\frac{E_p}{G_m^*}\right)^{-0.60}$

Table 2.3 Influence factors for use in Equation 2.4 for rigid piles

Reference / Shear Modulus Distribution	Horizontal I_{uH}	Rocking $I_{\theta M}$	Coupled $I_{uM}=I_{\theta H}$
Poulos (1971) Homogeneous $G = G_s$	$1.84\left(\frac{L}{R}\right)^{-1}$	$5.60\left(\frac{L}{R}\right)^{-3}$	$2.81\left(\frac{L}{R}\right)^{-2}$
Scott (1981) Homogeneous $G = G_s$	$0.83\left(\frac{L}{R}\right)^{-0.8}$	$1.90\left(\frac{L}{R}\right)^{-2.8}$	$0.85\left(\frac{L}{R}\right)^{-1.75}$

Poulos (1971) uses linear elastic theory instead of subgrade reaction theory (e.g., Scott, 1981; Hetenyi, 1946) because the subgrade reaction theory ignores the fact that the soil is a continuum. Many studies use subgrade reaction theory because it is mathematically convenient. Poulos (1971) analyzed the laterally loaded pile as a beam in an ideal, elastic, homogeneous, isotropic mass with constant Young's modulus, and looked at the factors that influence displacements and rotations in the pile. Figure 2.6 shows simplified Poulos (1971)'s influence factors for the displacement due to pure horizontal loading, coupled due to combined loading, and rotation due to pure moment loading. The simplification was performed to compare the influence factors with other models in Table 2.2 and Table 2.3.

In this simplified analysis, Poulos (1971) assumes uniform stress distribution across the width of the pile, because Poulos (1971) studied flexible piles, but is well aware that this assumption is not appropriate for rigid piles. One of the mayor disadvantages in using influence factors presented by Poulos (1971) for rigid piles is that horizontal shear stresses developed between the soil and the sides of the pile are ignored since these are not significant for flexible piles. Poulos (1971) considers the pile embedment length to diameter ratio (L/D) and the pile flexibility factor (K_R) to be the major variables influencing pile behavior.

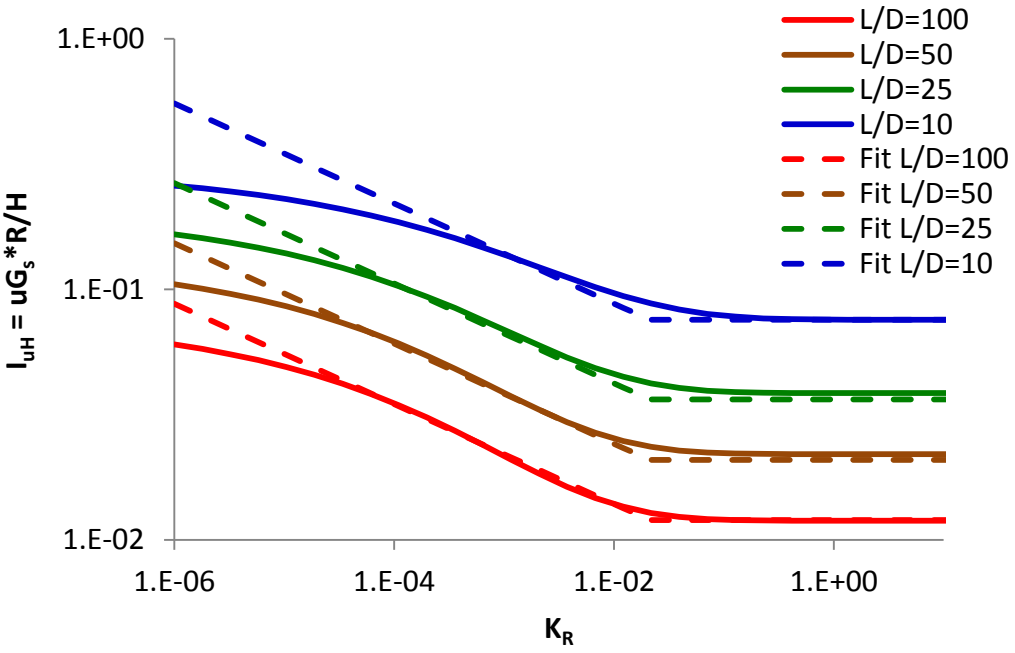

(a) Displacement influence factor for pure horizontal load

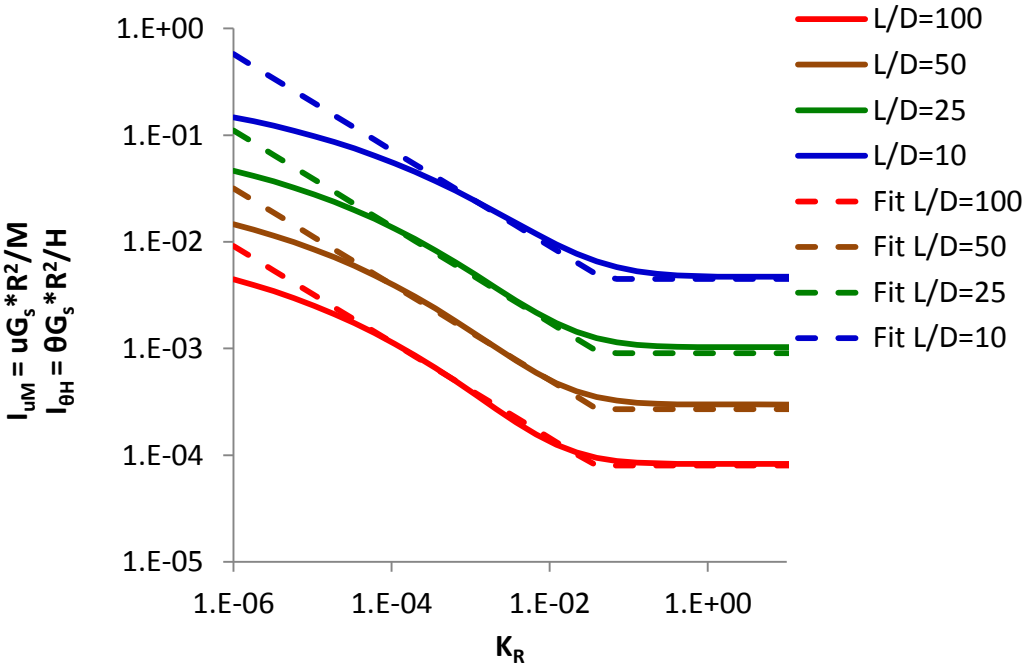

(b) Coupled influence factor for combined loading

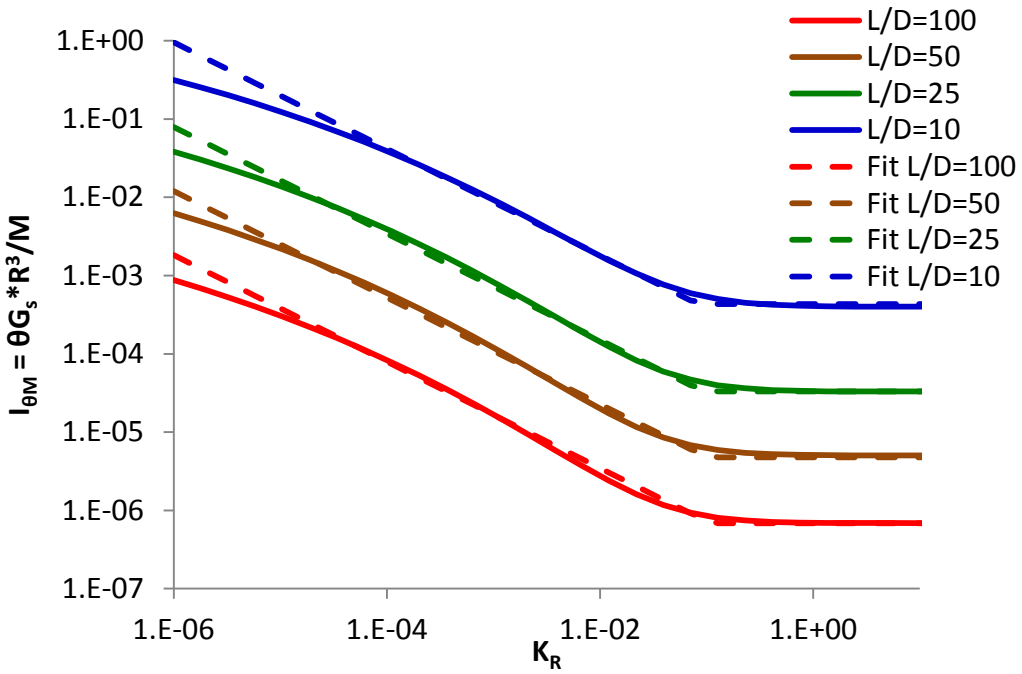

(c) Rotation influence factor for pure moment load

Figure 2.6 Poulos (1971) model and influence factors fitting

Randolph (1981) analysis also uses the linear elastic theory, treating the soil as an elastic continuum. Randolph (1981) develops influence factors for homogeneous stiffness and for soil stiffness proportional to depth using finite elements, considering flexible piles. Randolph (1981) analyzes flexible piles as cantilevered beam because flexible piles deflect more in the upper part of the pile taking the soil to failure, but there is a lower section where the soil has not failed yet. Randolph (1981) does not consider pile embedment length as an important parameter because he is looking at flexible piles that behave as infinitely long piles. Figure 2.7 to Figure 2.9 compares influence factors presented by Randolph (1981) and Poulos (1971).

As defined in Chapter 1, flexible piles have pile flexibility factors (K_R) that vary from 10^{-5} to 10^{-2}, and rigid piles from 10^{-2} to 1. Pile behavior can also be described by L/D ratio, generally flexible piles have L/D ratios higher than 15 and rigid piles lower than 12. It was observed that in the flexible range of K_R, Randolph (1981) produces I_{uH} that are higher than Poulos (1971) by 40% for piles with L/D=100, but lower by 20% for L/D=10. I_{uM} and $I_{\theta H}$ were lower by 20% for both L/D ratios, and $I_{\theta M}$ was higher by 10% for L/D=100, but lower by 10% for L/D=10. At the rigid range of K_R, I_{uH} for L/D=100 was lower by 40% and by 60% for L/D=10. I_{uM} and $I_{\theta M}$ were lower by 80 and 85%, respectively.

Considerable lower values were produced for displacement and rotations for rigid piles for Randolph (1981) in comparison to Poulos (1971), because the solution presented by Randolph (1981) was for flexible piles. However, Zaaijer (2005) applied Randolph (1981)'s solution for rigid piles outside of the design range.

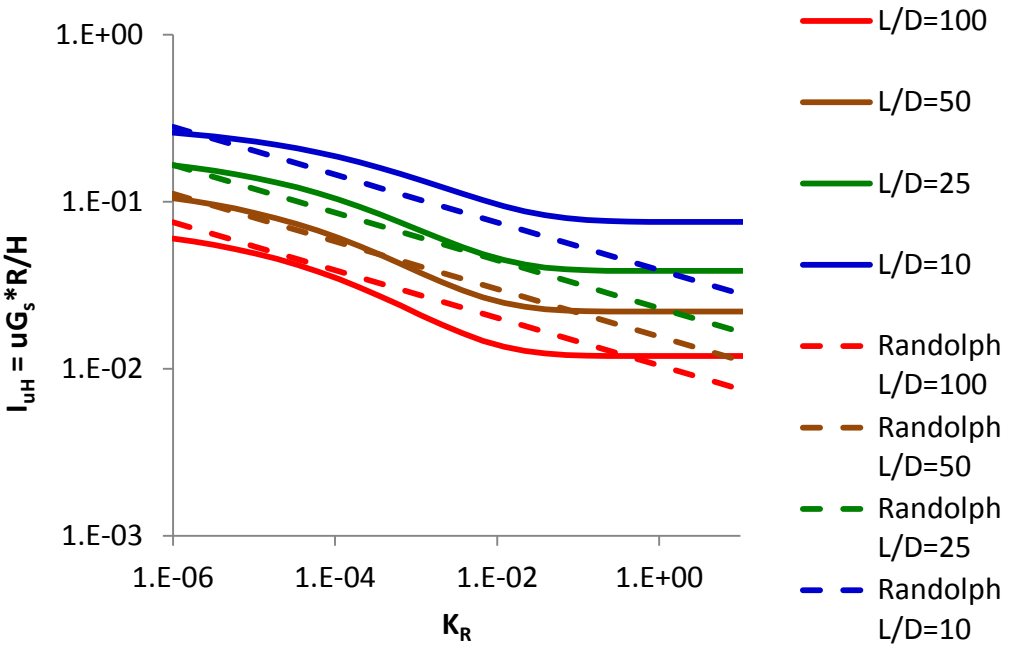

(a) Displacement influence factor for pure horizontal load

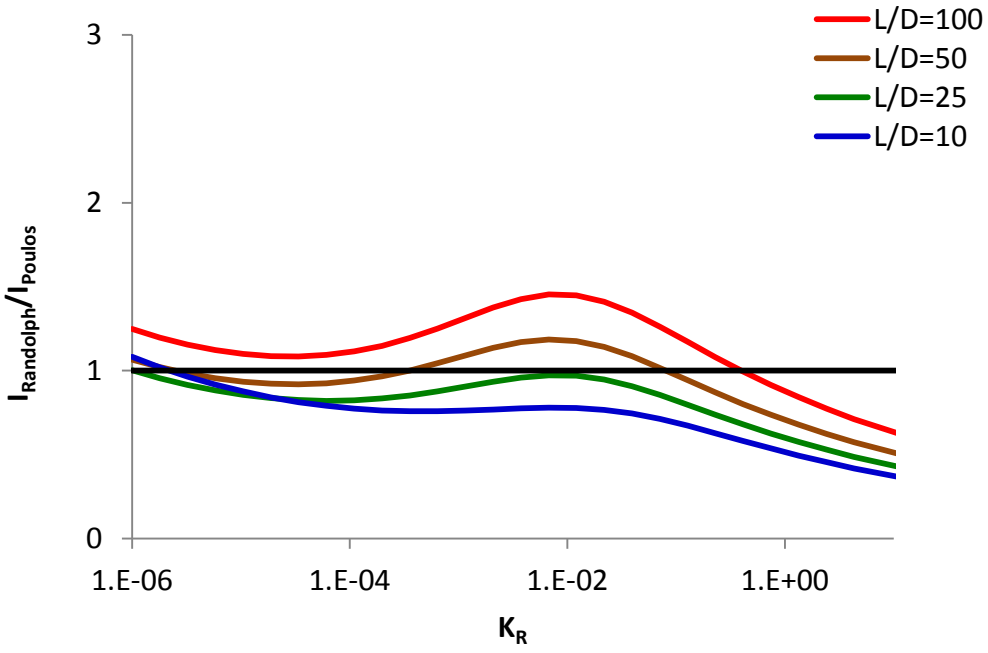

(b)

Figure 2.7 Influence factors presented by Randolph (1981) and Poulos (1971) for pure horizontal load

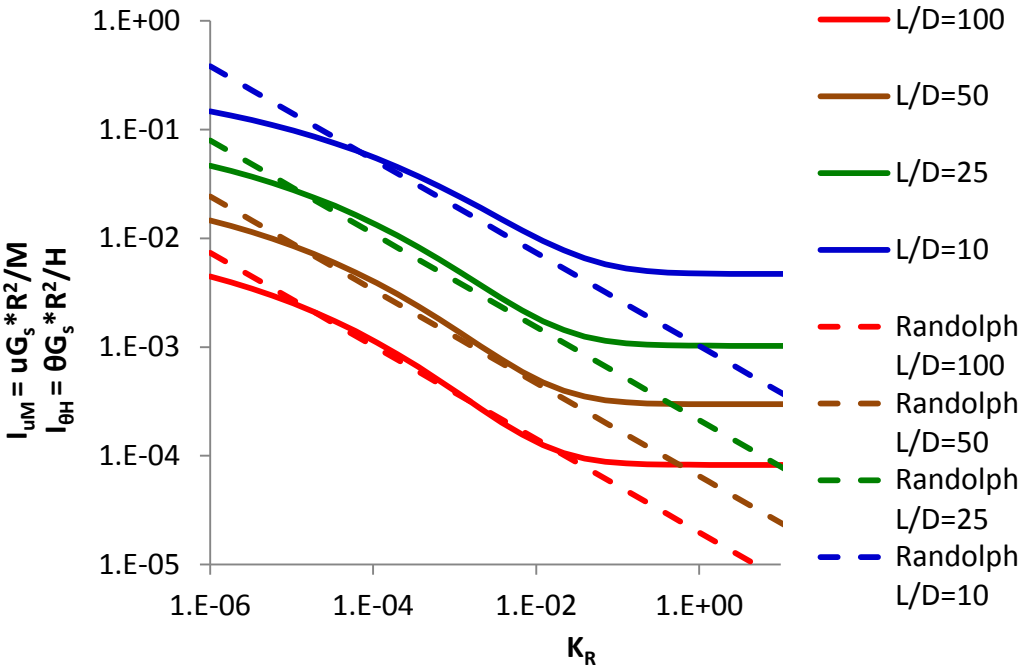

(a) Coupled influence factors for combined loading

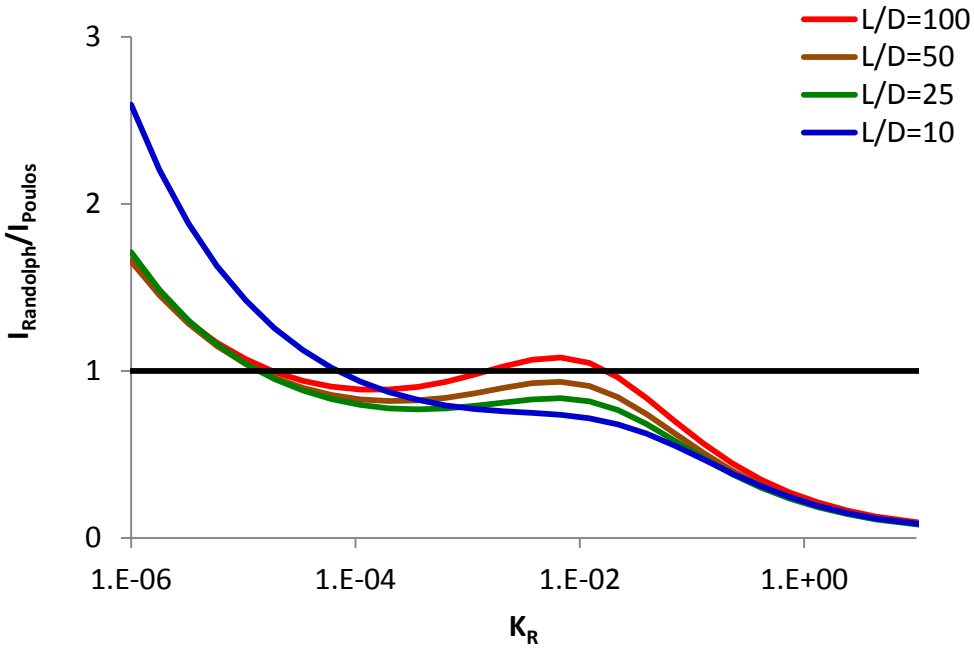

(b)

Figure 2.8 Influence factors presented by Randolph (1981) and Poulos (1971) for combined loading

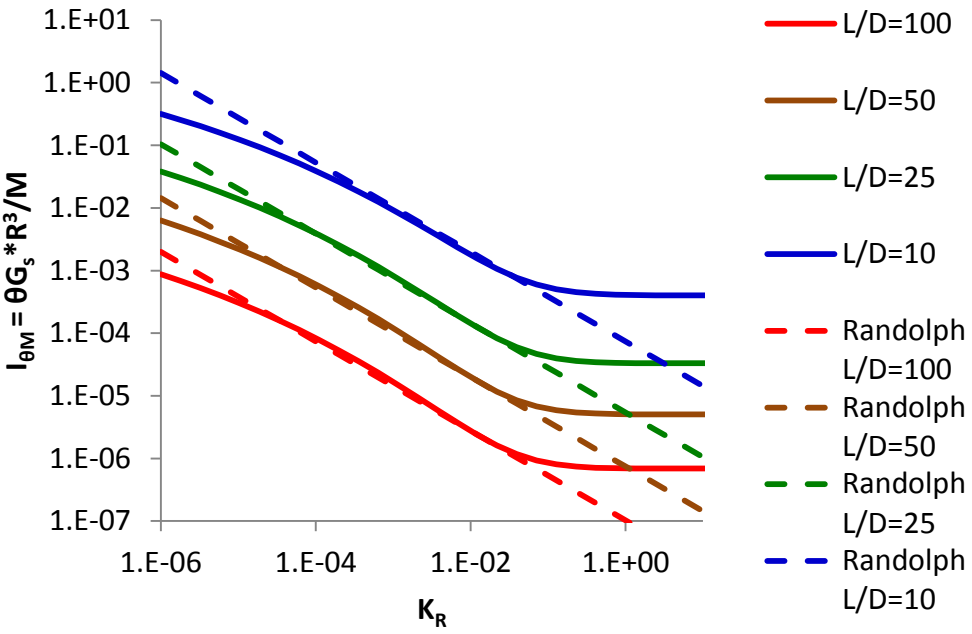

(a) Rotation influence factor for pure moment loading

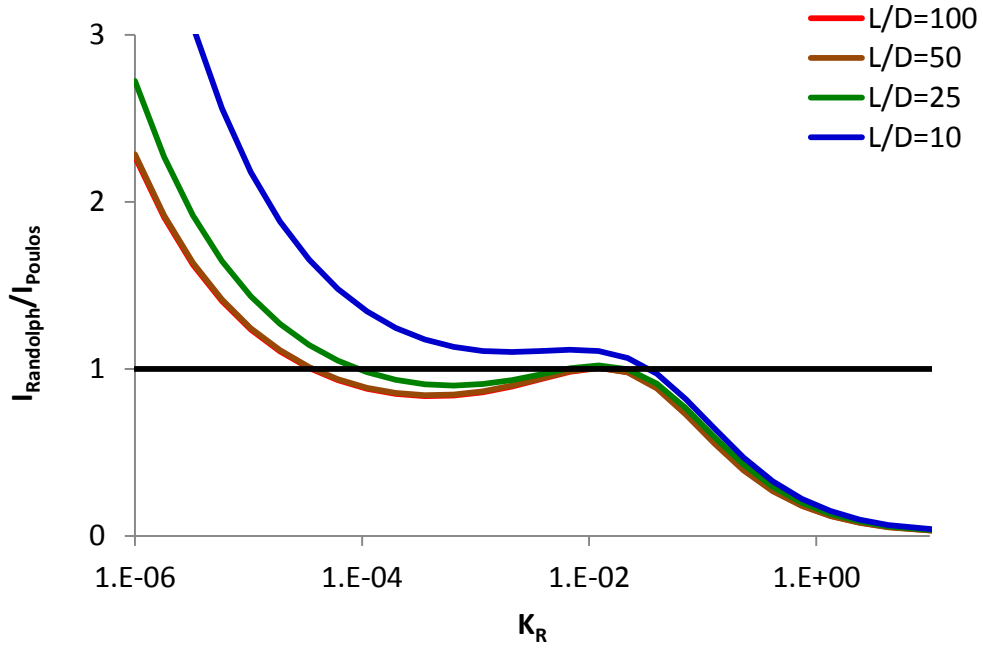

(b)

Figure 2.9 Influence factors presented by Randolph (1981) and Poulos (1971) for pure moment load

Scott (1981) analyzes the laterally loaded piles using rigid beam on elastic foundation (e.g., Hetenyi, 1946) with the subgrade reaction theory, or Winkler foundation model, which is a simplification of an elastic half-space, that requires at least two descriptive material properties (Young's modulus E_s and Poisson's ratio ν). The subgrade reaction coefficient (*k*) is extensively discussed by Scott (1981), and is specified that close predictions with linearly elastic theory can be achieved with the proper selection of *k*. For example, if it is desired that both theories, subgrade reaction and linearly elastic theory, have the same results of maximum moment, the *k* value is taken equal to E_s (Scott, 1981). But this only applies for typical material and beam properties, not for large offshore piles, as discussed by Scott (1981).

Winkler's foundation model assumes a uniform stress distribution at the surrounding of a thin beam, when one section of the pile is loaded and displaces, the displacement does not affect the next section. In reality, the soil is a continuum, adjacent areas are affected, and displacements dissipate with distance from the loaded point. And in the case of offshore monopiles, the diameter is large enough to affect behavior.

LPILE models, using p-y curves, were created to compare the equations proposed by Scott (1981) for flexible and rigid piles (see Appendix A). LPILE is a commercial software program published by Ensoft,Inc., that is often used for the analysis of laterally loaded piles, pile groups, and walls (Reese et al., 2004). The solutions using p-y curves match the solutions given in Scott (1981) for flexible piles, implying that *k* equals E_s. However, Poulos (1971) showed that this solution ignores L/D effects, and Randolph (1981) showed

that there were consistent errors induced with the assumption of modeling a pile as a thin vertical elastic strip where the stress distribution is assumed constant through the pile diameter (i.e., Scott, 1981; Poulos, 1971). This error is increased when the pile diameter is increased (Poulos, 1971).

When Scott's (1981) solution is compared to Poulos' (1971) solution, is observed that Scott (1981) underestimates I_{uH} by 20% for piles with L/D=100 in the flexible and rigid ranges of K_R, and overestimates I_{uH} by 20% for piles with L/D=10. For I_{uM} the underestimation was less than 20% for piles with L/D=100 in the flexible and rigid range of K_R. Overpredictions of 20 and 50% was observed for piles with L/D=10 in the flexible and rigid range of K_R, respectively. Large $I_{\theta M}$ overpredictions of 45 and 75% was observed for piles with L/D=10 in the flexible and rigid range of K_R, respectively.

Design recommendations presented by DNV/Risø (2001) are based on p-y curves, which consist on the construction of load-deformation curves in the length of the pile. Figure 2.13 to Figure 2.15 show large underestimations in the rigid range of K_R for displacements and rotations when assuming $k=E_s$, with values of 75% for I_{uH}, and 90% for I_{uM} and $I_{\theta M}$. Underestimations were also observed in the flexible range of K_R, with values of 35, 30, and 25% for I_{uH}, $I_{uM,}$ and $I_{\theta M}$, respectively.

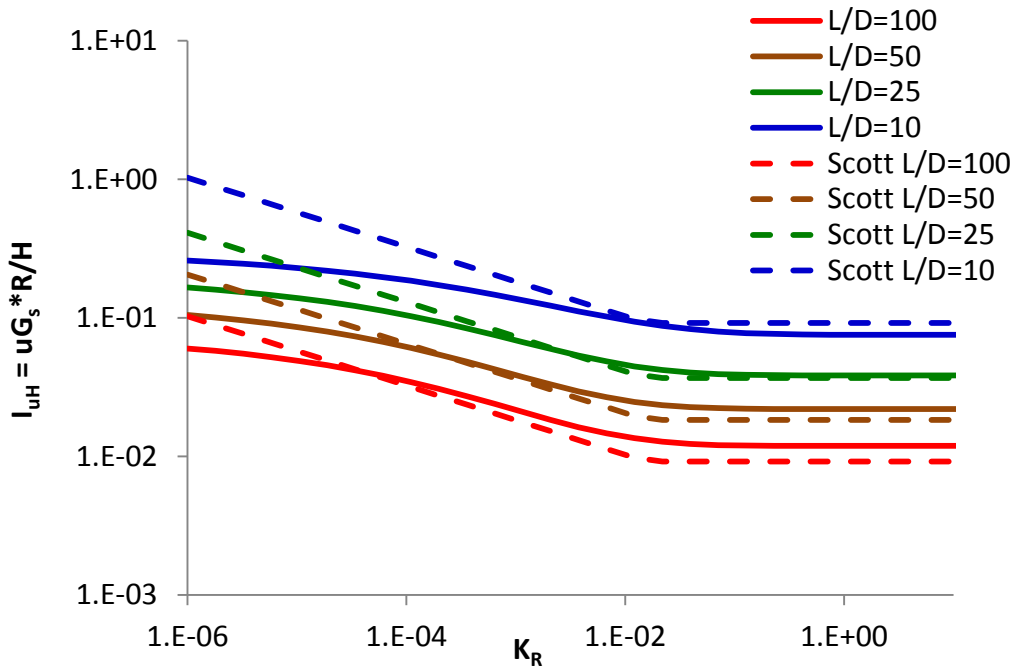

(a) Displacement influence factor for pure horizontal load

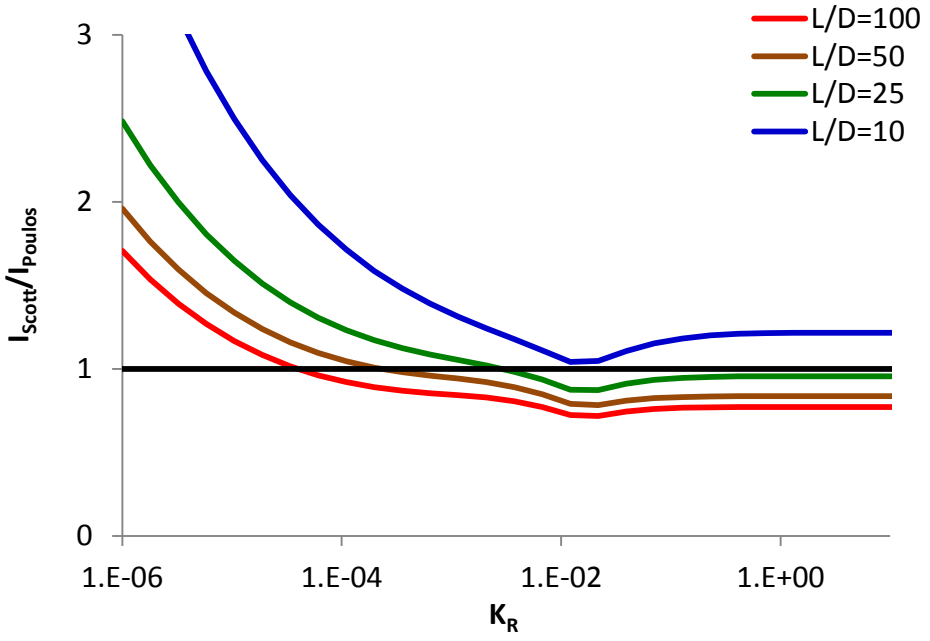

(b)

Figure 2.10 Influence factors presented by Scott (1981) and Poulos (1971) for pure horizontal load

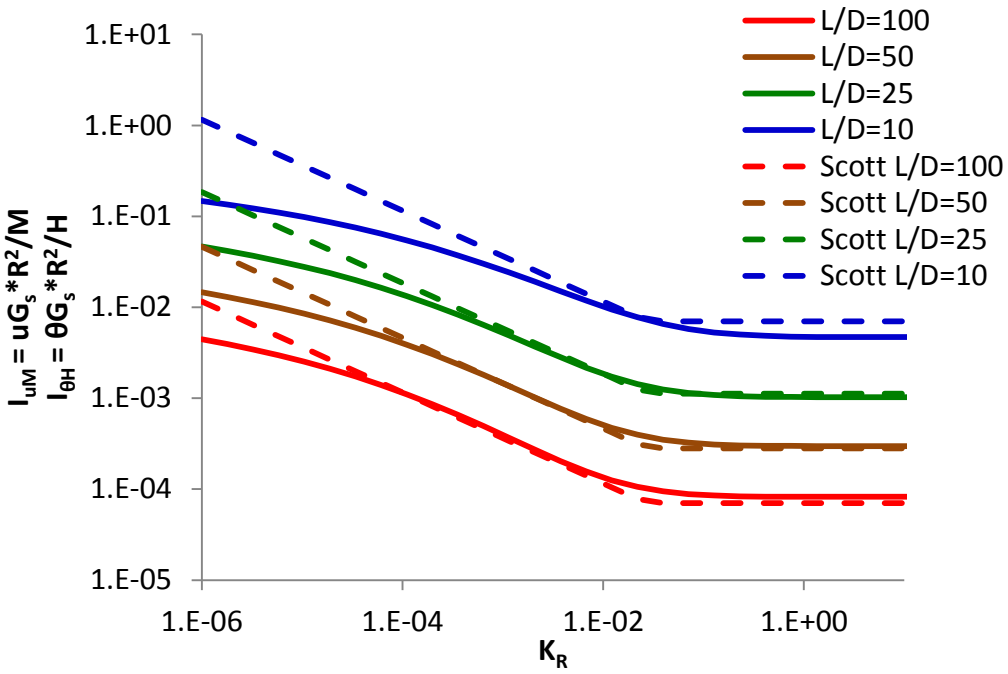

(a) Coupled influence factor for combined loading

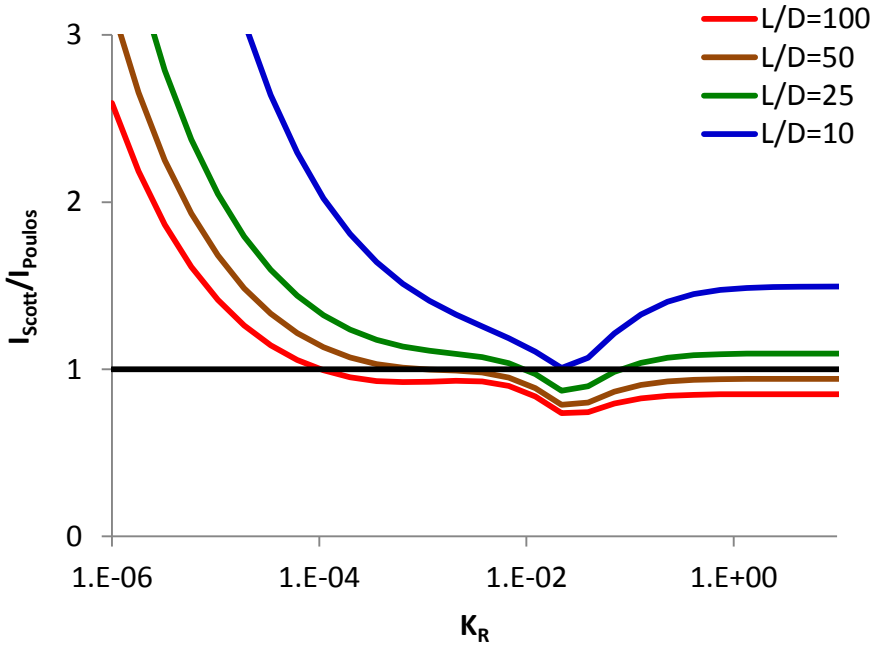

(b)

Figure 2.11 Influence factors presented by Scott (1981) and Poulos (1971) for combined loading

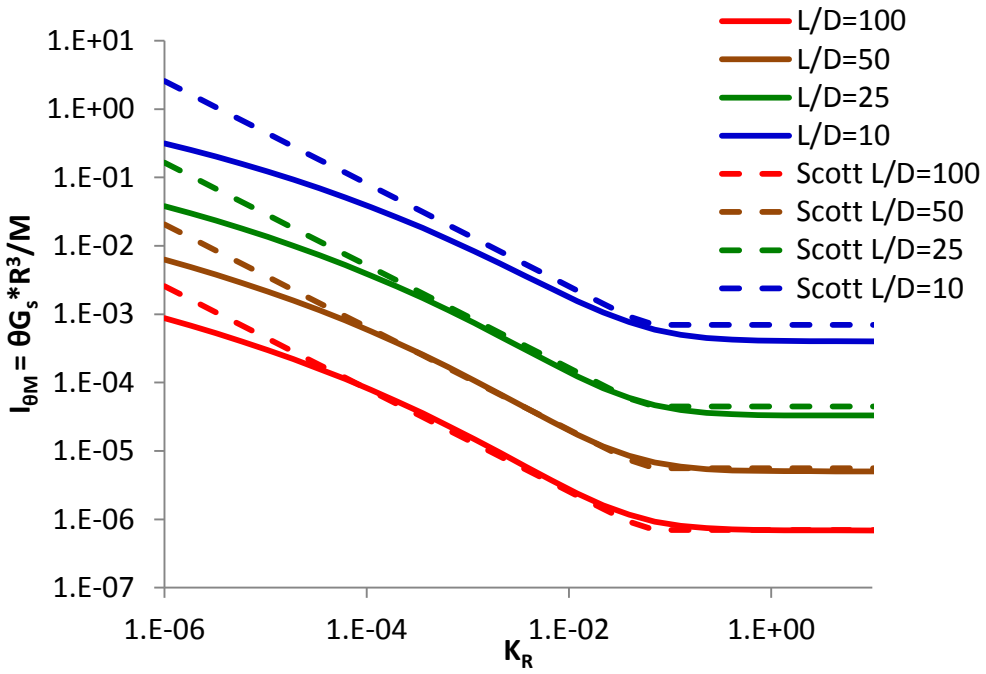

(a) Rotation influence factor for pure moment loading

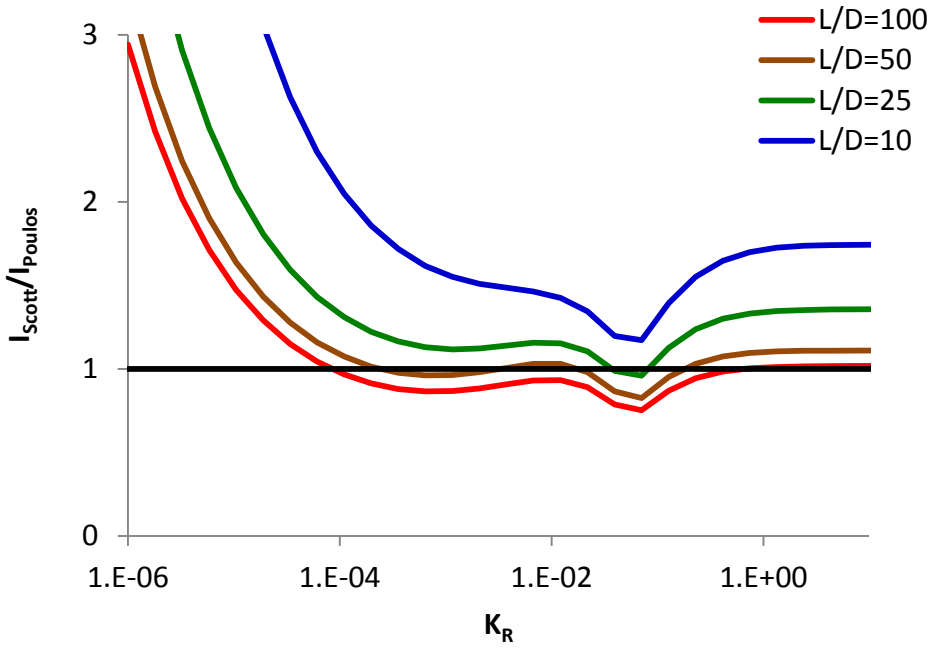

(b)

Figure 2.12 Influence factors presented by Scott (1981) and Poulos (1971) for pure moment load

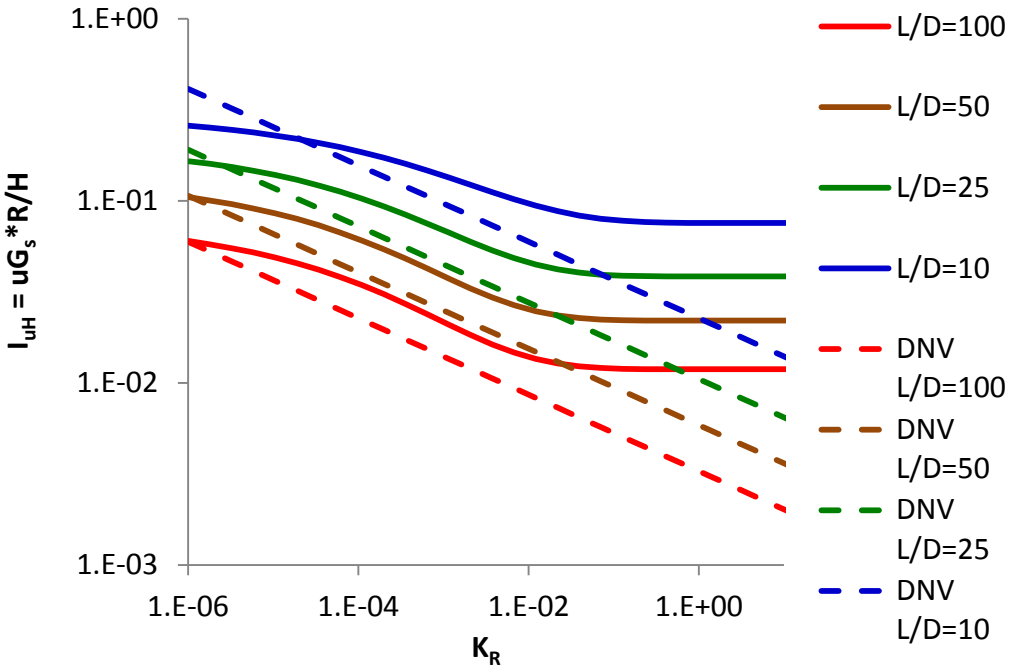

(a) Displacement influence factor for pure horizontal load

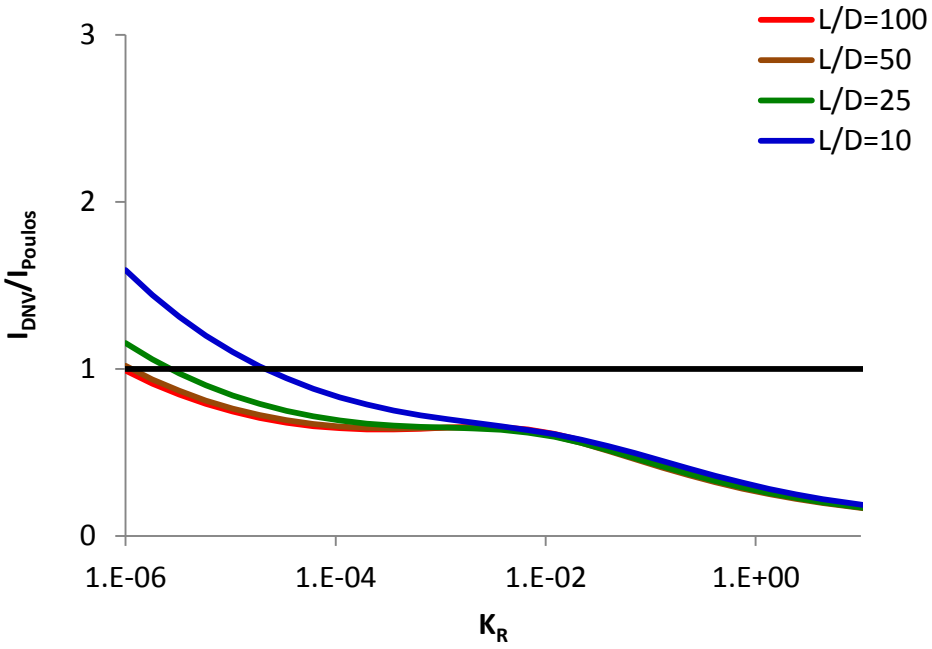

(b)

Figure 2.13 Influence factors presented by DNV/Risø (2001) and Poulos (1971) for pure horizontal load

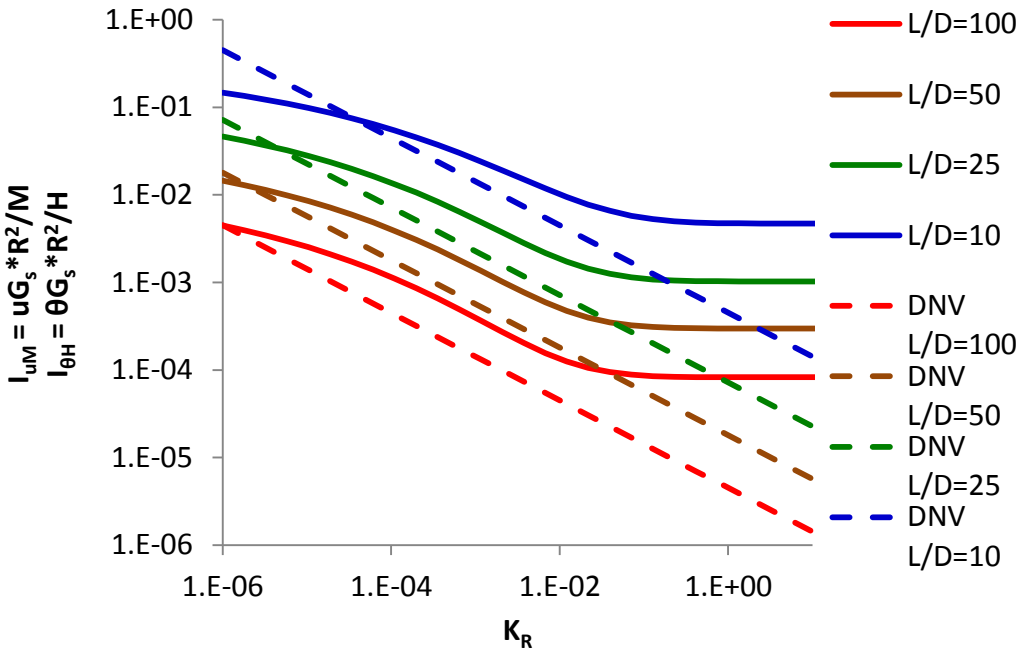

(a) Coupled influence factor for combined loading

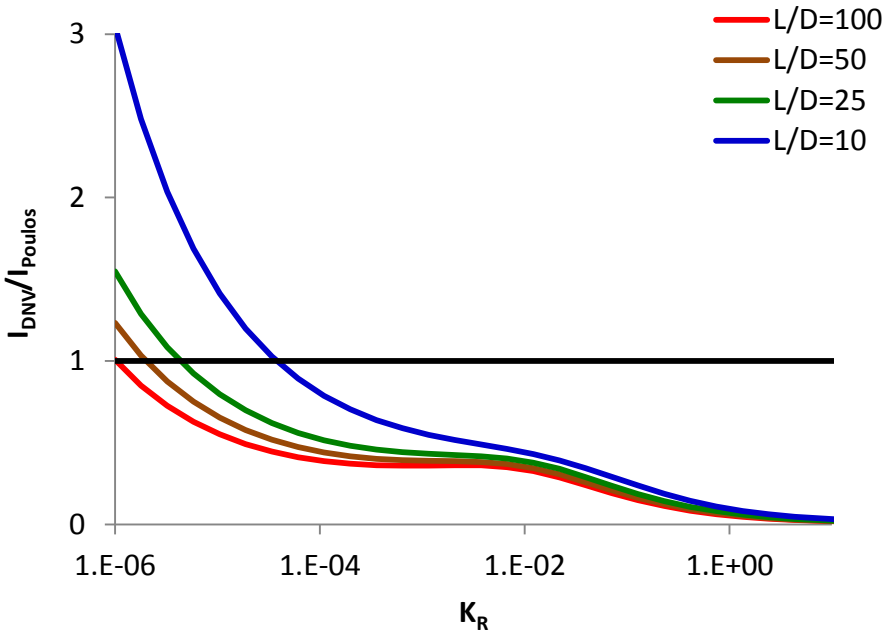

(b)

Figure 2.14 Influence factors presented by DNV/Risø (2001) and Poulos (1971)) for combined loading

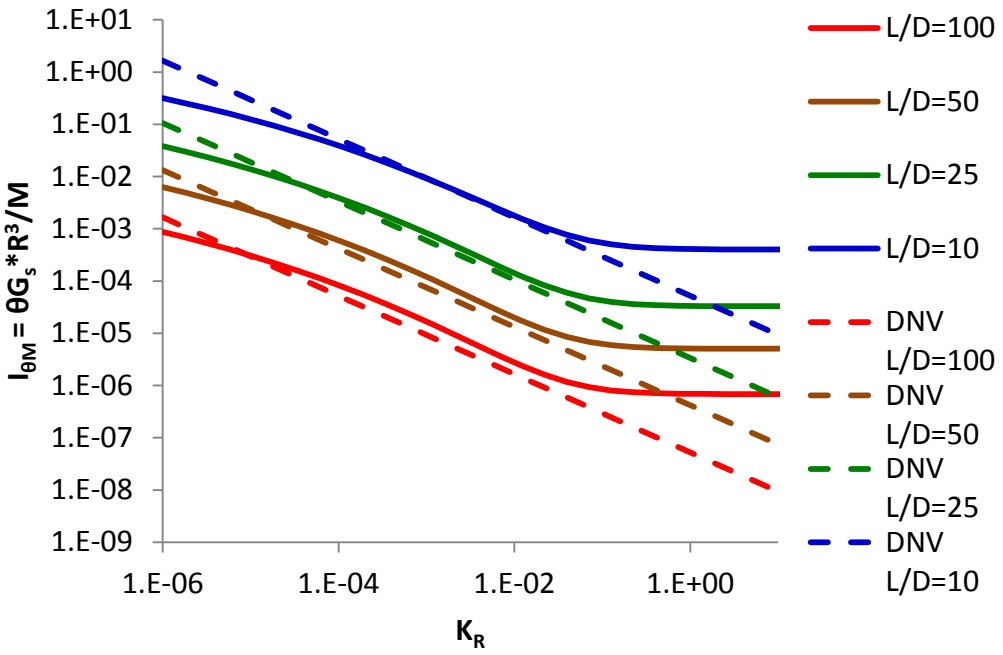

(a) Rotation influence factor for pure moment loading

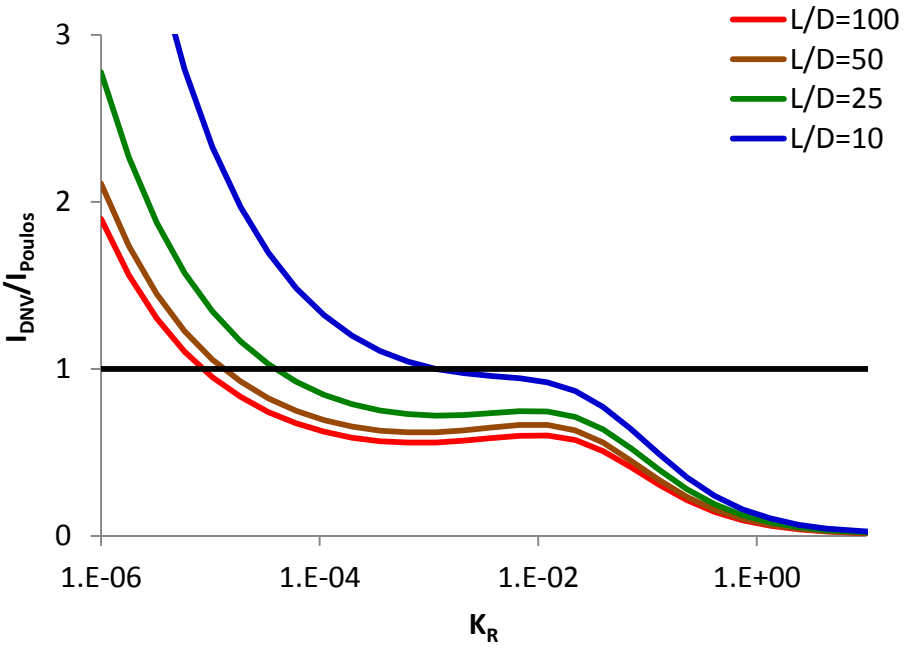

(b)

Figure 2.15 Influence factors presented by DNV/Risø (2001) and Poulos (1971) for pure moment load

Variation in the prediction of influence factors is observed for variations in K_R and variations in L/D. Large underestimations of rocking influence factors (e.g., DNV/Risø, 2001) are a concern in the design of offshore wind turbines, because of the small rotational tolerance (about 0.5° at mudline). Large rotations at hub height decrease wind turbine life, increase maintenance cost, and eventually reduces the power out of the wind farm.

Poulos (1971) does not have a linearly increasing stiffness model, then influence factors presented by Randolph (1981) and DNV/Risø (2001) are compared together in Figure 2.16. From previous analyses and graphs, is known that both methods underestimate the influence factors for rigid piles.

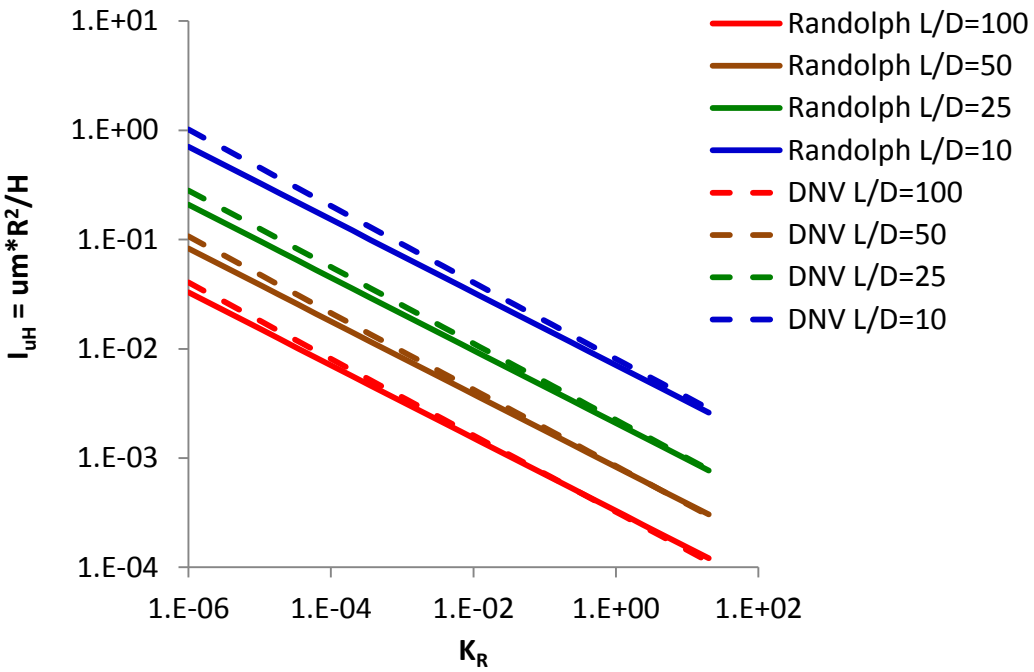

(a) Displacement influence factor for pure horizontal load

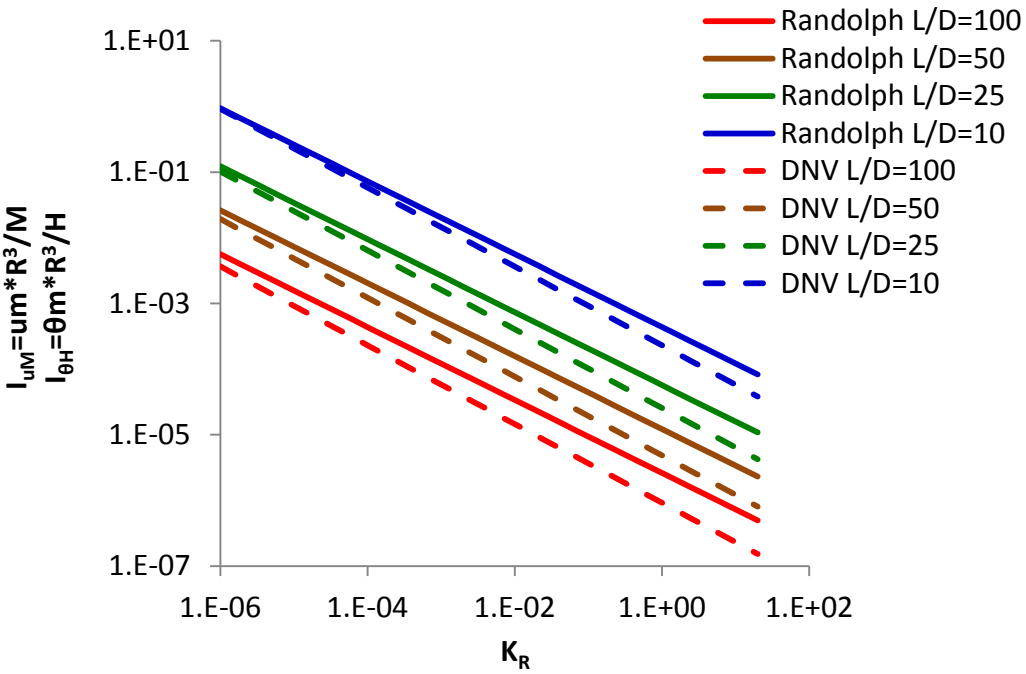

(b) Coupled influence factor for combined loading

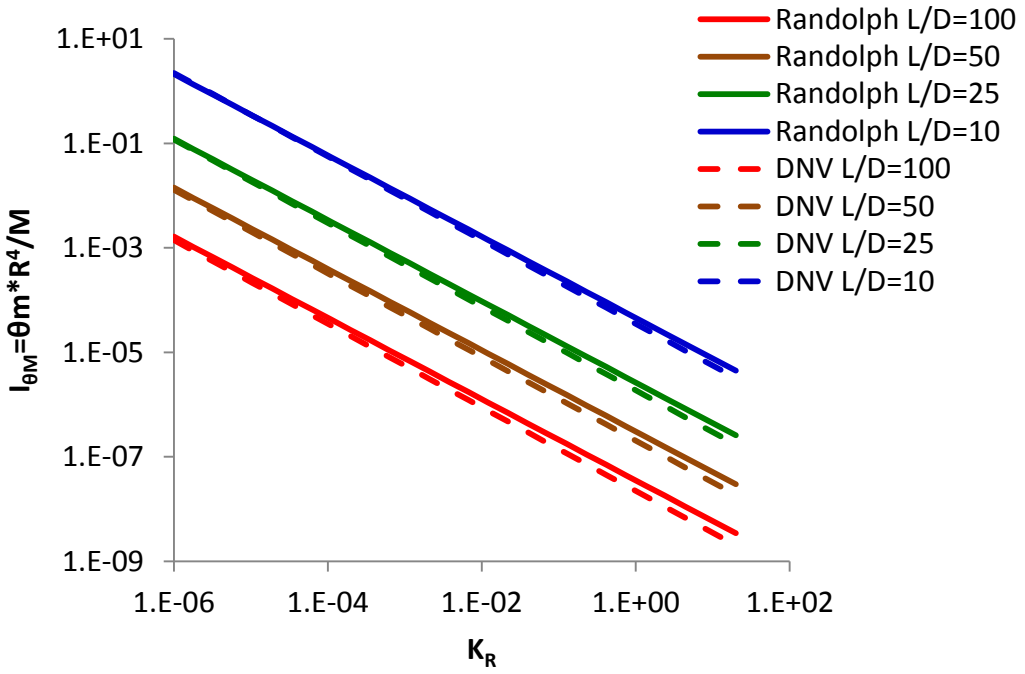

(c) Rotation influence factor for pure moment loading

Figure 2.16 Influence factors presented by DNV/Risø (2001) and Randolph (1981) for linearly increasing stiffness with depth

2.5. Soil Behavior

When soils are loaded with small loads, high stiffness is observed, as shown in Figure 2.17, until larger loads are applied. With larger loads, displacements increase rapidly, demonstrating nonlinearly soil behavior. Once the soil reaches a certain shearing strength, plastic deformations in the soil increase until yield is reached, at this point soil displacement increases greatly. When piles are loaded laterally, the soil at the surface surrounding the pile yields at low load levels, and as the load is increased the yielding progress down the pile (Scott, 1981).

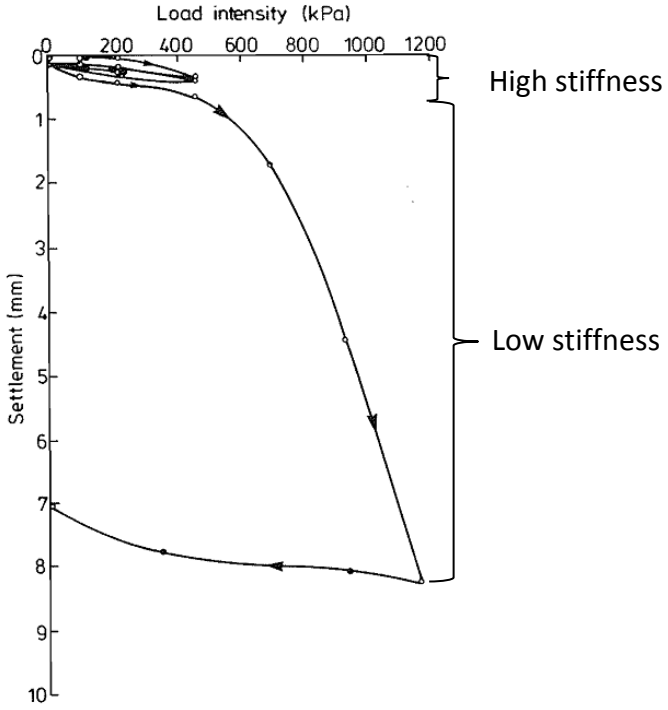

Figure 2.17 Load vs settlement plate test (Burland & Lord, 1969)

A test was performed by the U.S. Army Corps of Engineers in an Arkansas River site where they measured deflection at the surface and the moment distribution down the pile as the lateral load was increased. The results show the downward movement of the maximum moment as the load increases and as the soil yields (Scott, 1981). This behavior is an example of the non-elastic soil behavior.

When the soil is being loaded and unloaded continuously or with cyclic loads, there is an accumulation of strain. During testing, hysteretic behavior has been observed, which means that the soil is dissipating energy. This energy dissipation can be measured by the area of the hysteric loop, and is called hysteretic damping (Gerolymos & Gazetas, 2006).

2.5.1. Material Damping and Cyclic Response

Damping is the dissipation of energy of a system. There are different types of damping: radiation (or geometric) damping, due to the propagation of elastic waves in the soil mass; and material (or internal) damping, due to hysteretic losses in soil (Richart et al., 1970).

One way of measuring internal damping is by measuring the area of the hysteresis loop, one loop is one period of vibration or loading-unloading-reloading (Richart et al., 1970). This loop is considered the energy dissipation per every loading cycle. Figure 2.18(a) shows the hysteretic loop for a nonlinear-elastic foundation soil, where the loading-unloading follows the same curve. Figure 2.18(b) shows the same nonlinear-elastic soil behavior, but this time plastic behavior is also observed. Figure 2.18(c) shows large energy

dissipation of the soft soil, produced by the cyclic loading of the foundation and soil plastic deformations. With every cycle, the loop gets larger and more foundation rocking occurs.

Internal damping can be measured in the laboratory by using the resonant column test (Richart et al., 1970). Where a forced vibration in induced in the soil column, and when the forced is removed, the amplitude decay with time is recorded, and the damping is calculated.

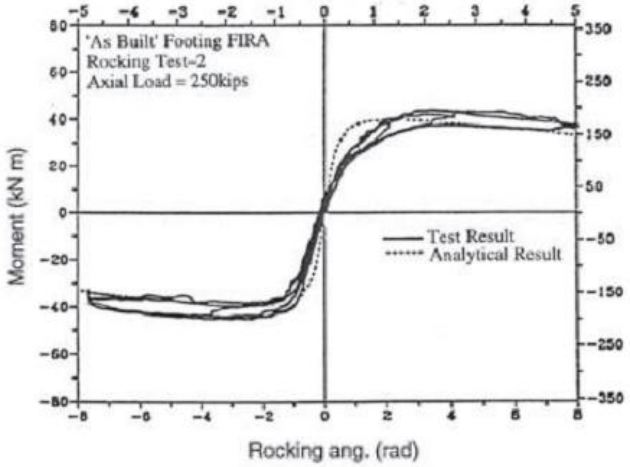

(a) very hard foundation soil

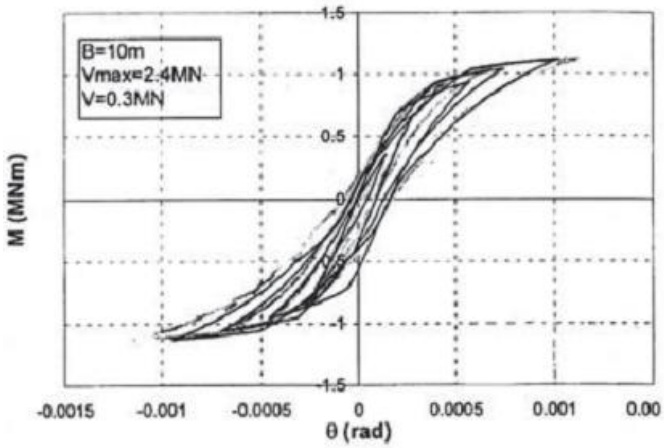

(b) intermediate stiffness foundation soil

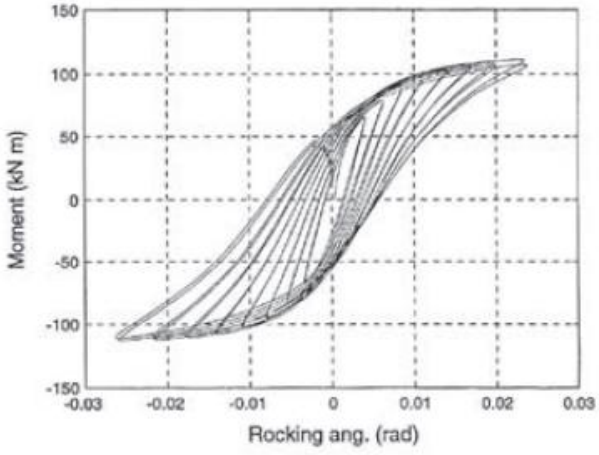

(c) very soft foundation soil

Figure 2.18 Hysteresis loops of a soil-structure interaction system (Gerolymos & Gazetas, 2006)

2.5.2. Constitutive Models

This section describes three constitutive models: linear elastic, linear elastic perfectly plastic (Mohr-Coulomb), and hardening soil with small-strain (HS-Small). These models, available in Plaxis 3D Foundation, describe the soil behavior response under different loading conditions.

The simplest model is the linear elastic (LE) model, based on Hooke's law, and requires two input parameters: Young's modulus (E) and Poisson's ratio (ν) (Holtz & Kovacs, 1981). Serviceability requirements for offshore wind turbines allows rotations at the mudline of 0.5°, for small rotations soil behavior is controlled by elasticity rather than plasticity. Essentially, small settlement and rotation of foundations are controlled by linear elastic soil behavior, as shown in Figure 2.17. The linear elastic model in Plaxis 3D allows for increased stiffness with depth.

The Mohr-Coulomb (MC) model is a linear elastic-perfectly plastic model that involves five principal parameters to define soil elasticity, plasticity, and dilatancy (Plaxis 3D Foundation Material Models Manual, 2011). The input parameters are Young's modulus (E), Poisson's ratio (ν), friction angle (φ), cohesion (c), and dilatancy angle (ψ). This model is convenient for initial assessment of soil behavior. This model contains a purely elastic region, where strains are reversible. Once the strains exceed this region, the behavior becomes plastic. The Mohr-Coulomb model in Plaxis 3D allows for increase of stiffness and cohesion with depth.

The hardening soil (HS) model is similar to the Mohr-Coulomb, but the stiffness parameters are defined differently, as described in Figure 2.19. The model requires four input parameters for stiffness: secant Young's modulus (E_{50}^{ref}), tangent Young's modulus (E_{oed}^{ref}), unload/reload Young's modulus ($E_{ur}^{ref} = 3E_{50}^{ref}$), and power of stress-level dependency of Young's modulus (m). These parameters are related by Equation 2.6 (Plaxis, 2011).

$$E_{oed} = E_{oed}^{ref} \left(\frac{c \cos\varphi - \sigma_1' \sin\varphi}{c \cos\varphi + p^{ref} \sin\varphi} \right)^m \qquad \text{Equation 2.6}$$

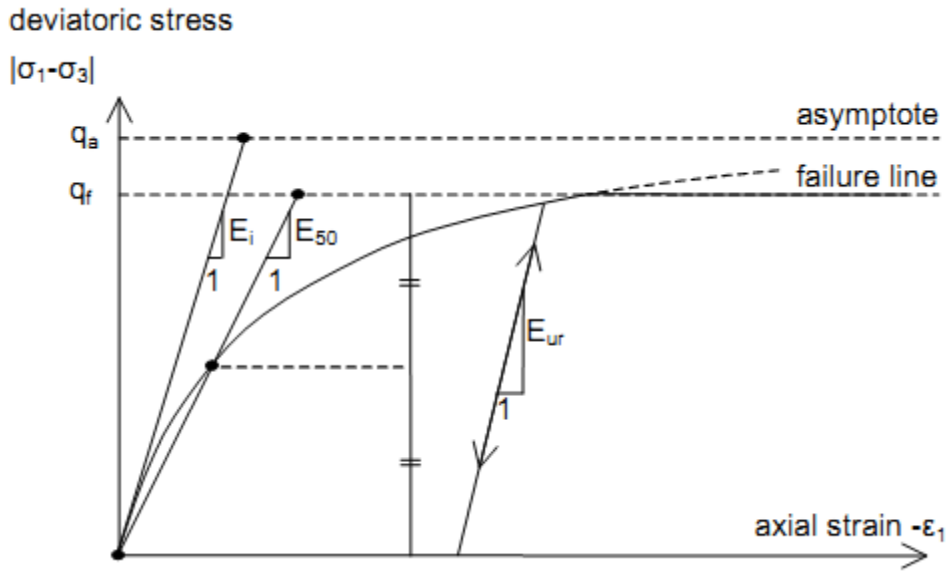

Figure 2.19 Hyberbolic stress-strain relation for a drained triaxial test (Plaxis 3D Foundation Material Models Manual, 2011)

The hardening soil model with small-strain (HS-Small) stiffness is an advance soil model that considers higher stiffness for soils that are deformed with small strains

(Plaxis, 2011). In addition to the input parameters used in the HS model, this model requires two more input parameters: initial small-strain shear modulus (G_0) and the shear strain level ($\gamma_{0.7}$) where the secant shear modulus is reduced 70% of G_0.

2.6. Dynamic Response

Dynamic response can be characterized based on the excitation frequencies (1P and 3P) relative to the fundamental frequency of the tower-foundation-turbine system (Kuhn, 1997). The 1P frequency is related to the rotor's rotational frequency, and the 3P frequency is the blade passing frequency for a three-bladed wind turbine (Ibsen, 2008). If both the 1P and 3P frequencies are less than the fundamental frequency of the structure (f_n), the system is considered stiff-stiff; if the 1P frequency is less than the fundamental frequency and 3P frequency is greater, the system is considered soft-stiff; and if both the 1P and 3P frequencies are greater than the fundamental frequency the system is considered soft-soft (Kuhn, 1997). Figure 2.20 shows these definitions in a frequency measurement of a wind turbine in operational mode.

While range of behavior is well characterized, there are still significant uncertainties in predicting the dynamic response characteristics of offshore wind turbines. For example, the Lely wind farm offshore monopile foundations, located in The Netherlands, were designed to display soft-soft structural dynamic characteristics. However, six months after installation, dynamic measurements showed that the foundation was behaving as soft-stiff

(Kuhn, 2000), indicating overprediction of the natural frequency. Calculation methods that have an overprediction of natural frequency may result in coincidence of the actual frequency of the structure and the frequency of the rotor causing resonance and the potential for structural damage and reduced turbine life. Currently, offshore wind turbines are design as soft-stiff (LeBlanc et al., 2009).

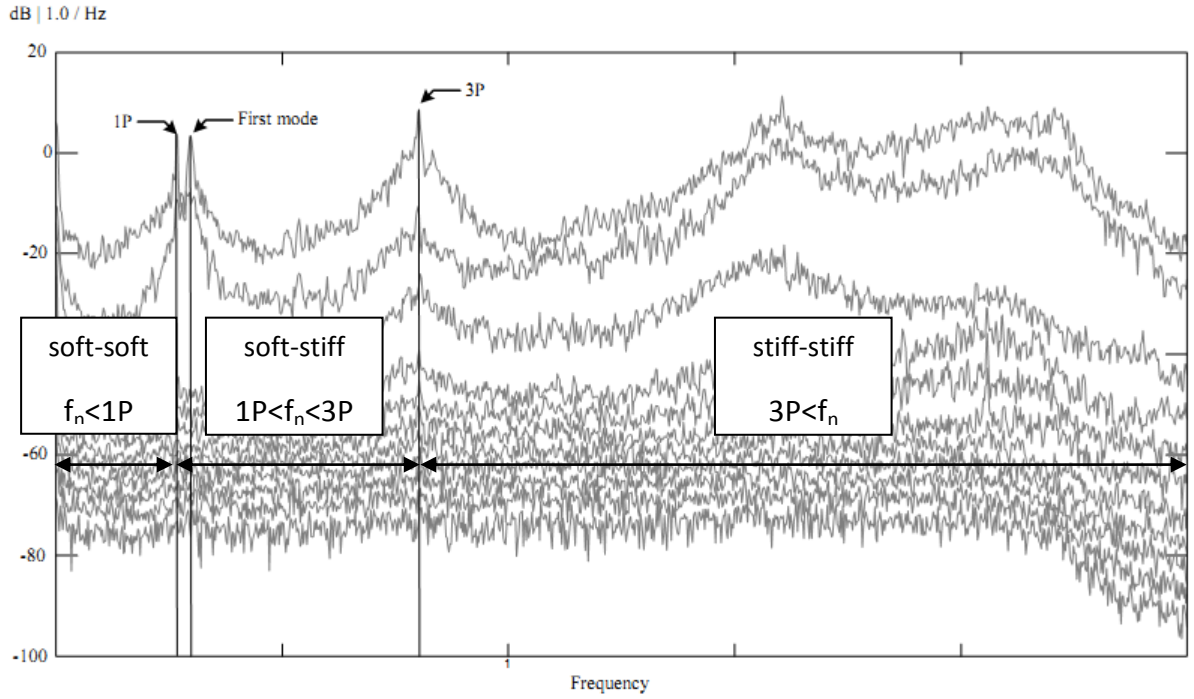

Figure 2.20 Frequency measurement of a Vestas V90 3.0 MW wind turbine in operational mode (Ibsen, 2008)

Zaaijer (2005) found that the first natural frequency of monopiles longer than their critical length can be predicted with an uncertainty of 9%, and sensitivity of 4%. If the pile is shorter than the critical length (i.e. rigid pile), more sensitivity to parameter variations is expected. Zaaijer (2005) also found that the natural frequency of the pile increases with

length, but the natural frequency reaches a limit where the length of the pile no longer affects its dynamic behavior.

2.7. Other Factors Influencing Monopile Response

In the previous sections, we have discussed how geometry, loading conditions, and soil behavior influences the monopile response, and how the design recommendations (e.g., DNV/Risø, 2007) take this into consideration. There are also other factors that influence the response of monopile foundations:

- cyclic loading during normal operation;
- torque induced by nacelle rotation and sudden stop;
- separation between soil and pile;
- loss of soil strength due to cyclic loading;
- water flow characteristics.

One of the mayor design concerns is the effect of cyclic loading on pile behavior. LeBlanc et al. (2009) studied the response of stiff piles in drained sand after long term cyclic lateral loading, applying 8000 to 60000 cycles of combined loading. It was found that cyclic degradation is a function of the loading characteristics and stiffness changes. LeBlanc et al. (2009) emphasizes that p-y curves used by API (2000) and DNV/Risø (2001) are designed to estimate ultimate lateral capacity and do not take into account accumulated rotation and displacement, as well as stiffness changes in the soil-pile system.

The author proposes to incorporate a method for the deterioration of the moment-rotation curves, where the soil reaction is reduced based on the number of cycles applied.

Water flow characteristics are also important to assess during cyclic loading. Water flow characteristics are related to how fast water can flow through soil pores versus how fast the soil is loaded, and can be measured by the coefficient of consolidation (Holtz & Kovacs, 1981). Soils with low coefficients of consolidation and loaded rapidly will develop pore water pressures that will dissipate with time (Schneider & Senders, 2010). Drainage effects can be quantified using the normalized velocity (V):

$$V = \frac{v \times d}{c_v}$$

where v is the pile velocity, d is the pile diameter, and c_v is the coefficient of consolidation. Randolph (2004) observed that excess pore pressures decay to zero when V is approximately 0.1, and from undrained to partially drained condition when V is around 100.

3. Finite Element Analysis of Flexible and Rigid Piles in Elastic Soil

3.1. Introduction

Finite element analysis (FEA) models were created to investigate the behavior of laterally loaded large-diameter piles. The program used for all the FEA was Plaxis 3D Foundation. The numerical models were validated with theoretical models presented by Randolph (1981), and good agreement was found for flexible piles in homogeneous and linearly increasing stiffness with depth soil profiles. As observed in Figure 3.1(a), the soil stratum reaches 5 to 10 m deeper than the pile base, having no influence on the response. Finite element meshes were verified to ensure that the displacements were insignificant prior to reach the boundaries, example in Figure 3.1(b). Smaller elements were used in the surroundings of the pile to increase accuracy of results.

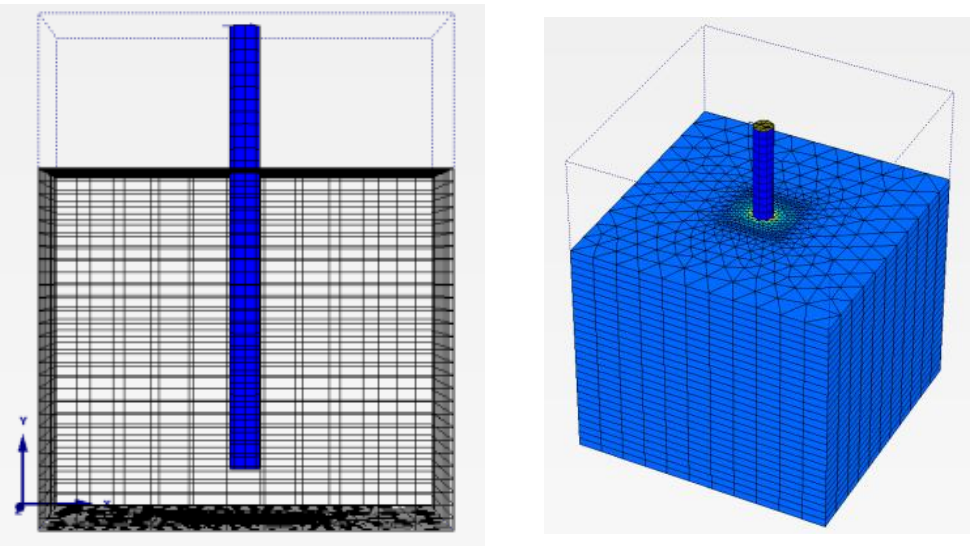

Figure 3.1 Plaxis 3D Foundation model (a) deformed mesh and (b) displacements

3.2. Overview of Plaxis 3D Foundations

Plaxis is a collection of finite element programs for geotechnical engineering and design, including analysis of deformation and stability of structures. For this study, Plaxis 3D Foundation V2.2 was used.

The first step in the *Model Mode* for each new project is defining boreholes. The boreholes define soil layer properties and water table location. Soils with a variety of shear modulus were used to vary the soil-pile system stiffness and the water table was maintained at the soil surface. For the material, you must select between five material models types: (i) linear elastic, (ii) Mohr-Coulomb, (iii) hardening soil model, (iv) HS small, and (v) soft soil creep model; and three models of soil behavior: (i) drained, (ii) undrained, and (iii) non-porous material.

The second step is defining the work planes. The work planes are horizontal planes with different elevations used to define structural objects, construction stages, and loads. The program allows to define the pile stiffness properties at different work planes by varying the thickness of the pile wall and changing material strength. The eccentricities to diameter ratios (e/D) used for this study were 0, 5, and 20. Work planes were created at 0, 5 and 20 m for the 1 m diameter piles, and at 0, 30 and 120 m for 6 m diameter piles, to apply point loads at these eccentricities. Zero eccentricity was used to simulate pure horizontal loading. Additional floors, without weight but with stiffness, were added at the load height to increase the stiffness and measure rotation of the pile at the mudline.

For piles we can use volume piles or embedded piles, volume piles were selected. Volume piles do not take into consideration the installation effects, but interfaces can be added to inner and outer surfaces to consider reduced or increase soil strength at the pile-soil interface (Plaxis, 2011). No changes in effective stress due to installation were considered in this study. Embedded piles are modeled like beam elements that interacts (skin and toe resistance) with the subsoil using special interfaces. This pile option does not occupy volume, but soil around is taken into consideration (Plaxis, 2011). When creating embedded piles, no geometry points are included, then embedded piles does not influence the finite element mesh. Once the boreholes are defined, the work planes are created, the structural elements are placed and loadings defined, we can proceed to create the finite element mesh.

The finite element mesh can be optimized by local and global refinement. Finer element results in accurate numerical results but higher calculation times, finer elements were used in the surrounding of the pile to increase accuracy of the displacements. Plaxis manual recommends creating the 2D mesh and used to verify local and global refinement needs. Once the refinements are done, you can proceed to generate the 3D mesh, and with this step the geometry modeling is completed.

Finite element calculation is performed in the *Calculation Mode.* In this mode, calculation phases, that corresponds to construction or loading phases, are defined. The initial phase is based on the initial stress field using gravity loading or K_0 procedure. For the next phases, the calculation type and the starting point for that phase are defined. The

types of calculations that can be performed are the plastic calculation, consolidation analysis, and phi-c reduction. In this case, plastic calculations for elastic-plastic deformation analysis are used. Once all the calculation stages are defined, the program is instructed to perform the calculation. The output program is run to obtain the results.

The output given by Plaxis is a table with the coordinates and displacement in the three Cartesian directions (x, y, and z). For the analysis displacement at the mudline and at a certain height were obtained. The displacement at the mudline is accurate and precise. The rotation at the mudline is taken as the rotation of the first pile section, which is accurate but not precise, because the pile section above the soil surface also deforms due to eccentric horizontal load.

3.3. Validation Studies

Finite element models were created to validate the models prior to use them for analysis of large-diameter piles. Influence factors developed by Randolph (1981) for flexible piles were compared to Plaxis 3D Foundation models for variations in pile flexibility factor (K_R). Plaxis models for validation have 1 m diameters, constant L/D ratio of 60, and eccentricity to diameter ratio (e/D) varying from 0 to 20, see Table 3.1. A large L/D ratio means that the pile behaves as flexible piles, deflecting in the upper part.

Good agreement was found between displacement and rotation influence factors for homogeneous stiffness distribution presented by Randolph (1981) and Plaxis 3D

Foundation models, shown in Figure 3.2. Figure 3.3 presents the finite element results for displacement and rotation influence factors for linearly increasing stiffness with depth compared to Randolph (1981).

Table 3.1 Validation studies with R=0.5 m and L=60 m

ID	E_p (kPa)	G* (kPa)	e/D	H (kN)	u_{plaxis} (m)	θ_{plaxis} (degrees)	K_R	E_p/G^*
eD001	1.6E+07	5.0E+05	0	1.0E+04	6.9E-03	-	5.6E-08	3.2E+01
eD002	1.6E+07	5.0E+05	0	1.0E+06	6.9E-01	-	5.6E-08	3.2E+01
eD003	1.6E+07	6.1E+05	0	1.0E+04	5.8E-03	1.4E-01	4.6E-08	2.6E+01
eD004	1.6E+07	2.5E+04	0	1.0E+04	8.3E-02	-	1.1E-06	6.4E+02
eD005	1.6E+07	2.5E+03	0	1.3E+04	7.2E-01	6.2E+00	1.1E-05	6.4E+03
eD006	1.6E+07	2.5E+01	0	2.5E+02	5.2E-01	-	1.1E-03	6.4E+05
eD007	1.6E+07	2.5E-01	0	4.5E+01	6.1E+00	-	1.1E-01	6.4E+07
eD008	1.6E+07	1.5E+01	0	1.0E+01	3.5E-02	8.1E-02	1.9E-03	1.1E+06
eD009	1.6E+07	2.5E-02	0	1.0E+00	1.4E+00	-	1.1E+00	6.4E+08
eD010	1.6E+07	2.5E+01	0	1.0E+01	2.3E-02	6.1E-02	1.1E-03	6.4E+05
eD501	1.6E+07	6.1E+05	5	1.0E+04	1.9E-02	2.6E+00	4.6E-08	2.6E+01
eD502	1.6E+07	6.1E+05	5	1.0E+04	1.8E-02	2.6E+00	4.6E-08	2.6E+01
eD503	1.6E+07	3.1E+05	5	7.0E+03	2.2E-02	2.2E+00	9.1E-08	5.3E+01
eD504	1.6E+07	3.1E+04	5	1.5E+03	2.6E-02	9.4E-01	9.1E-07	5.3E+02
eD505	1.6E+07	3.1E+03	5	3.0E+02	2.7E-02	4.1E-01	9.1E-06	5.3E+03
eD506	1.6E+07	3.1E+02	5	3.0E+02	1.4E-01	9.8E-01	9.1E-05	5.3E+04
eD507	1.6E+07	3.1E+01	5	1.0E+01	2.4E-02	8.6E-02	9.1E-04	5.3E+05
eD2001	1.6E+07	6.1E+05	20	6.7E+02	3.8E-03	4.4E-01	4.6E-08	2.6E+01
eD2002	1.6E+07	6.1E+05	20	6.7E+02	5.6E-03	5.4E-01	4.6E-08	2.6E+01
eD2003	1.6E+07	3.1E+05	20	5.0E+02	6.6E-03	5.0E-01	9.1E-08	5.3E+01
eD2004	1.6E+07	3.1E+04	20	5.0E+01	2.7E-03	9.8E-02	9.1E-07	5.3E+02
eD2004	1.6E+07	3.1E+03	20	1.0E+01	2.2E-03	3.9E-02	9.1E-06	5.3E+03
eD2006	1.6E+07	3.1E+02	20	2.0E+00	1.8E-03	1.6E-02	9.1E-05	5.3E+04
eD2007	1.6E+07	3.1E+01	20	5.0E-01	2.0E-03	8.7E-03	9.1E-04	5.3E+05

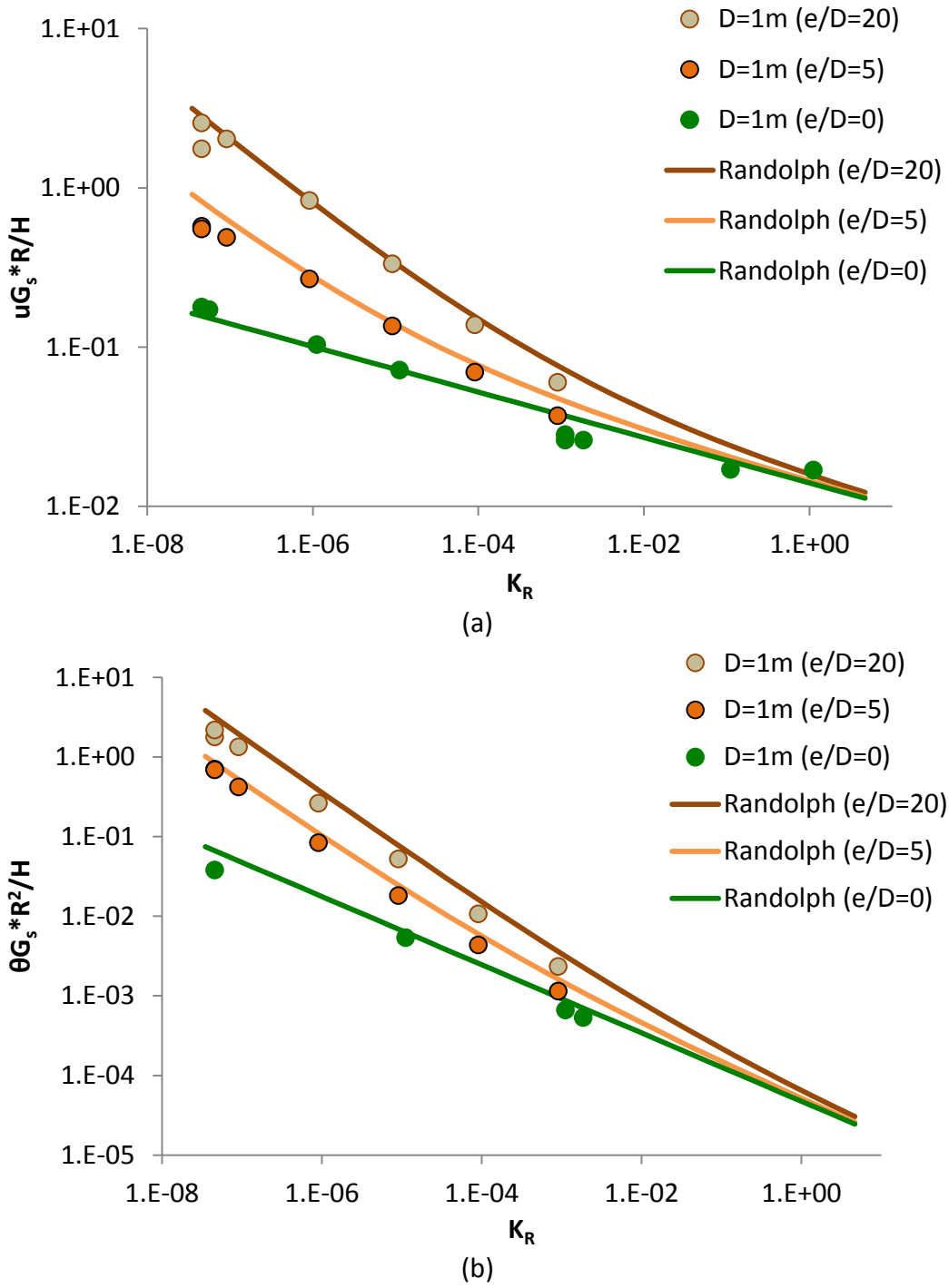

Figure 3.2 Influence factor for (a) displacement and (b) rotation of combined loading in homogeneous stiffness distribution with L/D=60

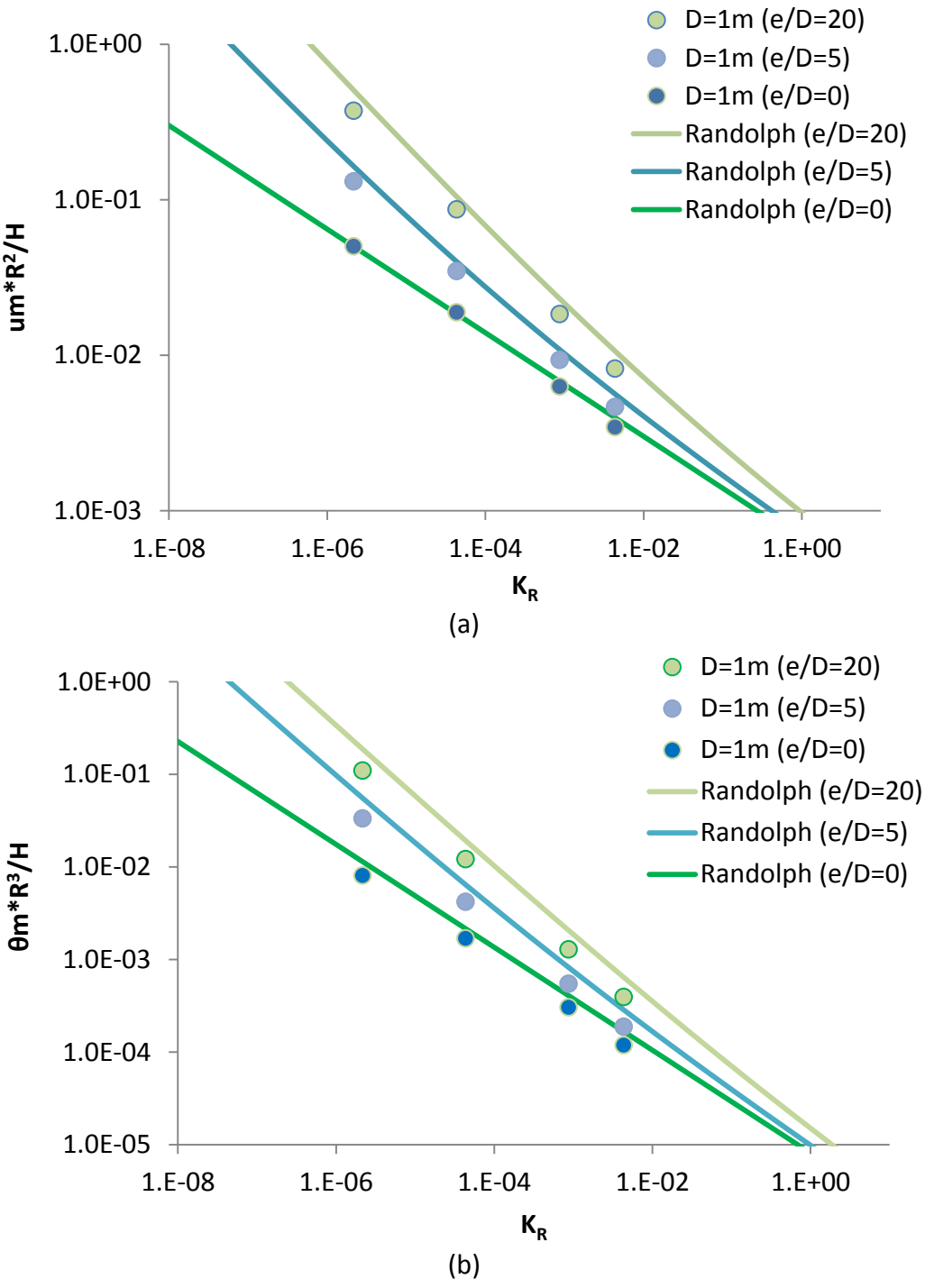

Figure 3.3 Influence factors for (a) displacement and (b) rotations of combined loading in linearly increasing stiffness distribution with L/D=60

3.4. Analysis of Lateral Deformations

Lateral deformations were analyzed in different stiffness distribution soil profiles and compared to influence factors presented by Randolph (1981). Homogeneous and linearly increasing stiffness with depth (z) soil profiles were analyzed for horizontal (H) and moment (M) loading. Small-diameter piles are represented with 1 m diameter, and large-diameter piles with 6 m diameter. The load eccentricities to diameter ratios (e/D) selected were 0, 5 and 20. To have different pile flexibility ratios (K_R), length to diameter ratios (L/D) ranged from 4 to 15 and soil shear modulus was also varied. Load magnitudes were varied depending on the shear modulus of the soil (G_s) selected.

The same pile geometries were used for soils with homogenous stiffness distribution with depth and for soils with stiffness increasing with depth in the FEA models. The results were graph using Randolph (1981)'s framework. Deviations were observed for large-diameter piles, and for small-diameter and large-diameter piles for large values of K_R. The following sections, 3.4.1. Homogeneous Stiffness with Depth and 3.4.2. Stiffness Increasing with Depth, present the FEA results for both stiffness distributions.

3.4.1. Homogeneous Stiffness with Depth

A homogeneous stiffness with depth profile is a typical assumption for overconsolidated clays (Scott, 1981). This section will present the results of FEA studies and a comparison to the solution presented by Randolph (1981). The FEA results are compared to

Randolph (1981) because good agreement was found for flexible piles, and similar behavior was observed for rigid piles in the flexible region of the pile flexibility factor (K_R). Table 3.2 presents a summary of all the analyses performed for homogeneous stiffness distribution with depth.

Figure 3.4 shows the displacement and rotation influence factors for a flexible pile with small-diameter and L/D=15, compared to the solutions by Randolph (1981). The correspondence between the solutions by FEA and Randolph (1981) shows that the uniform stress distribution is negligible for L/D=15, as stated by Poulos (1971). Figure 3.5(a) shows the influence factors for displacements and Figure 3.5(b) for rotations for pile geometries with L/D=4 for small (1 m) and large (6 m) diameter with small (e/D=5) and large (e/D=20) eccentricities. Good agreement in the influence factors is observed for flexible piles, $K_R=10^{-2}$, where the 6 m diameter pile has a larger rotation influence factor than the one predicted by the formulation by Randolph (1981). As K_R increases, the pile changes behavior from flexible to rigid and underestimation of pile displacement (u) and rotation (θ) at the mudline is observed, even for the small-diameter pile.

Figure 3.6 show the finite element analysis results for L/D=10 ratio for large-diameter piles and two eccentricities. Large-diameter piles show flexible behavior at $K_R=10^{-4}$, but as K_R increases underestimation is observed for displacement influence factor and large underestimations for rotational influence factors. These results show the need to assess diameter effects for flexible piles and L/D ratio effects for rigid piles.

Table 3.2 Summary of analyses for homogeneous stiffness with depth

ID	R (m)	L (m)	E_p (kPa)	G* (kPa)	e/D	H (kN)	u_{plaxis} (m)	θ_{plaxis} (degrees)	K_R	E_p/G^*
eD5D1L15a	0.5	15	1.5E+07	1.5E+05	5	500	2.8E-03	2E-01	4.4E-05	1.0E+02
eD5D1L15b	0.5	15	1.5E+07	6.8E+04	5	500	5.0E-03	2E-01	1.0E-04	2.3E+02
eD5D1L15c	0.5	15	1.5E+07	4.4E+04	5	500	6.9E-03	2E-01	1.6E-04	3.5E+02
eD5D1L15d	0.5	15	1.5E+07	3.1E+02	5	500	2.9E-01	2E+00	2.2E-02	5.0E+04
eD5D1L4a	0.5	4	1.5E+07	1.5E+05	5	500	2.9E-03	2E-01	8.8E-03	1.0E+02
eD5D1L4b	0.5	4	1.5E+07	6.8E+04	5	500	5.5E-03	2E-01	2.0E-02	2.3E+02
eD5D1L4c	0.5	4	1.5E+07	4.4E+04	5	500	8.0E-03	3E-01	3.1E-02	3.5E+02
eD5D1L4d1	0.5	4	1.5E+07	3.1E+02	5	500	9.6E-01	2E+01	4.4E+00	5.0E+04
eD20D1L4a	0.5	4	1.5E+07	1.5E+05	20	500	8.5E-03	6E-01	8.8E-03	1.0E+02
eD20D1L4b	0.5	4	1.5E+07	6.8E+04	20	500	1.6E-02	8E-01	2.0E-02	2.3E+02
eD20D1L4c	0.5	4	1.5E+07	4.4E+04	20	500	2.3E-02	9E-01	3.1E-02	3.5E+02
eD20D1L4d1	0.5	4	1.5E+07	3.1E+02	20	1	5.9E-03	1E-01	4.4E+00	5.0E+04
eD5D6L24a	3	24	5.5E+08	5.5E+06	5	500	2.0E-05	1E-03	8.8E-03	1.0E+02
eD5D6L24b	3	24	5.5E+08	8.7E+04	5	500	6.8E-04	5E-03	5.6E-01	6.4E+03
eD5D6L24c	3	24	5.5E+08	4.4E+04	5	500	1.2E-03	7E-03	1.1E+00	1.3E+04
eD5D6L24d	3	24	5.5E+08	1.1E+01	5	500	3.8E+00	1E+01	4.4E+03	5.0E+07
eD5D6L24e	3	24	5.5E+08	5.5E+00	5	500	7.6E+00	3E+01	8.8E+03	1.0E+08
eD20D6L24a	3	24	5.5E+08	5.5E+06	20	1	1.0E-07	7E-06	8.8E-03	1.0E+02
eD20D6L24b	3	24	5.5E+08	8.7E+04	20	500	2.0E-03	2E-02	5.6E-01	6.4E+03
eD20D6L24c	3	24	5.5E+08	4.4E+04	20	500	3.5E-03	2E-02	1.1E+00	1.3E+04
eD20D6L24d	3	24	5.5E+08	1.1E+01	20	500	1.1E+01	4E+01	4.4E+03	5.0E+07
eD20D6L24e	3	24	5.5E+08	5.5E+00	20	500	2.1E+01	6E+01	8.8E+03	1.0E+08
eD5D6L60a	3	60	5.5E+08	5.5E+06	5	500	2.0E-05	1E-03	2.2E-04	1.0E+02
eD5D6L60b	3	60	5.5E+08	2.8E+03	5	500	7.3E-03	2E-02	4.5E-01	2.0E+05
eD5D6L60c	3	60	5.5E+08	1.4E+03	5	500	1.3E-02	3E-02	8.9E-01	4.0E+05
eD5D6L60d	3	60	5.5E+08	1.1E+01	5	500	1.5E+00	2E+00	1.1E+02	5.0E+07
eD5D6L60e	3	60	5.5E+08	5.5E+00	5	500	3.1E+00	4E+00	2.2E+02	1.0E+08
eD20D6L60a	3	60	5.5E+08	5.5E+06	20	500	6.1E-05	4E-03	2.2E-04	1.0E+02
eD20D6L60b	3	60	5.5E+08	2.8E+03	20	500	1.9E-02	6E-02	4.5E-01	2.0E+05
eD20D6L60c	3	60	5.5E+08	1.4E+03	20	500	3.2E-02	8E-02	8.9E-01	4.0E+05
eD20D6L60d	3	60	5.5E+08	1.1E+01	20	500	3.4E+00	5E+00	1.1E+02	5.0E+07
eD20D6L60e	3	60	5.5E+08	5.5E+00	20	500	6.8E+00	1E+01	2.2E+02	1.0E+08

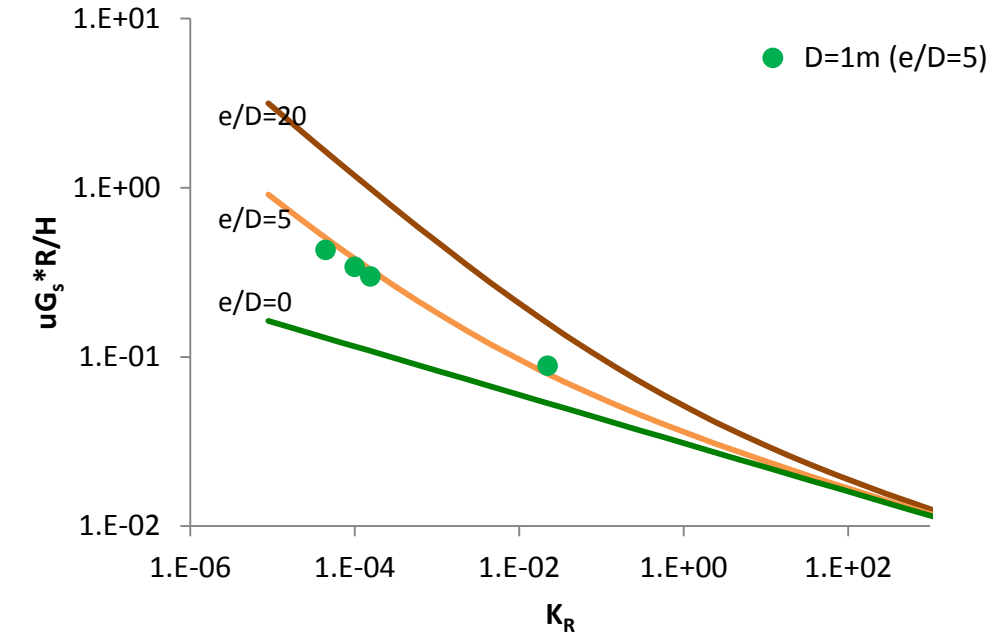

(a)

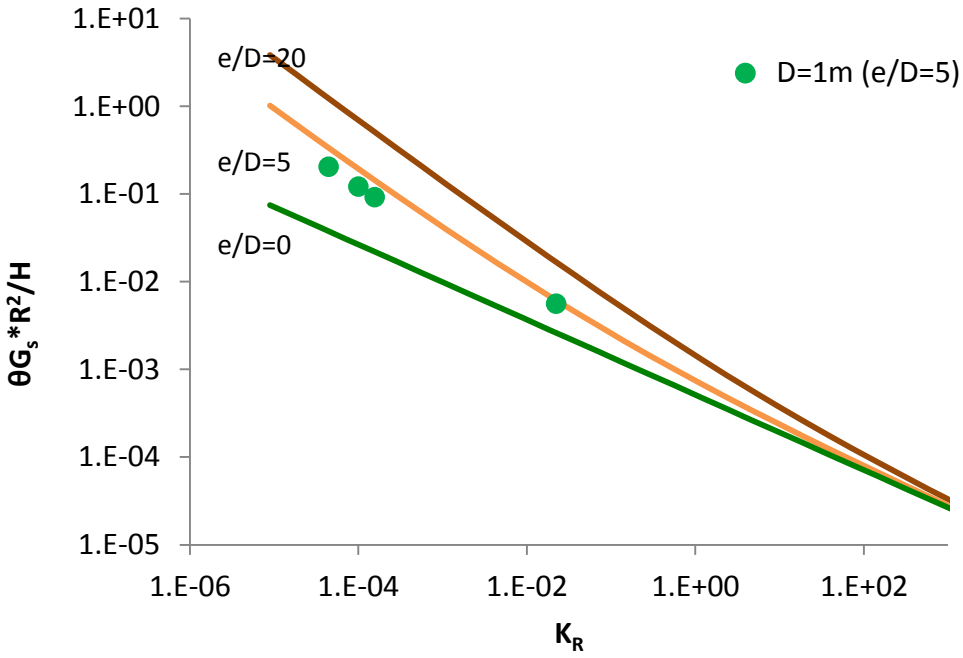

(b)

Figure 3.4 Variations in pile (a) displacement and (b) rotation influence factors with stiffness ratio in homogeneous soils for L/D=15

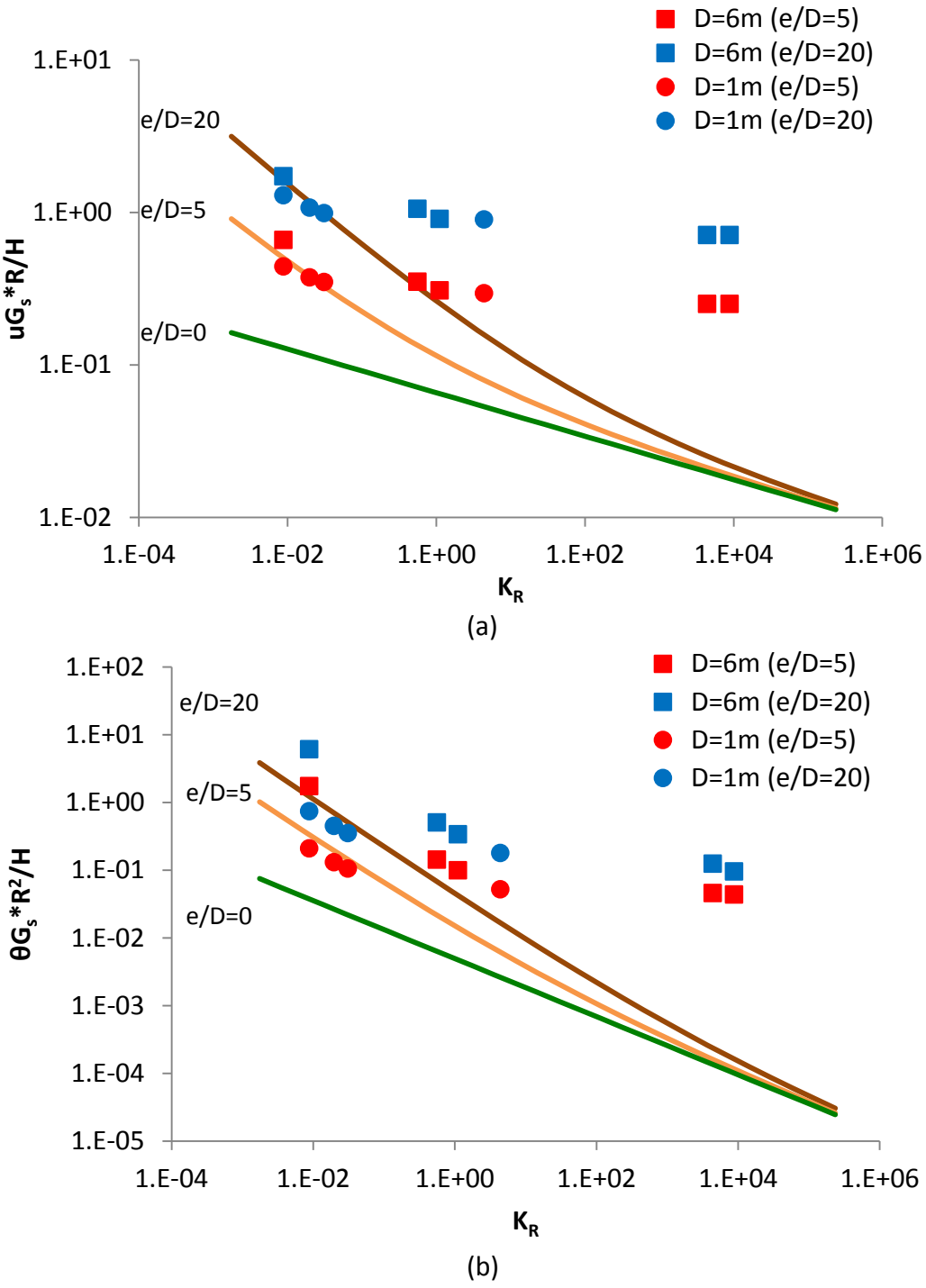

Figure 3.5 Variations in pile (a) displacement and (b) rotation influence factors with stiffness ratio in homogeneous soils for L/D=4

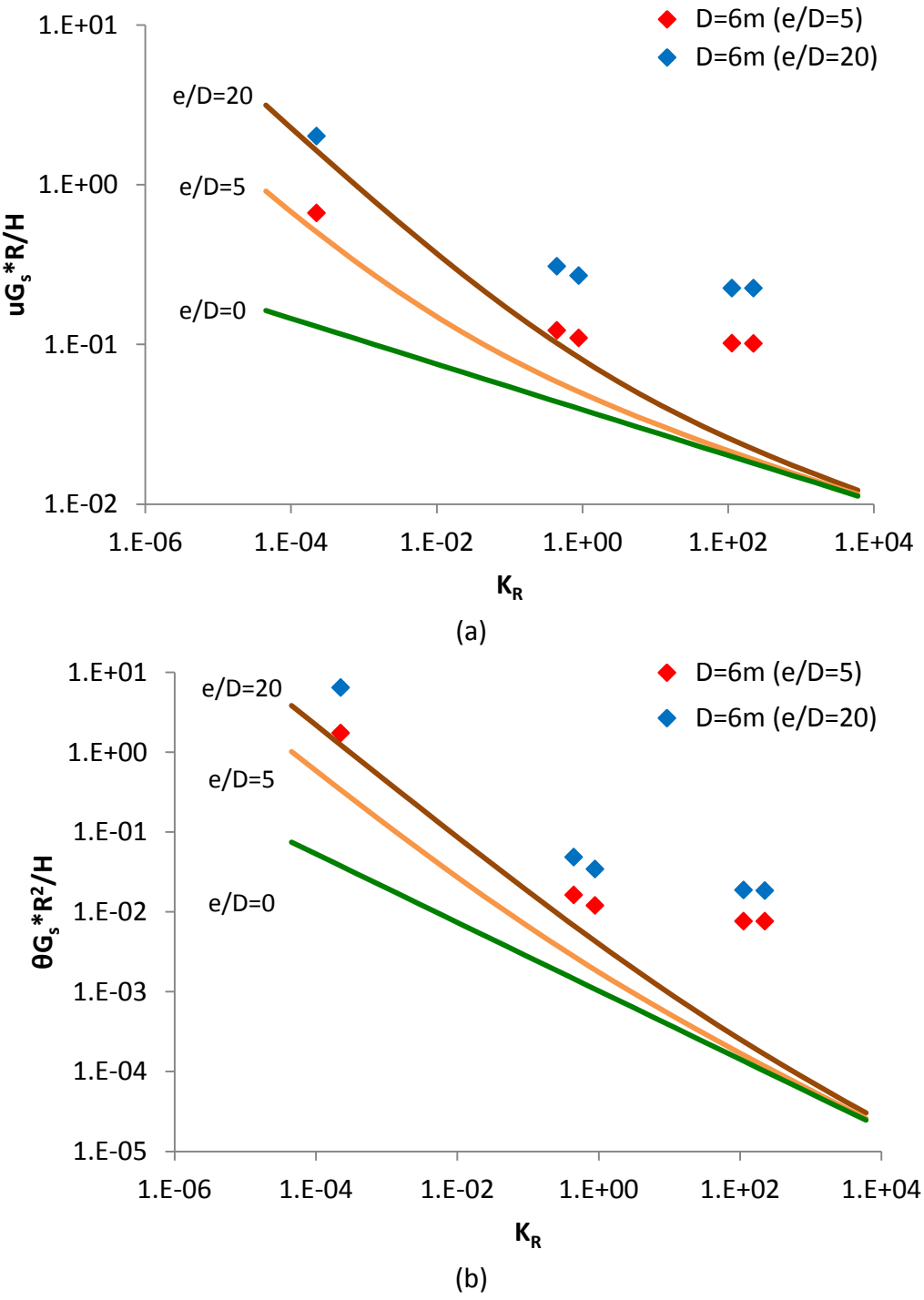

Figure 3.6 Variations in pile (a) displacement and (b) rotation influence factors with stiffness ratio in homogeneous soils for L/D=10

The ratio between Plaxis results and Randolph (1981)'s solution is presented in Figure 3.7. Large differences between both methods are observed for displacements and rotations influence factors for K_R>1, defined before as perfectly rigid pile region. Large differences are also observed for large-diameter piles with K_R<1. In both cases the Randolph (1981) solution is not applicable.

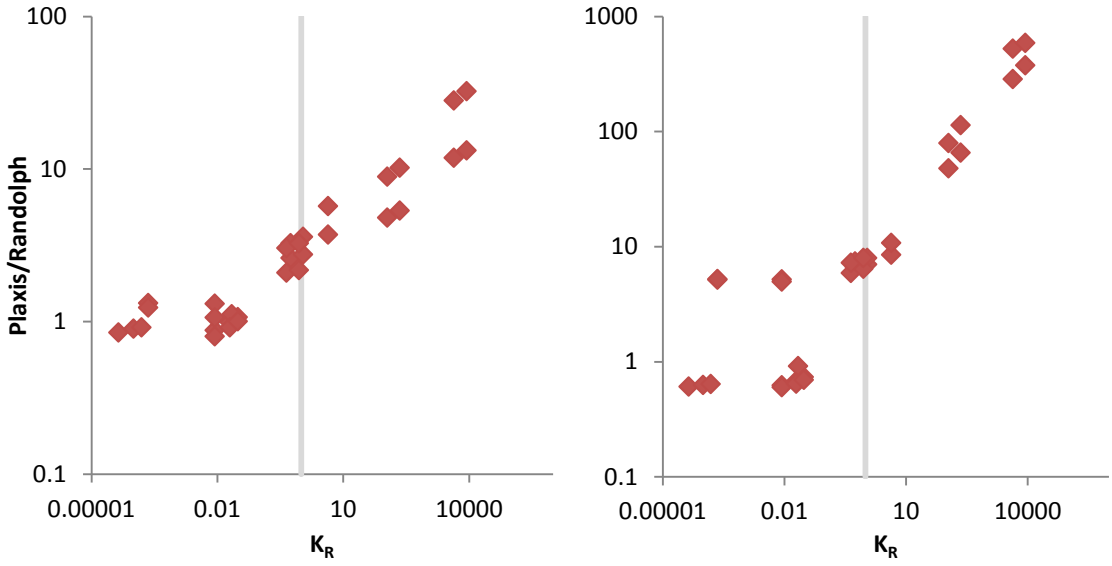

Figure 3.7 Comparison between Plaxis and Randolph (1981) for (a) displacement and (b) rotation influence factors

3.4.2. Stiffness Increasing with Depth

Even though is mathematically convenient and simple analysis can be done with a homogeneous stiffness distribution soil profile, in reality the increasing overburden pressure with depth causes deeper materials to have a higher stiffness than the material closer to the surface. Stiffness increasing with depth is a typical consideration for sands (Scott, 1981). This section will present the results of FEA studies and comparison to the solution presented by Randolph (1981) for linearly increasing stiffness with depth. Table 3.3 presents a summary of the analyses performed for linearly increasing stiffness with depth.

Figure 3.8 and Figure 3.9 presents the displacement and rotation influence factors, respectively, for small-diameter and large-diameter piles with L/D=4 compared to Randolph (1981). Good agreement in the influence factors is observed for K_R<1 for small-diameter piles. The large-diameter piles show an underestimation of the influence factor presented by Randolph (1981) for flexible behavior.

Figure 3.10 and Figure 3.11 show the displacement and rotation influence factors, respectively, for piles with small-diameters and large-diameters with L/D=10. Similar behavior to piles with L/D=4 are observed, but piles with L/D=10 behave more flexible than L/D=4. As the K_R increases, larger influence factors than the ones predicted by Randolph (1981) formulation are observed. Both pile diameters appear to have same influence factors for rigid behavior.

Table 3.3 Summary of analyses for linearly increasing stiffness with depth

ID	R (m)	L (m)	E_p (GPa)	G* (MPa)	e/D	H (kN)	u_{plaxis} (m)	θ_{plaxis} (degrees)	K_R	E_p/G*
eD5LD4D1m01	0.5	4	15	1.4E-02	5	1	3.3E-01	5.7E+00	2.2E+03	2.5E+07
eD5LD4D1m2	0.5	4	15	3.3E-01	5	100	9.0E-01	1.5E+01	4.4E+01	5.0E+05
eD5LD4D1E20	0.5	4	15	2.0E+01	5	500	3.1E-02	6.9E-01	2.9E-01	3.3E+03
eD5LD4D1m02	0.5	4	15	4.5E+01	5	500	1.5E-02	4.0E-01	1.1E-01	1.3E+03
eD20LD4D1m01	0.5	4	15	1.4E-02	20	100	9.0E+01	8.8E+01	2.2E+03	2.5E+07
eD20LD4D1m2	0.5	4	15	3.3E-01	20	100	2.5E+00	3.7E+01	4.4E+01	5.0E+05
eD20LD4D1E20	0.5	4	15	2.0E+01	20	500	8.6E-02	2.1E+00	2.9E-01	3.3E+03
eD20LD4D1m02	0.5	4	15	4.5E+01	20	100	8.6E-03	2.6E-01	1.1E-01	1.3E+03
eD5LD10D1m01	0.5	10	15	1.4E-02	5	1	6.8E-02	4.9E-01	5.6E+01	2.5E+07
eD5LD10D1m2	0.5	10	15	3.3E-01	5	100	1.6E-01	1.2E+00	1.1E+00	5.0E+05
eD5LD10D1E20	0.5	10	15	2.0E+01	5	500	1.9E-02	6.4E-01	7.3E-03	3.3E+03
eD20LD10D1m01	0.5	10	15	1.4E-02	20	1	1.4E-01	1.1E+00	5.6E+01	2.5E+07
eD20LD10D1E20	0.5	10	15	2.0E+01	20	500	5.1E-02	1.3E+00	7.3E-03	3.3E+03
eD20LD10D1m02	0.5	10	15	4.5E+01	20	100	6.8E-03	2.2E-01	2.8E-03	1.3E+03
eD0LD4D6m01	3	24	551	1.1E-01	0	1	4.3E-03	1.2E-02	1.3E+04	1.5E+08
eD0LD4D6E20	3	24	551	1.7E+02	0	100	7.8E-05	2.7E-04	1.7E+00	2.0E+04
eD0LD4D6m02	3	24	551	3.7E+02	0	500	2.0E-04	7.5E-04	6.6E-01	7.5E+03
eD5LD4D6m01	3	24	551	1.1E-01	5	1	9.4E-03	2.8E-02	1.3E+04	1.5E+08
eD5LD4D6E20	3	24	551	1.7E+02	5	500	1.1E-03	7.0E-03	1.7E+00	2.0E+04
eD5LD4D6m02	3	24	551	3.7E+02	5	100	1.4E-04	1.1E-03	6.6E-01	7.5E+03
eD20LD4D6m01	3	24	551	1.1E-01	20	1	2.6E-02	8.0E-02	1.3E+04	1.5E+08
eD20LD4D6E20	3	24	551	1.7E+02	20	500	3.4E-03	2.4E-02	1.7E+00	2.0E+04
eD20LD4D6m02	3	24	551	3.7E+02	20	100	4.1E-04	3.8E-03	6.6E-01	7.5E+03
eD20LD4D6E20	3	24	551	4.9E+04	20	100	7.0E-04	4.9E-03	1.7E-03	2.0E+01
eD0LD10D6m01	3	60	551	1.1E-01	0	1	1.1E-03	1.3E-03	3.4E+02	1.5E+08
eD0LD10D6E20	3	60	551	1.7E+02	0	100	7.7E-05	2.7E-04	4.4E-02	2.0E+04
eD0LD10D6m02	3	60	551	3.7E+02	0	500	2.0E-04	7.8E-04	1.7E-02	7.5E+03
eD5LD10D6m01	3	60	551	1.1E-01	5	10	1.8E-02	2.1E-02	3.4E+02	1.5E+08
eD5LD10D6E20	3	60	551	1.7E+02	5	500	1.1E-03	6.8E-03	4.4E-02	2.0E+04
eD5LD10D6m02	3	60	551	3.7E+02	5	100	1.3E-04	1.1E-03	1.7E-02	7.5E+03
eD20LD10D6m01	3	60	551	1.1E-01	20	100	3.7E-01	4.8E-01	3.4E+02	1.5E+08
eD20LD10D6E20	3	60	551	1.7E+02	20	500	3.3E-03	2.3E-02	4.4E-02	2.0E+04
eD20LD10D6m02	3	60	551	3.7E+02	20	100	4.1E-04	3.8E-03	1.7E-02	7.5E+03

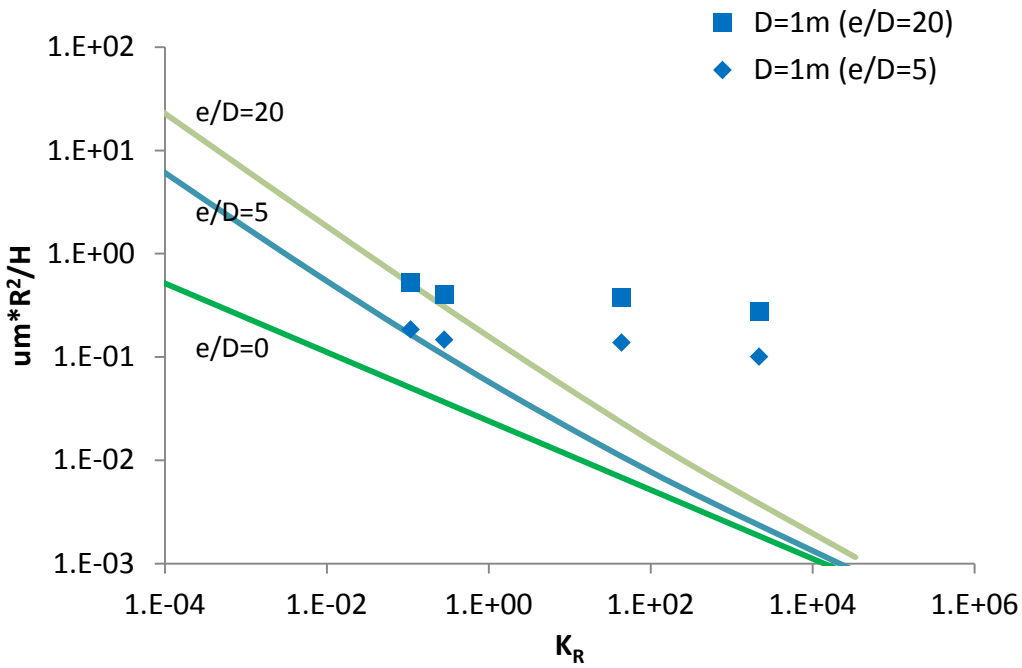

(a)

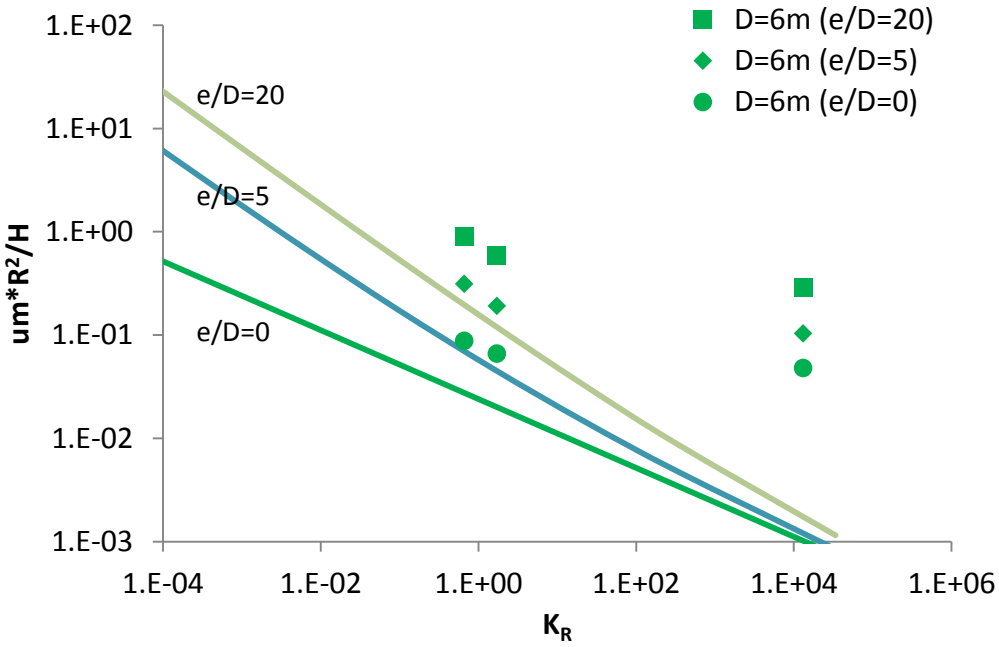

(b)

Figure 3.8 Displacement influence factors for piles with (a) D=1 m and (b) D=6 m, and L/D=4

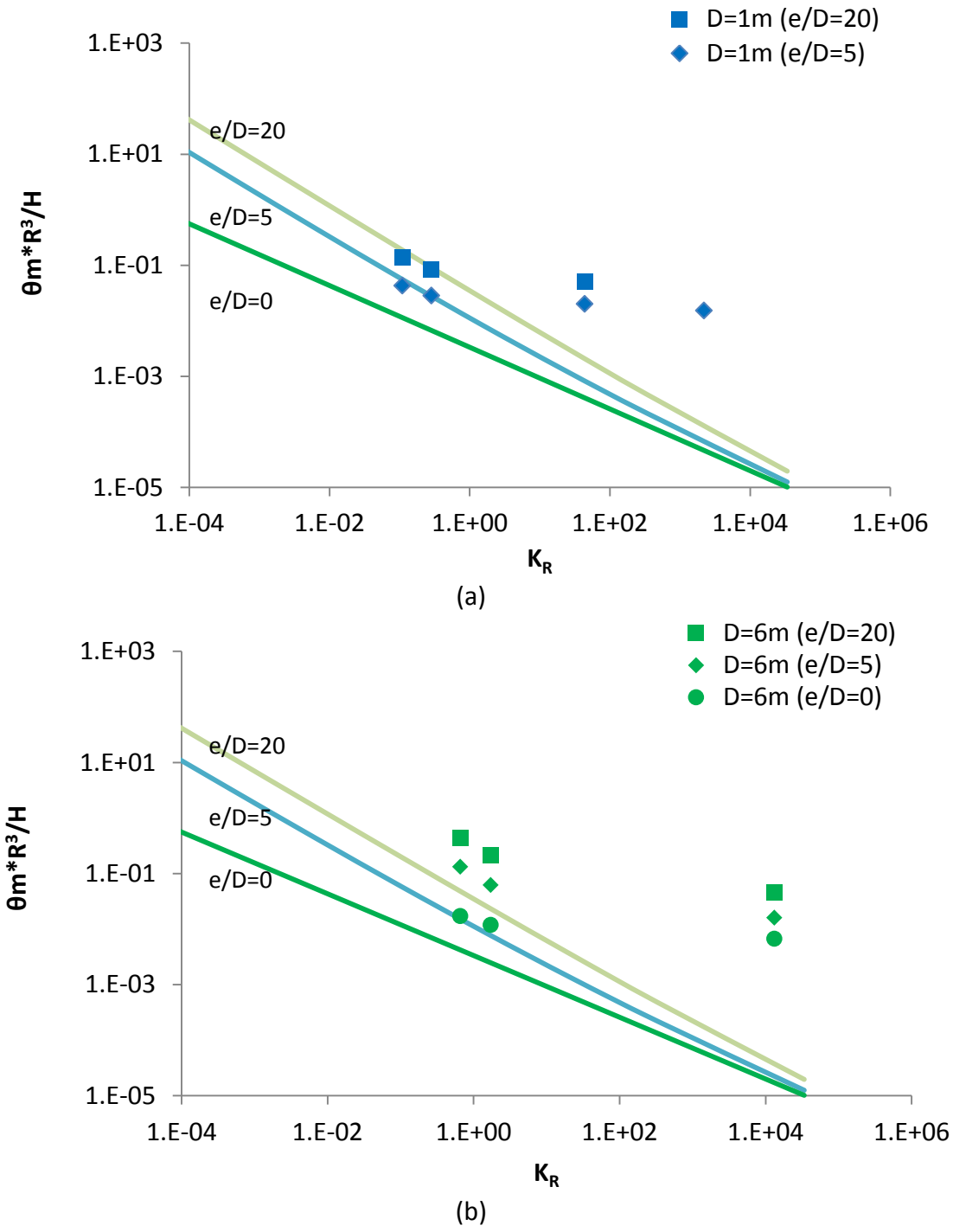

Figure 3.9 Rotation influence factors for piles with (a) D=1 m and (b) D=6 m, and L/D=4

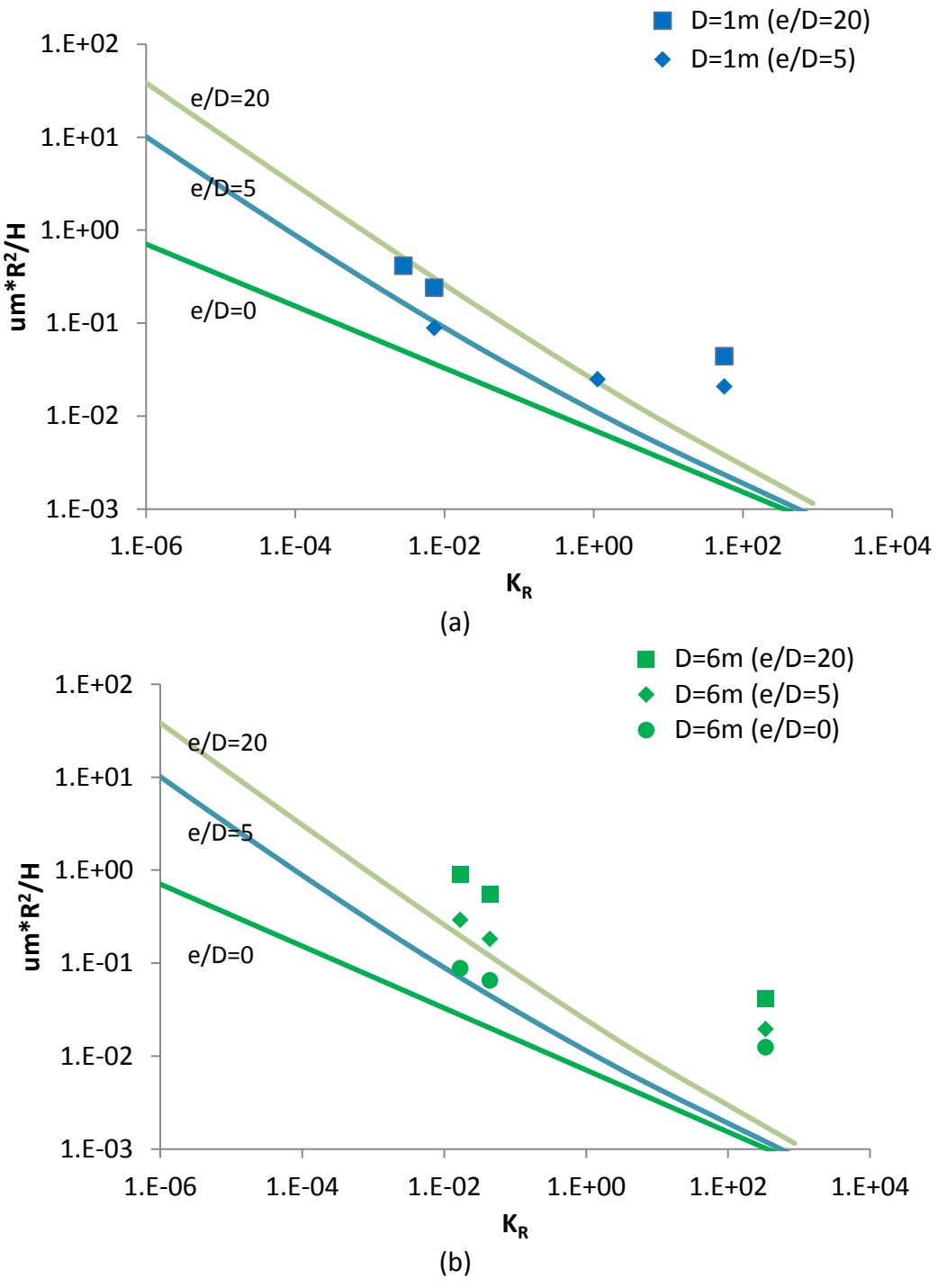

Figure 3.10 Displacement influence factors for piles with (a) D=1 m and (b) D=6 m, and L/D=10

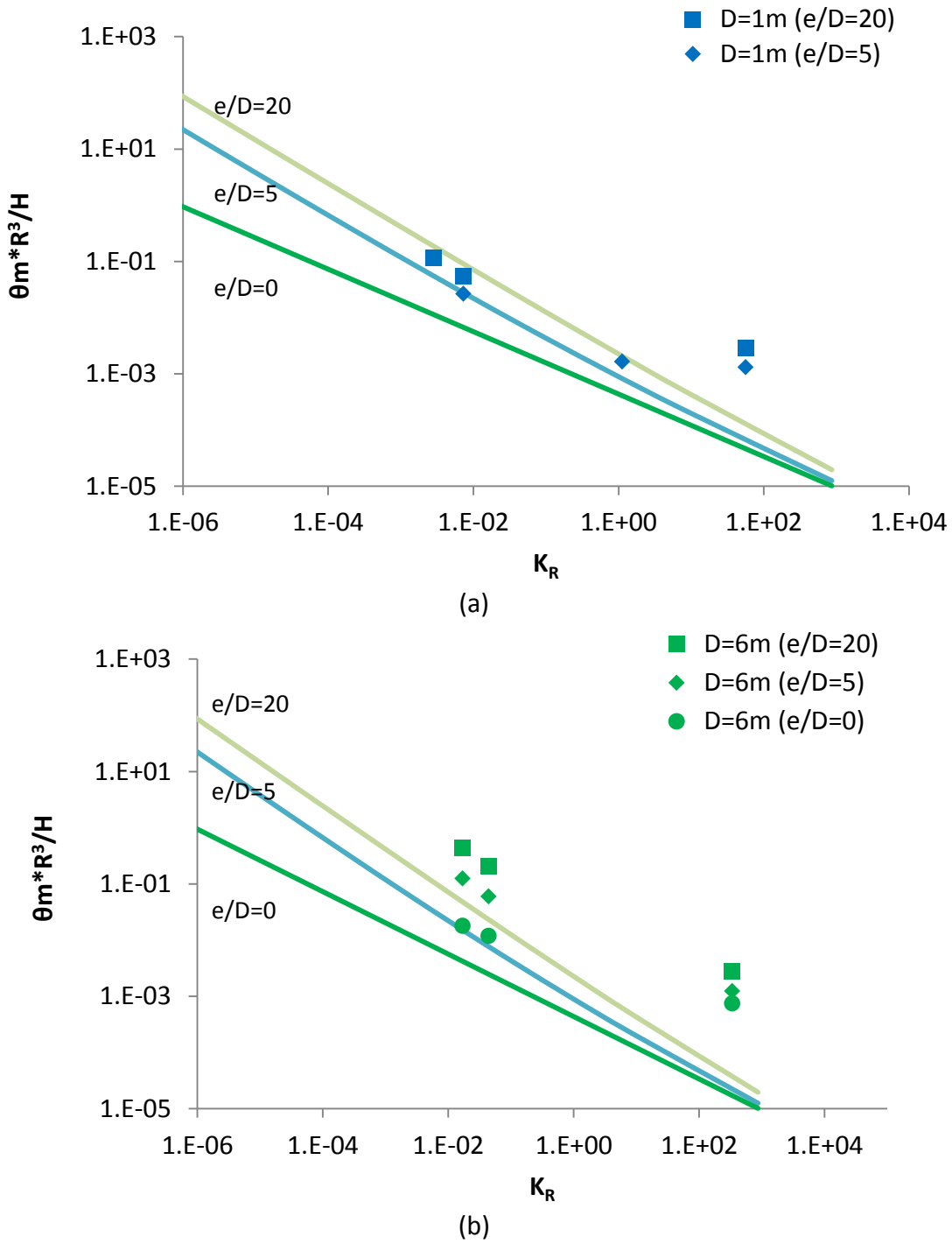

Figure 3.11 Rotation influence factors for piles with (a) D=1 m and (b) D=6 m, and L/D=10

The ratio between Plaxis results and the solution presented by Randolph (1981) is presented in Figure 3.12. Large differences between both methods are observed for displacements influence factors for K_R>1, defined before as perfectly rigid pile region, and for large-diameter piles. Considerable scatter is also observed for rotational influence factors in all K_R values.

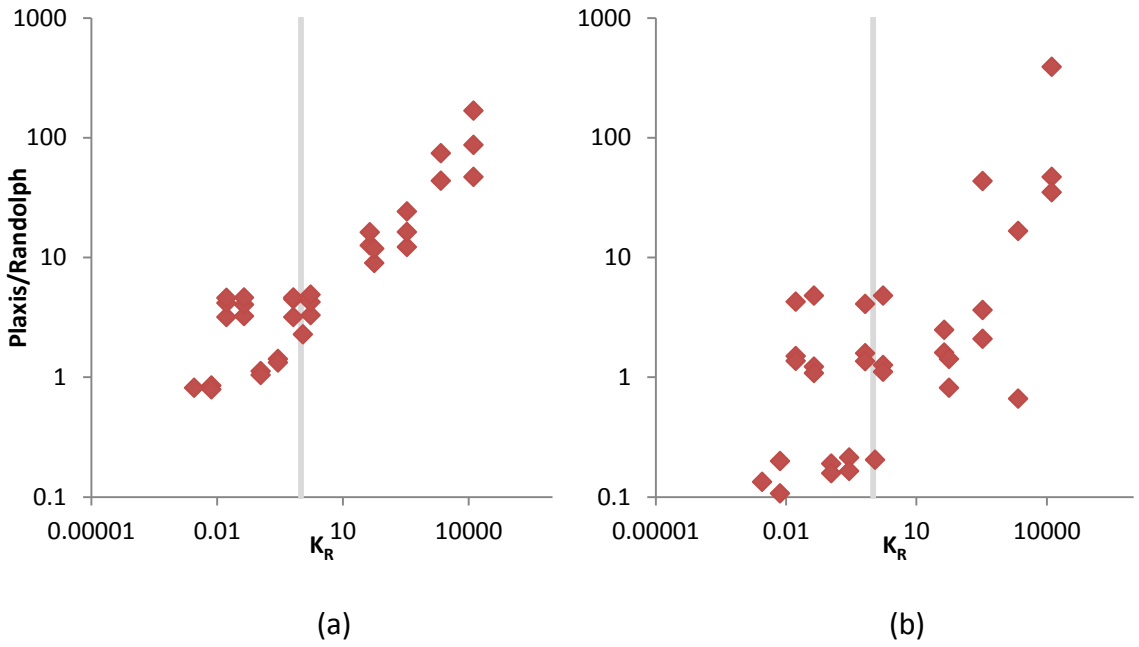

Figure 3.12 Comparison between Plaxis and Randolph (1981) for (a) displacement and (b) rotation influence factors

3.5. Development of Functional Form for Design Equations

In Section 3.4 the analysis of laterally loaded piles was presented. It was observed that pile to soil stiffness controls the behavior of flexible piles, and large-diameters also have an effect in the behavior, increasing influence factors. Rigid pile behavior is controlled by L/D ratio, no change in influence factors was observed for changes in pile to soil stiffness ratio. A new set of influence factors that consider L/D effects is proposed for rigid piles. Also diameter effects are added to influence factors presented by Randolph (1981). Development of a functional form for design equations to calculate displacement and rotations due to horizontal and moment loading is a three step process.

1. Develop a design equation for displacement as a function of pure horizontal loading.
2. Develop a design equation for displacement as a function of pure moment loading.
3. Develop a design equation for rotation as a function of pure moment.

Equation 3.1 presented by Randolph (1981), same as Equation 2.4, use radius instead of diameter, then for the proposed influence factors we will also use radius.

$$\frac{u}{R} = I_{uH}\frac{H}{G^*R^2} + I_{uM}\frac{M}{G^*R^3} \qquad \text{Equation 3.1a}$$

$$\theta = I_{\theta H}\frac{H}{G^*R^2} + I_{\theta M}\frac{M}{G^*R^3} \qquad \text{Equation 3.1b}$$

Influence factors for the homogeneous stiffness with depth soil profile were developed in the format:

$$I_{xx} = max\left(a\left(\frac{E_p}{G^*}\right)^{-n}\left(\frac{R}{R_{ref}}\right)^{m}, b\left(\frac{L}{R}\right)^{-n*}\right) \quad \text{Equation 3.2}$$

where a, n, m, b, and n* are fitting coefficients; E_p/G^* is the pile to soil stiffness ratio; R is the radius of the pile; R_{ref} is the reference radius; and L is the pile embedment length. Influence factors for the linearly increasing stiffness with depth soil profile were developed in the similar way using:

$$I_{xx} = max\left(a\left(\frac{E_p}{G_m^*}\right)^{-n}\left(\frac{R}{R_{ref}}\right)^{m}, b\left(\frac{L}{R}\right)^{-n*}\right) \quad \text{Equation 3.3}$$

where $G_m^* = m^* R$, and m* is the increasing shear modulus with depth.

For the displacement influence factor it was observed that the influence factor for pure horizontal loading (I_{uH}) has a minor contribution to horizontal displacement once there is a moment applied. Then the influence factor for displacement due to moment (I_{uM}) is the major contributor in the determination of the displacement influence factor. Similarly, the influence factor for rotation due to pure moment loading ($I_{\theta M}$) is the major contributor in the rotation prediction.

3.5.1. Homogeneous Stiffness with Depth

Influence factors for homogeneous stiffness with depth were developed using Equation 3.2. The results obtained are presented in Table 3.4 for flexible and rigid pile behavior. Plaxis 3D Foundation results, previously compared to Randolph (1981), are compared to the proposed model in Figure 3.13 to Figure 3.16.

Table 3.4 Influence factors for homogeneous stiffness with depth

Pile behavior	Horizontal I_{uH}	Rocking $I_{\theta M}$	Coupled $I_{uM}=I_{\theta H}$
Flexible	$0.25\left(\frac{E_p}{G^*}\right)^{-1/7}\left(\frac{R}{R_{ref}}\right)^{0.33}$	$0.8\left(\frac{E_p}{G^*}\right)^{-5/7}\left(\frac{R}{R_{ref}}\right)^{1}$	$0.27\left(\frac{E_p}{G^*}\right)^{-3/7}\left(\frac{R}{R_{ref}}\right)^{0}$
Rigid	$0.48\left(\frac{L}{R}\right)^{-2/3}$	$1.1\left(\frac{L}{R}\right)^{-2.8}$	$0.12\left(\frac{L}{R}\right)^{-1}$

Where R_{ref}=0.38 m (30 inches, typical diameter for current piles).

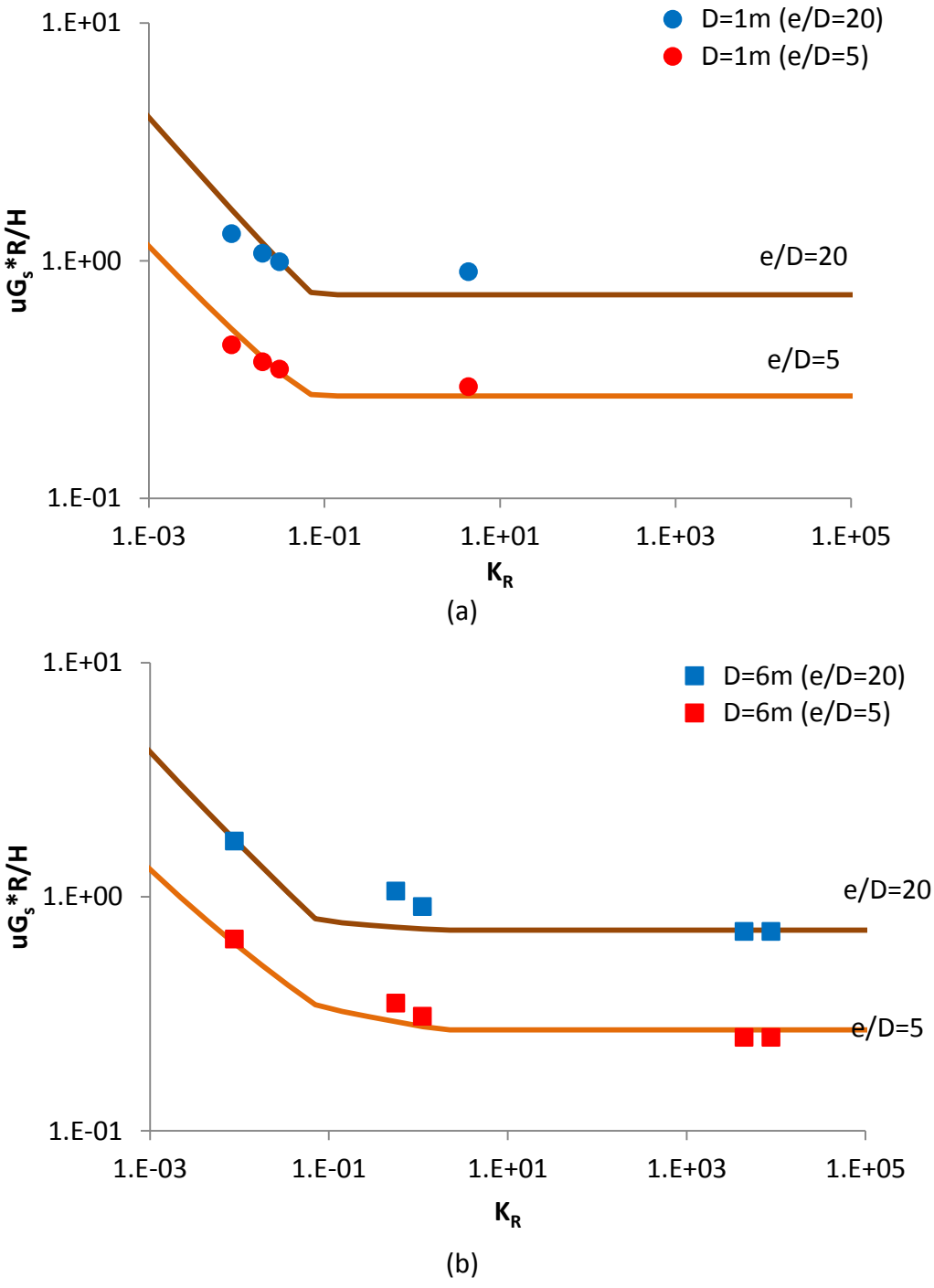

Figure 3.13 Displacement influence factors for piles with (a) D=1 m and (b) D=6 m, and L/D=4

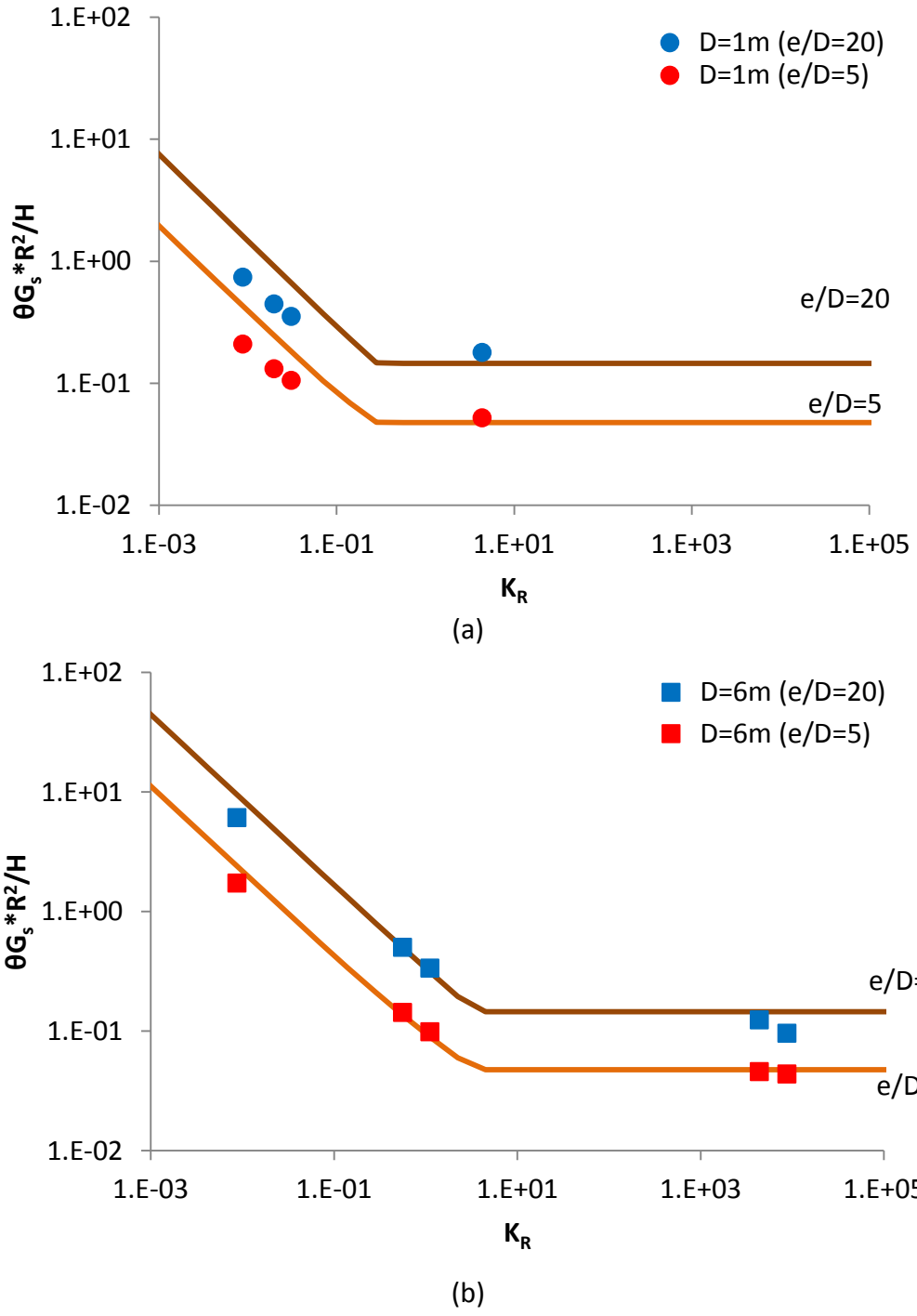

Figure 3.14 Rotational influence factors for piles with (a) D=1 m and (b) D=6 m, and L/D=4

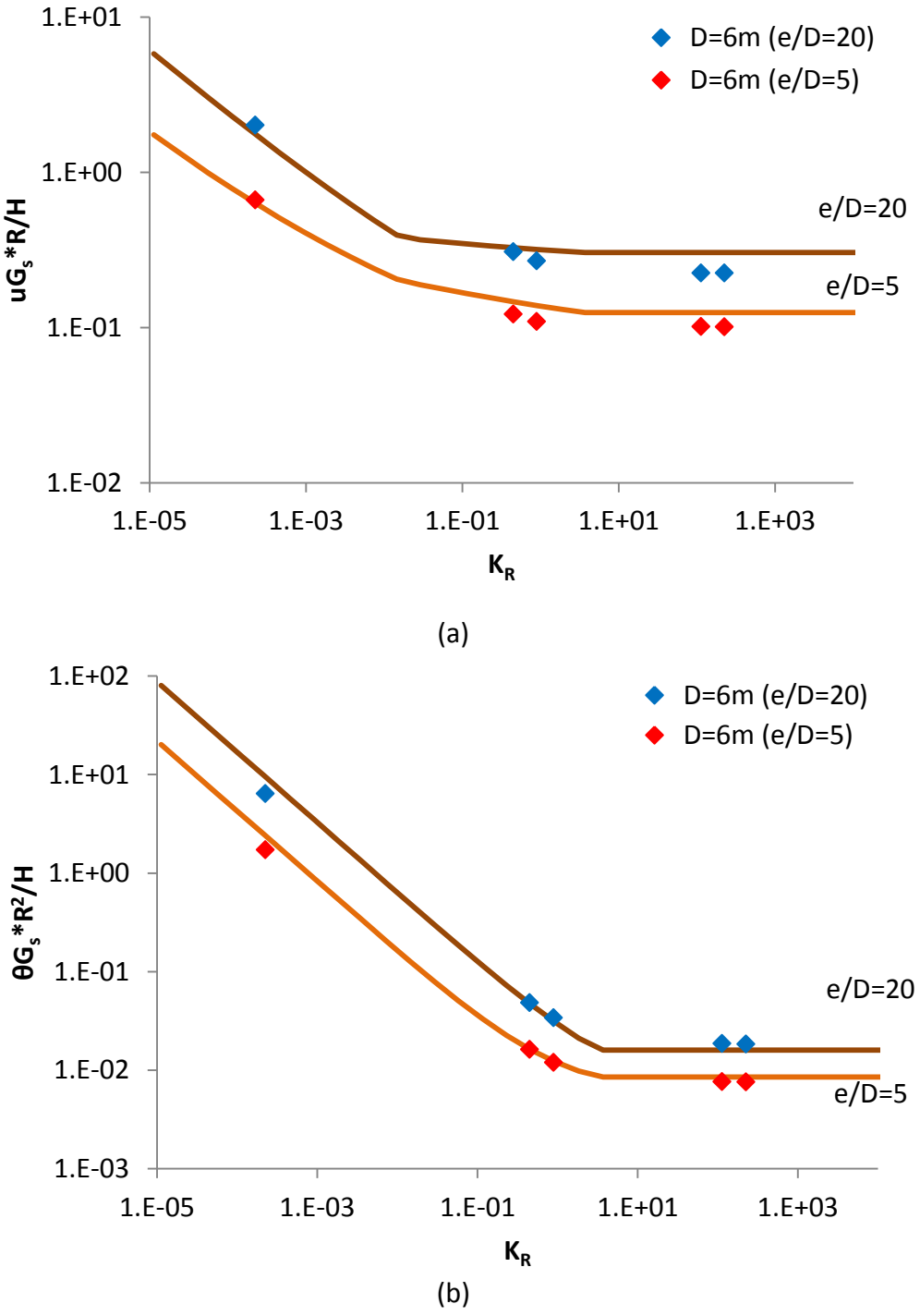

Figure 3.15 Influence factors for (a) displacement and (b) rotation of piles with L/D=10

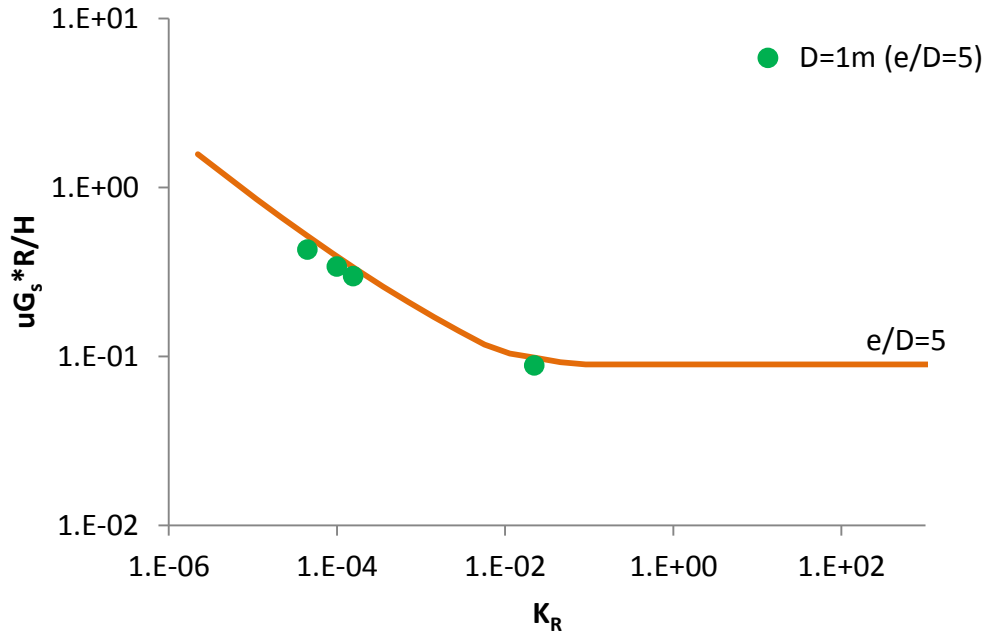

(a)

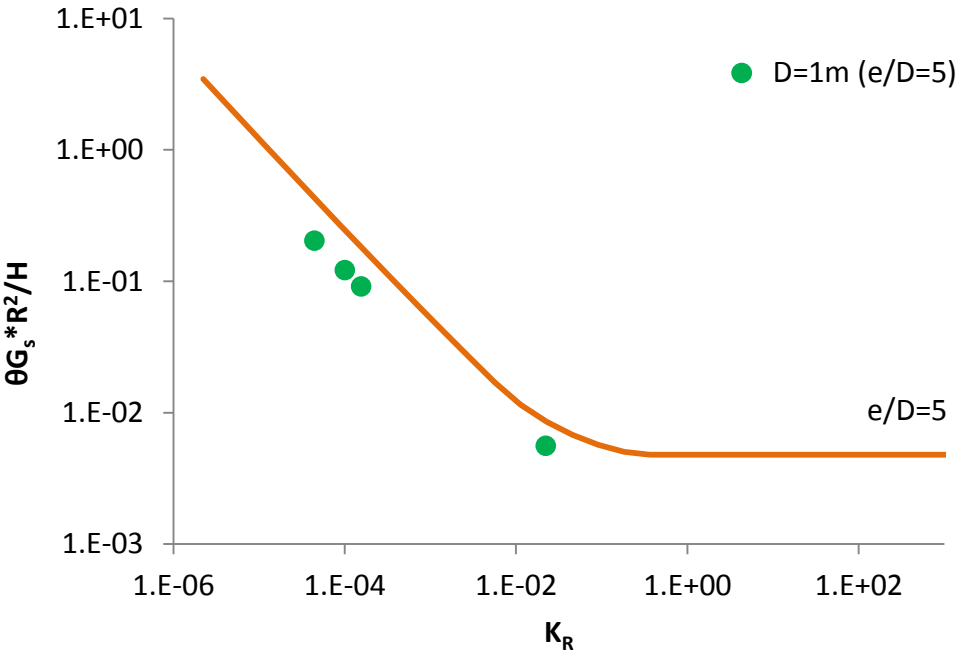

(b)

Figure 3.16 Influence factors for (a) displacement and (b) rotation of piles with L/D=15

The ratio between Plaxis results and the two models prediction, Randolph (1981) and the proposed model, are presented in Figure 3.17. The proposed model is capable of predicting displacements and rotations influence factors for a wide range of pile flexibility factors with low coefficients of variation. The coefficient of variation of Plaxis to the proposed model ratio is 0.17 for displacement influence factor and 0.31 for rotational influence factor, showing low variations.

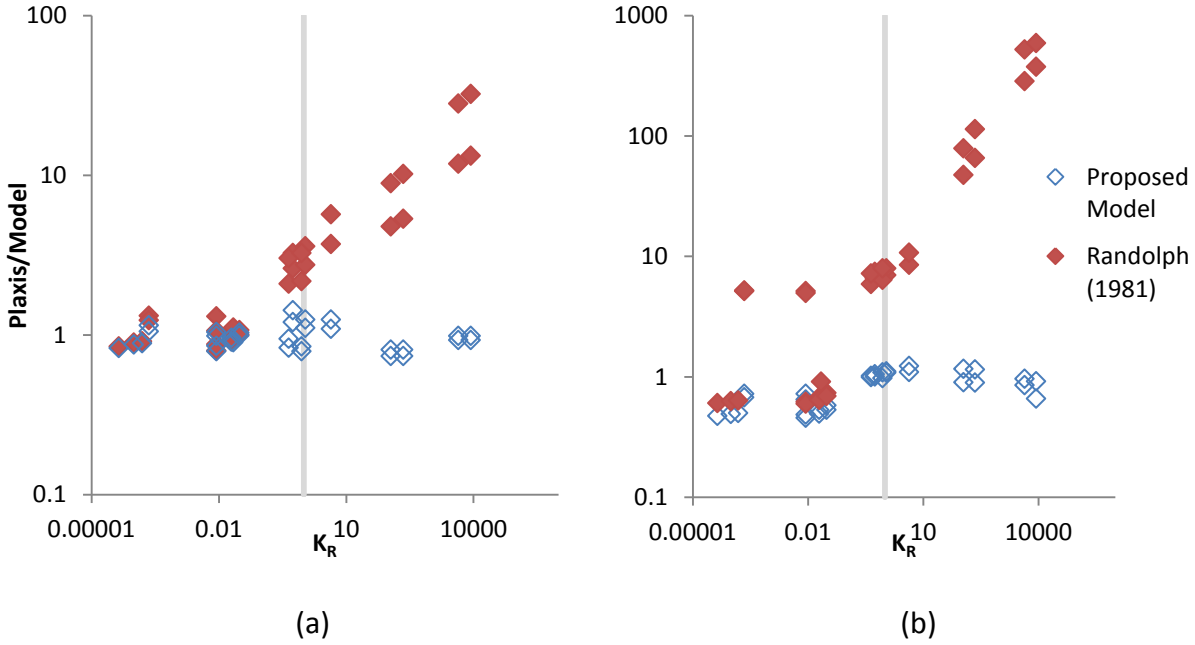

Figure 3.17 Comparison between the two models and Randolph (1981) for (a) displacement and (b) rotation influence factors

3.5.2. Stiffness Increasing with Depth

Influence factors for linearly increasing stiffness with depth were developed using Equation 3.3. The results obtained are presented in Table 3.5 for flexible and rigid pile behavior. Plaxis 3D Foundation results, previously compared to Randolph (1981), are compared to the proposed model in Figure 3.18 to Figure 3.21.

Table 3.5 Influence factors for linearly increasing stiffness with depth

Pile behavior	Horizontal I_{uH}	Rocking $I_{\theta M}$	Coupled $I_{uM}=I_{\theta H}$
Flexible	$0.54\left(\frac{E_p}{G_m^*}\right)^{-3/9}\left(\frac{R}{R_{ref}}\right)^{0.33}$	$1.13\left(\frac{E_p}{G_m^*}\right)^{-7/9}\left(\frac{R}{R_{ref}}\right)^{1}$	$0.6\left(\frac{E_p}{G_m^*}\right)^{-5/9}\left(\frac{R}{R_{ref}}\right)^{0.8}$
Rigid	$0.10\left(\frac{L}{R}\right)^{-0.5}$	$0.15\left(\frac{L}{R}\right)^{-2.5}$	$0.38\left(\frac{L}{R}\right)^{-2}$

Where R_{ref}=0.38 m (30 inches, typical diameter for current piles).

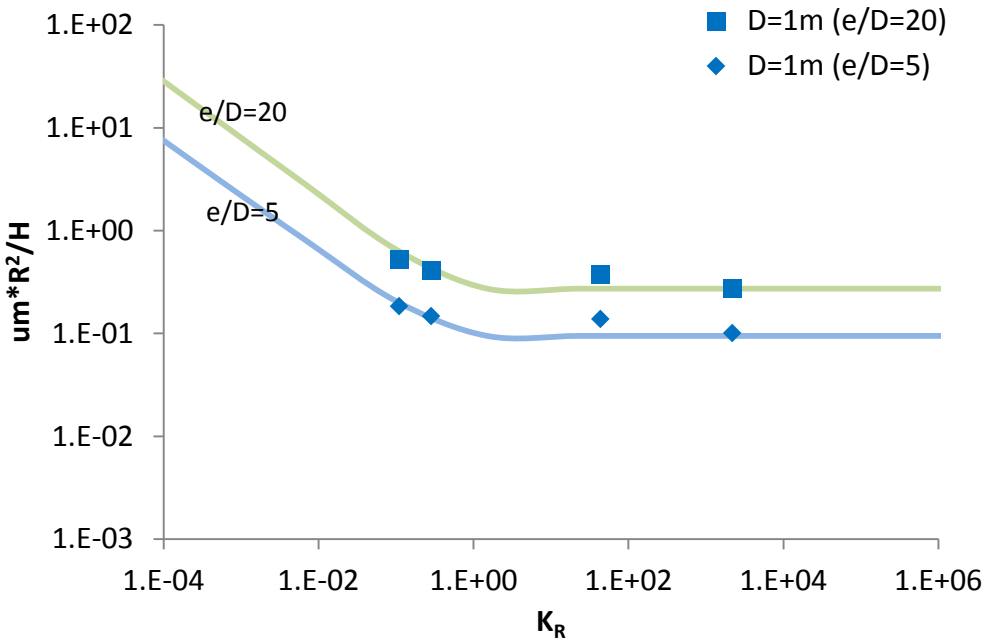

(a)

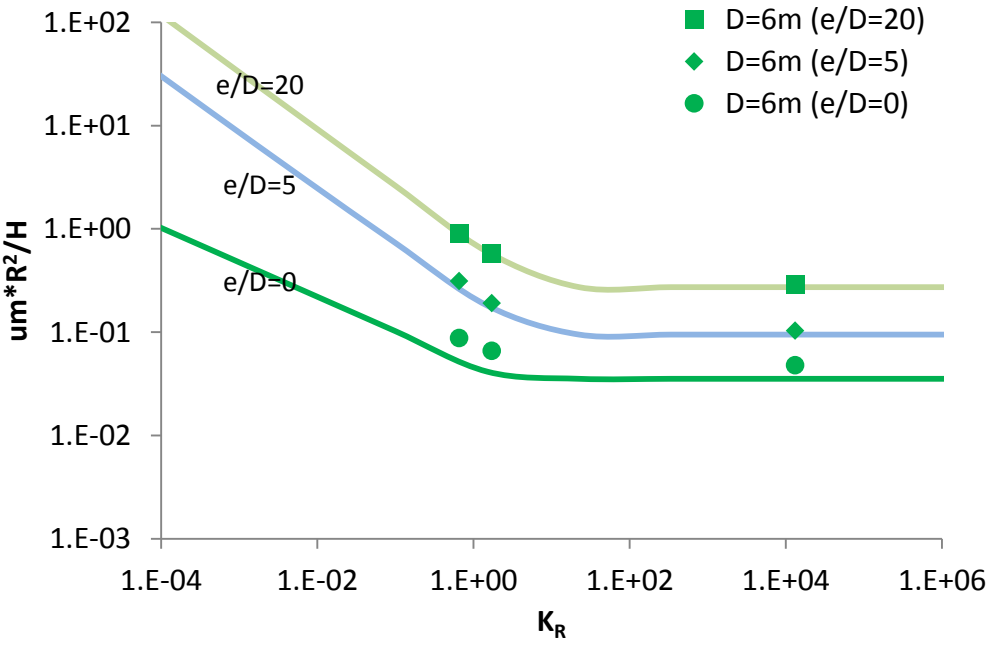

(b)

Figure 3.18 Displacement influence factors for piles with (a) D=1 m and (b) D=6 m, and L/D=4

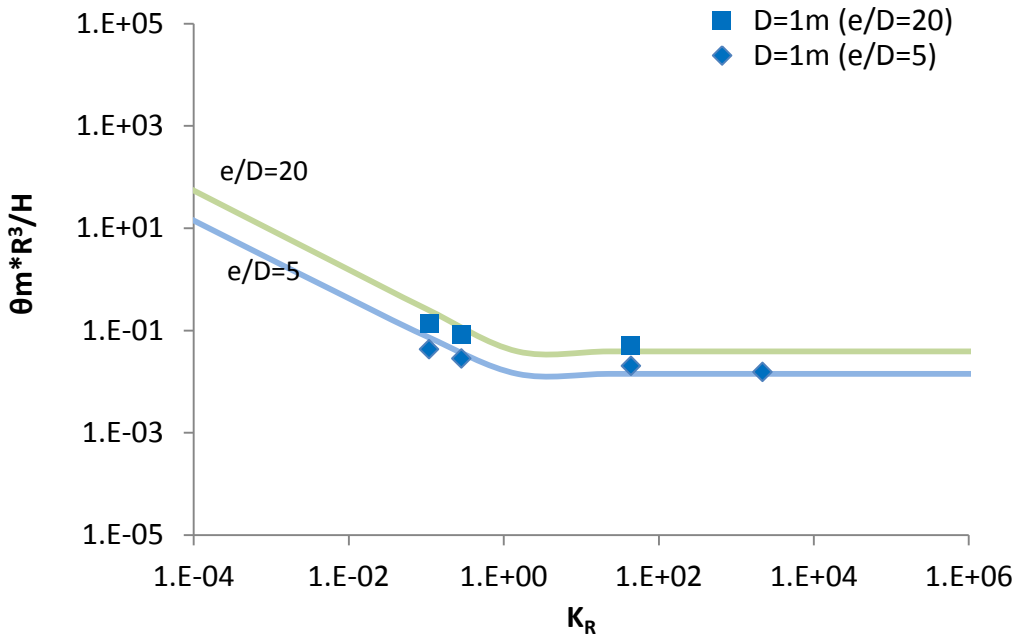

(a)

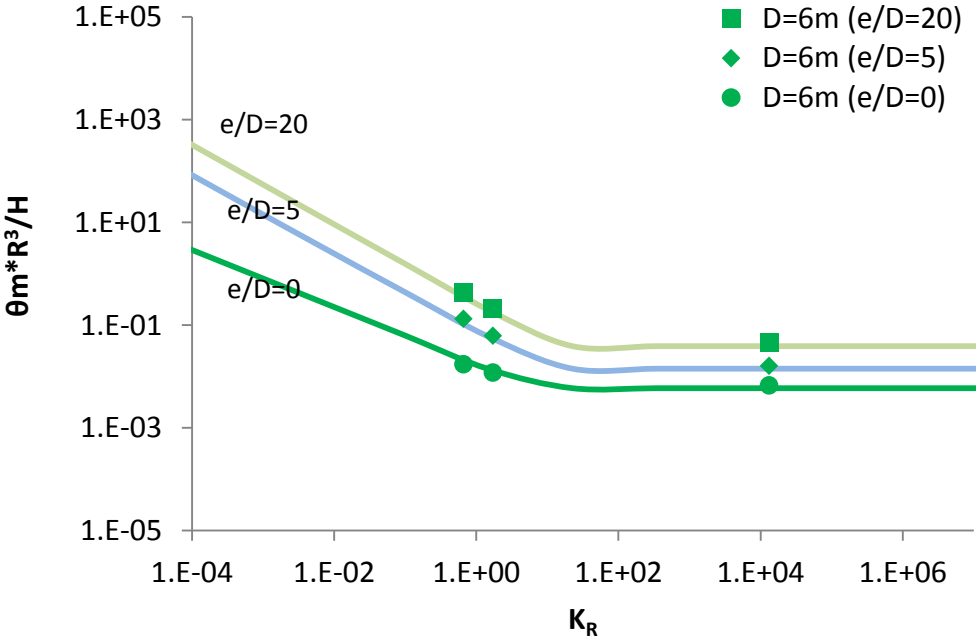

(b)

Figure 3.19 Rotational influence factors for piles with (a) D=1 m and (b) D=6 m, and L/D=4

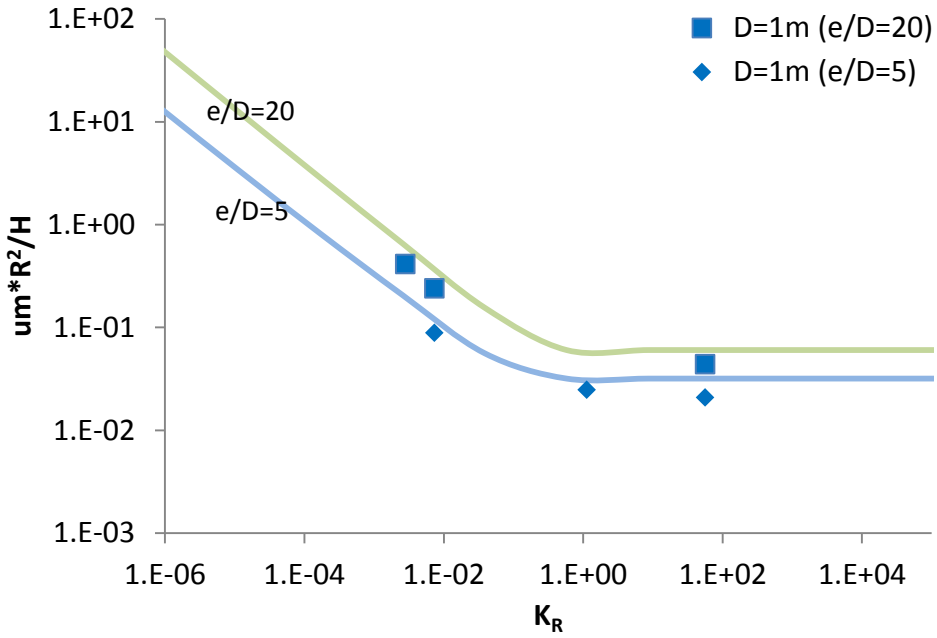

(a)

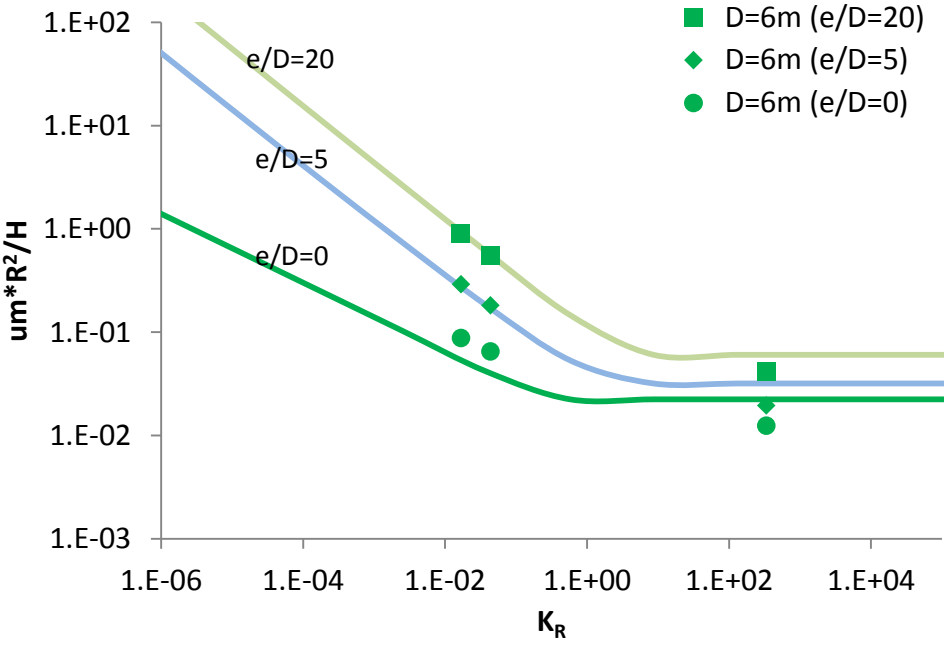

(b)

Figure 3.20 Displacement influence factors for piles with (a) D=1 m and (b) D=6 m, and L/D=10

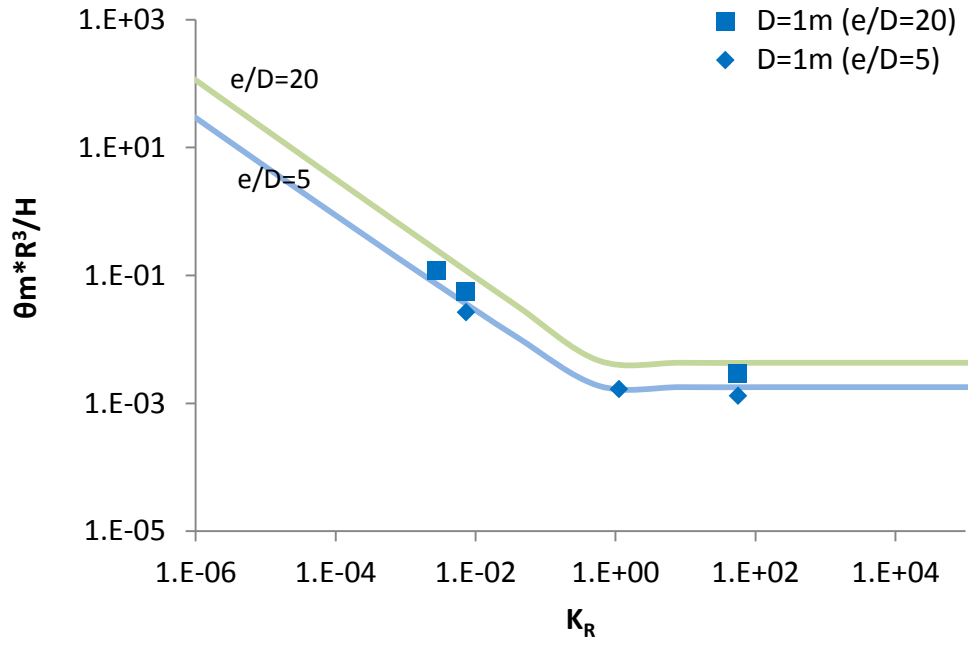

(a)

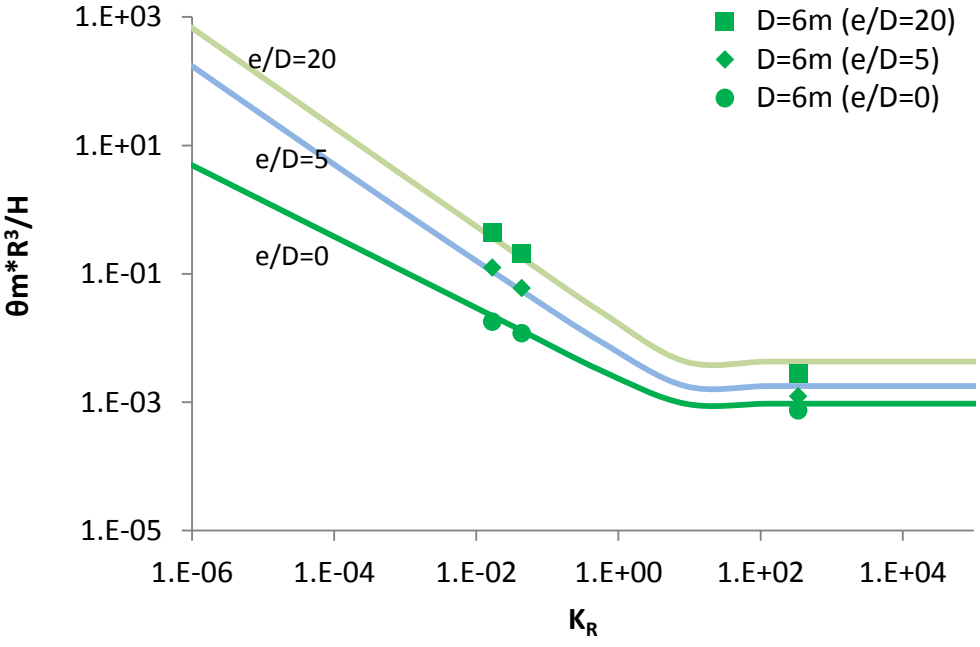

(b)

Figure 3.21 Rotational influence factors for piles with (a) D=1 m and (b) D=6 m, and L/D=10

The ratio between Plaxis results and the two models prediction, Randolph (1981) and the proposed model, are presented in Figure 3.22. The proposed model is capable of predicting displacements influence factors for a wide range of pile flexibility factors. The coefficient of variation of Plaxis to the proposed model ratio is 0.31 for displacement influence factor. A high coefficient of variation for the rotations of stiffness linearly increasing with depth of 0.79 was calculated, which may support the use of finite element analysis for monopile design, rather than attempting to use simplified design equations.

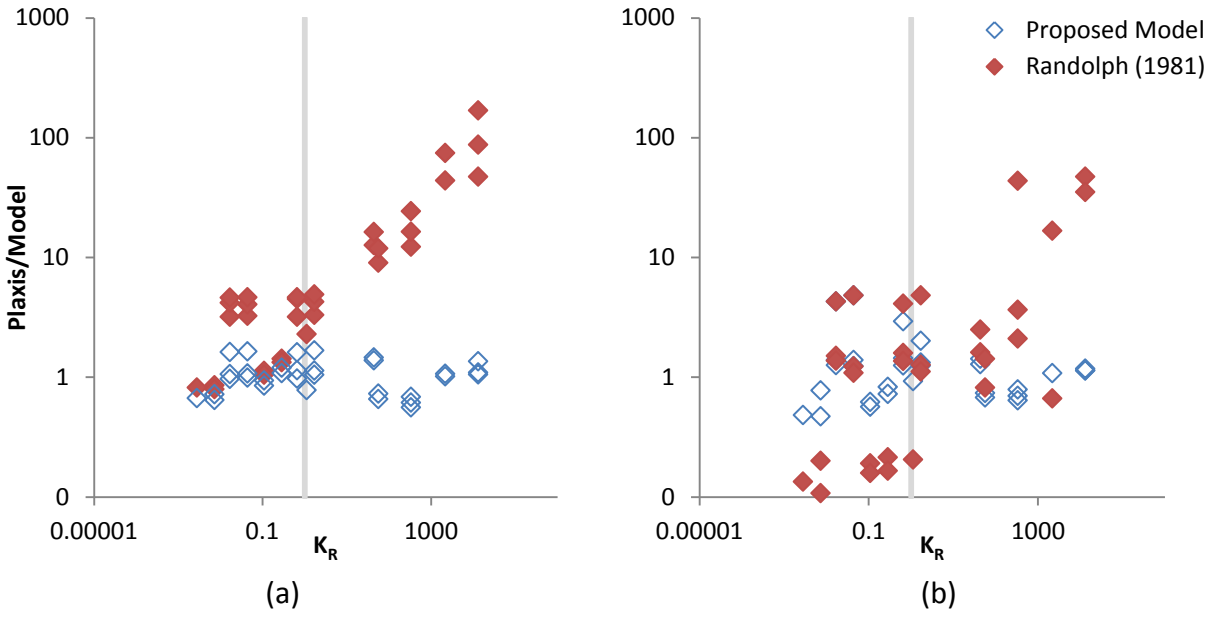

Figure 3.22 Comparison between the two models and Randolph (1981) for (a) displacement and (b) rotation influence factors

3.6. Discussion

Influence factors have been developed here based on finite element analysis studies. The influence factors are presented here to facilitate the calculation of lateral displacement and rotations at the mudline for flexible and rigid piles. These influence factors consider soil properties and pile geometries, allowing for a wide range of application.

Previous studies (e.g., Poulos, 1971) simplify the analysis by using the subgrade reaction coefficient equal to the soil Young's modulus, also not considering horizontal shear stresses developed between the soil and the sides of the pile. The uniform stress distribution simplification is acceptable for flexible piles, but in large-diameter piles this stresses are significant (Gerolymos & Gazetas, 2006). Displacement and rotation underestimation might be due to soil shearing in the circumference of the pile.

Figure 3.23 show the proposed displacement and rotation influence factors for homogeneous stiffness with depth with variations in pile flexibility factors (K_R). Small-diameter (D=1 m) and large-diameter (D=6 m) piles are graph for L/D ratios of 4 and 10, and e/D=20. As mentioned before, no diameter effects were observed for displacement influence factors for moment loading, since this is the major contributor for the displacement influence factor, no diameter effect is observed in Figure 3.23(a). If we plot displacement and rotation influence factors using pile to soil stiffness ratio defined as E_p/G_s, as in Randolph (1981), diameter and length to diameter ratio effects are easier to identify. Figure 3.24 show influence factors with variations in E_p/G_s.

Figure 3.25 show the proposed displacement and rotation influence factors for linearly increasing stiffness with depth, using same pile geometries as Figure 3.23. Diameter effects are significant in both influence factors, probably due to low stiffness at the surface. Figure 3.26 show influence factors with variations in E_p/G_s.

From this analysis we learned that as long as the flexible pile behavior assumption is maintained, the Randolph (1981) formulation works. When the L/D is decreased, we can see how the displacements and rotations are being underestimated; this underestimation is increased when the moment at the mudline is increased.

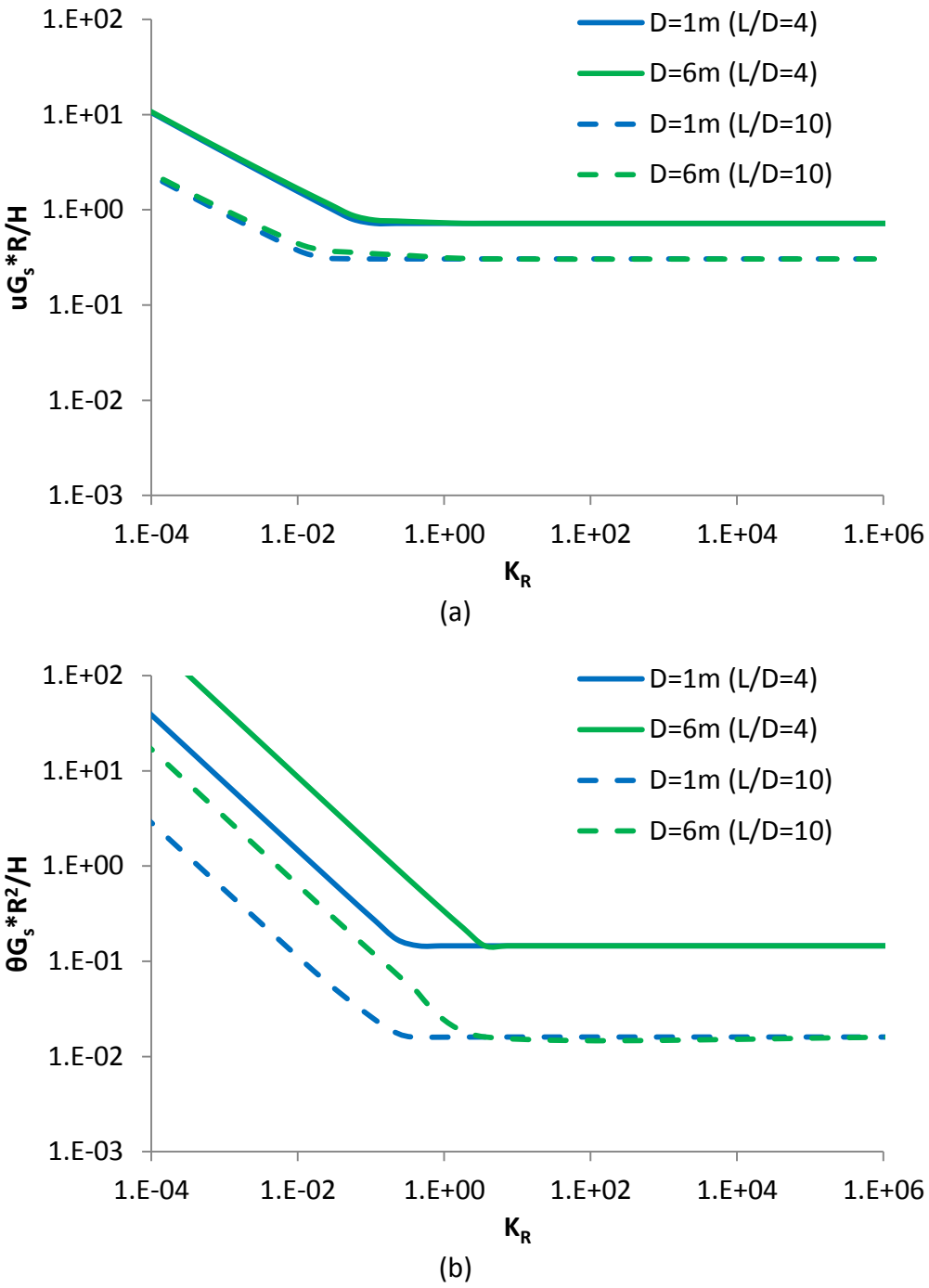

Figure 3.23 Proposed influence factors comparison for (a) displacements and (b) rotations for soils with homogeneous stiffness distribution with depth

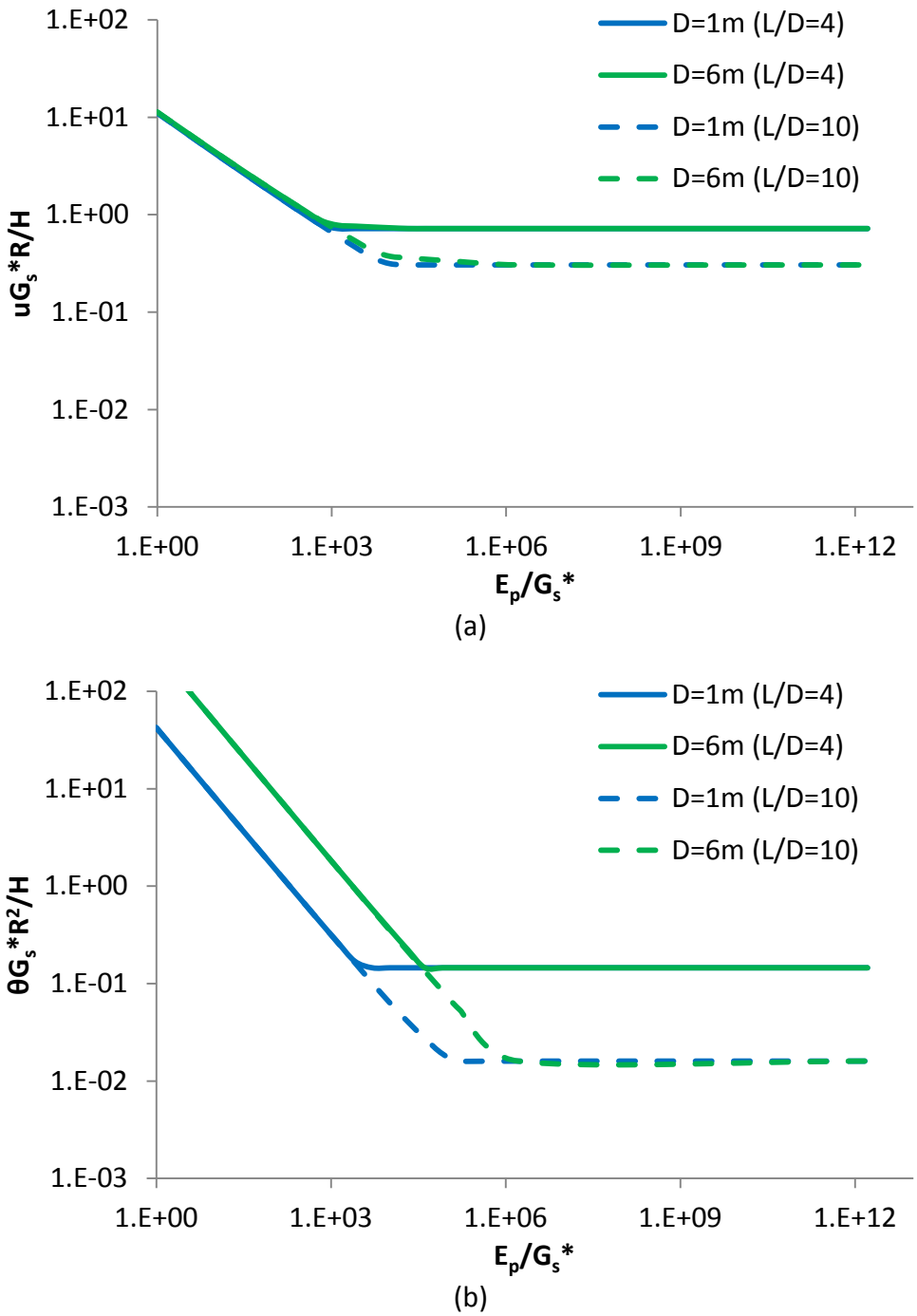

Figure 3.24 Proposed influence factors comparison for (a) displacements and (b) rotations for soils with homogeneous stiffness distribution with depth

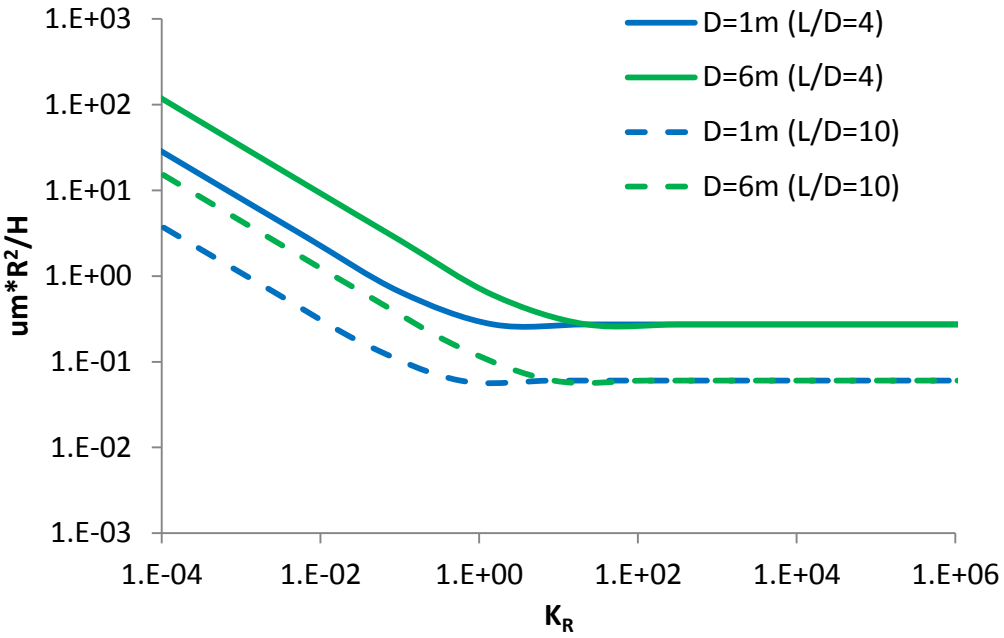

(a)

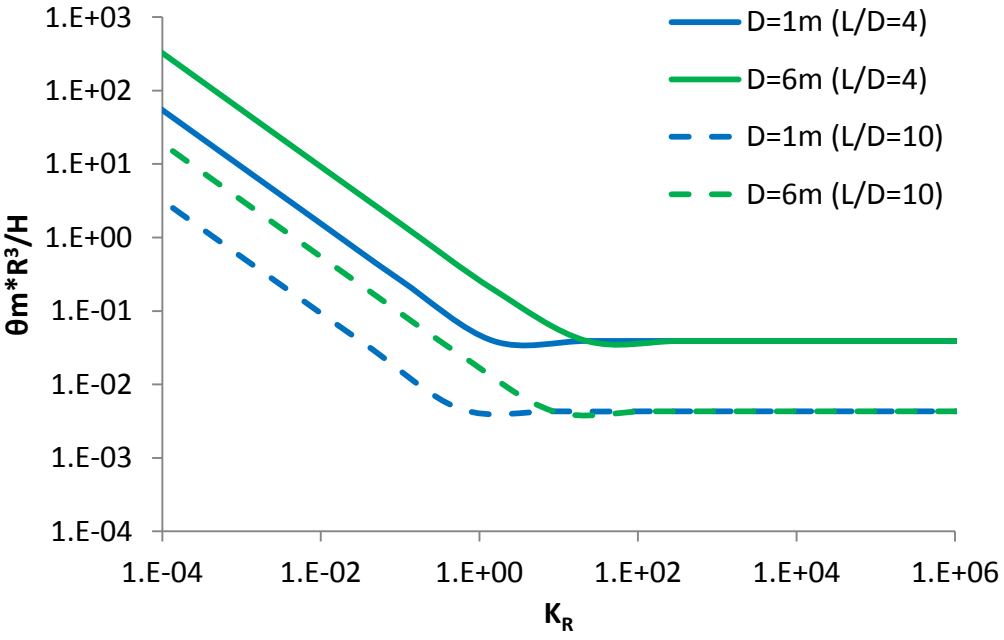

(b)

Figure 3.25 Proposed influence factors comparison for (a) displacements and (b) rotations for soils with linearly increasing stiffness distribution with depth

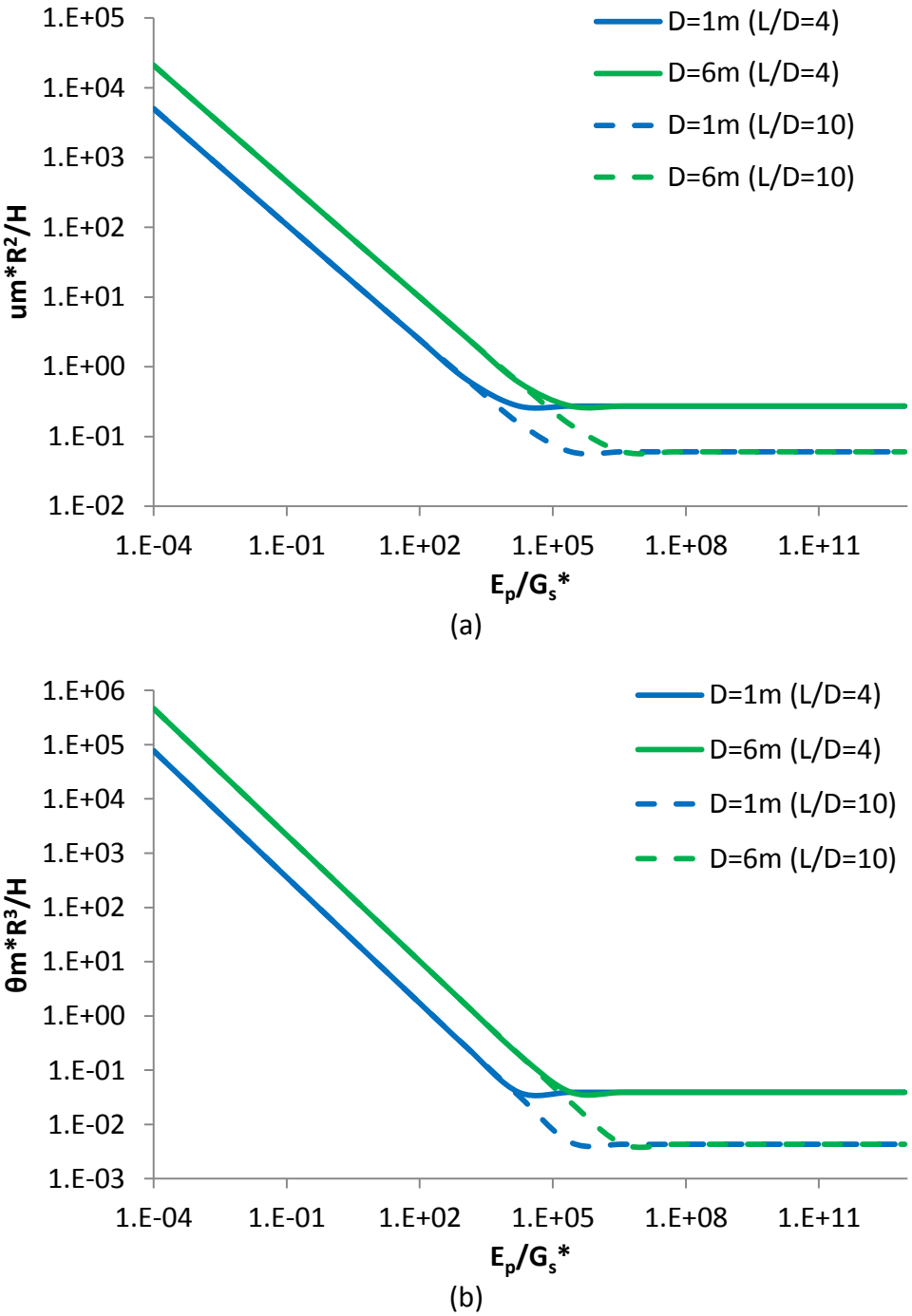

Figure 3.26 Proposed influence factors comparison for (a) displacements and (b) rotations for soils with linearly increasing stiffness distribution with depth

4. Experimental Studies

4.1. Introduction

A set of experimental studies were performed in order to evaluate the importance of dynamic response of a model offshore wind turbine founded in monopiles. Results are also discussed in Martinez-Chaluisant et al. (2010). The data obtained from the small scale experimental studies was used to evaluate the effects of pile-soil flexibility in damping and natural frequency predictions. The structural response to free vibrations was monitored using micro electro-mechanical systems (MEMS) accelerometers.

The dynamic experimental results of natural frequency were compared to analytical solutions given by the Rayleigh's energy method, based on the principle of conservation of energy as explained by (Timoshenko et al., 1974). In our system there are small damping forces. The damping forces primarily affect the amplitude of the dynamic response rather than the value of the measured dominant frequency, and the Rayleigh's method is considered applicable in this application. The parameters studied include (i) pile material; (ii) foundation material; (iii) water level; (iv) turbine and rotor mass; and (v) load characteristics. Good agreement was found for concrete and stiff soil as subbottom material, however for soft soils the natural frequency was over predicted by 40%.

Damping of the system was determined experimentally using the data obtained during the dynamic tests. Two methods were used: the half power bandwidth and the logarithmic decrement method. Results were compared to the data sets in the time and

frequency domain using the signal and the frequency response spectrum, respectively. Accurate damping calculations were achieved with the logarithmic decrement method in all cases. It was observed that damping ratio increases as pile-soil stiffness ratio increases.

4.2. Equipment

A vertical arrangement of six MEMS accelerometers equally spaced were placed in the tower physical models for data collection. Three towers were used, PVC, copper short and copper long, to cover a wide range of stiffness of pile-soil systems. Table 4.1 shows the properties of the model tower materials. In an attempt to model the effects of nacelle and rotor, masses of 257.5 g and 450 g were added to the free end of the tower as shown in Figure 4.1.

Table 4.1 Properties of model tower materials

Tower Material	PVC	Copper Short	Copper Long
Tower Length, L (mm)	2096	2099	2299
Wall Thickness, t (mm)	3.2	1.0	1.0
Outer Diameter, D_o (mm)	21.3	16.1	16.1
D_o/t	6.6	15.4	15.4
Inner Diameter, D_i (mm)	14.9	14.2	14.2
Cross Sectional Area, A (mm^2)	183.5	49.1	49.1
Density, ρ (kg/m^3)	1400	8500	8500
Young's Modulus, E (GPa)	3	100	100
Moment of Inertia, I (mm^4)	7524	1383	1383

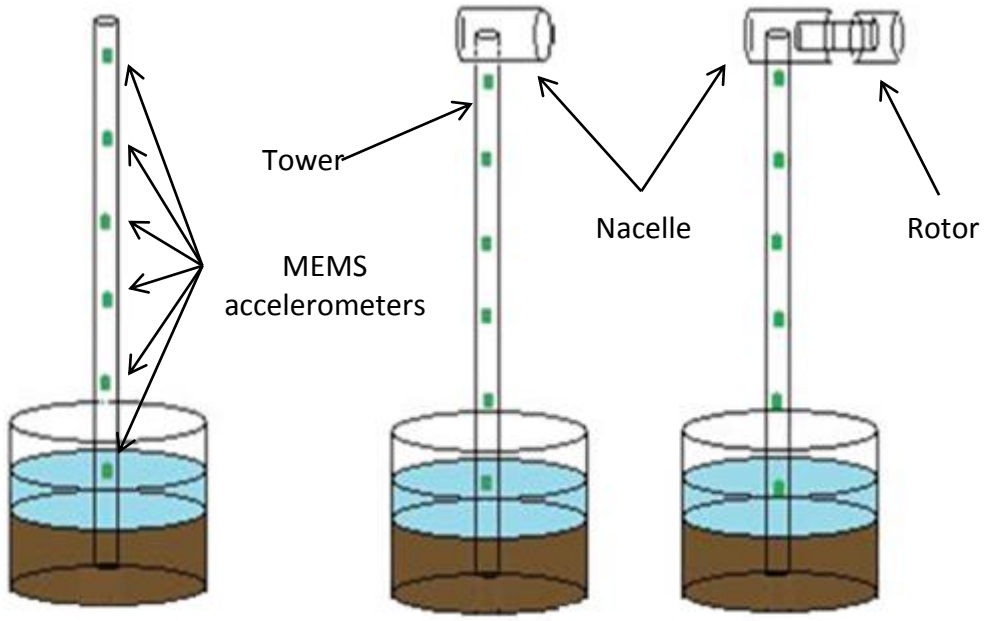

Figure 4.1 Diagram of test setup

Three foundation materials were used for the tests: concrete, sand, and a very soft clay. Several tests were performed with each foundation material and simulating different conditions. For the tests with the concrete as the foundation material surface water was added to some of the tests. With the soil as the foundation material, surface water depth was about 75 mm. In the sand tests, a donut shaped 4.55 kg mass was added at the surface to increase the effective stress on the surface of the sand so the soil strength and stiffness of the foundation soil was increased. Shear wave velocity (V_s) was measured for the foundation materials to determine the small strain shear modulus (G_0) in the concrete and clay:

$$G_0 = \rho V_s^2 \qquad \text{Equation 4.1}$$

where ρ is the soil density. For the sand soil conditions, the shear modulus was estimated from the void ratio ($e=V_v/V_s$) and confining stress. Table 4.2 shows the properties of the foundation materials.

Table 4.2 Properties of foundation materials

Foundation Material	Concrete	Sand	Clay
Shear Wave Velocity, V_s (m/s)	3300	NA	12
Unit Weight, ɣ (kN/m^3)	24	21.8	14.3
Density, ρ (kg/m^3)	2.45	2.22	1.46
Void Ratio, e	NA	0.40	3.0
Small Strain Shear Modulus, G_0 (MPa)	7,500 to 10,000	25	0.2

4.3. Methods

The experimental method consisted of apply lateral displacements to the free end of the tower and record the dynamic response of the system. Different conditions were tested for the foundation and tower material, and are summarized in Table 4.3.

The signals obtained with the MEMS accelerometers need to be processed prior to apply the methods to get the natural frequency and damping. First, the DC component of the signal was removed by averaging the signal. To enhance the frequency resolution, the zero padding technique was used. The zero padding method consists of appending zeros at the end of the signal, which may cause discontinuities if the cycles showing the decay are truncated (Santamarina & Fratta, 2005).

The Fast Fourier Transform (FFT) was applied to the signal in the time domain to decompose the signal in the different frequency components. A window was applied to filter the signal in the frequency domain, this is done in order to remove higher frequencies that are not of interest for this study. Once the signal is filtered in the frequency domain, the Inverse Fast Fourier Transform (IFFT) was applied to obtain the filtered signal in the time domain. All the signal processing was done using MATLAB.

Table 4.3 Experimental tests

Foundation Material	**Tower Material**	**Nacelle (258 g)**	**Rotor (450 g)**	**Water Depths (mm)**
Concrete	Copper Long	x	x	0, 75, 150, 225
		x		
	Copper Short	x	x	
		x		
	PVC	x	x	
		x		
Sand 16D	PVC	x	x	
		x		
Sand 8D	PVC	x		
90 mm Soil Layer/Concrete	PVC	x	x	83
	Copper Short	x	x	
	Copper Long	x	x	
Clay	Copper Short	x	x	
		x		
	PVC	x	x	
		x		

4.3.1. Rayleigh's Energy Method

The Rayleigh's energy method is based on the principle of conservation of energy of a cantilever beam, similar to the one shown in Figure 4.2. The natural frequency of vibration is obtained from:

$$f = \frac{1}{2\pi}\sqrt{\frac{3EIg}{L^3\left(W+\frac{33}{140}\overline{w}L\right)}} \qquad \text{Equation 4.2}$$

where *f* is the natural frequency, E is the tower Young's modulus, I is the tower moment of inertia, g is the acceleration of gravity, L is the tower length above fixity point (initially the mudline), W is the weight of the mass at the free end of the tower, and $\overline{w}$ is the tower weight per unit length. Derivation of the Rayleigh's energy method can be found in Prakash (1981, pp. 30-33). To compare the cantilever beam to an offshore tower, the model can be rotated, as shown in Figure 4.3.

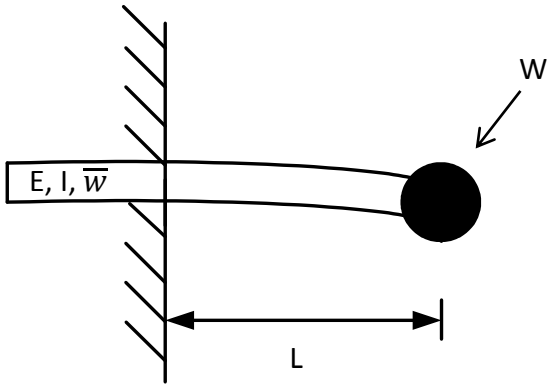

Figure 4.2 Cantilevered horizontal beam

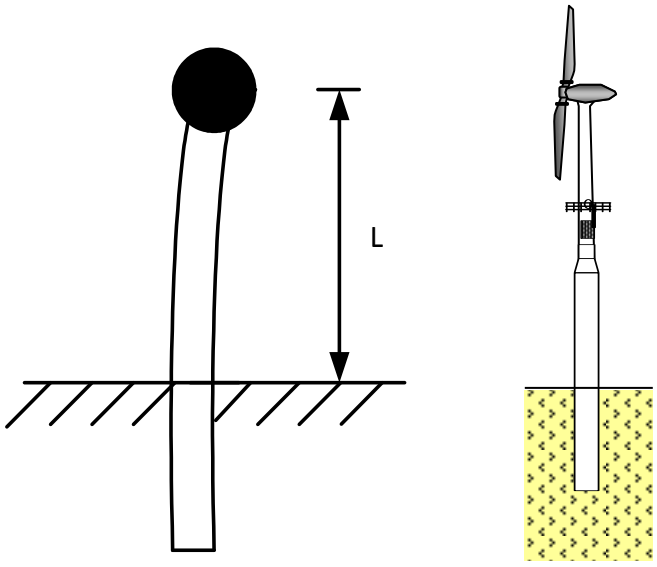

Figure 4.3 Rotated cantilever beam to have a structure with similar boundary conditions

The Rayleigh's energy method assumes fixity at the mudline. This was the initial condition for all the tests. During testing, some changes in this initial condition were observed for the models with clay as the subbottom material. Modifications were applied to the method to consider the changes in the system.

4.3.2. Half Power Bandwidth Method

Half power bandwidth is obtained from the frequency response curve. To calculate damping, the maximum value of the frequency response is divided by $\sqrt{2}$, at these two points the frequency values are determined, see Figure 4.4. Once the two frequencies are determined, the half power bandwidth is defined as the ratio of the frequency difference at the two half power points to the natural frequency at this mode of excitation:

$$\xi = \frac{f_2 - f_1}{2f_n}$$ Equation 4.3

where ξ is the damping ratio, f_1 and f_2 are the frequencies at the half power, and f_n is the natural frequency of excitation. Derivation of the method can be found in Prakash (1981, pp. 34-35).

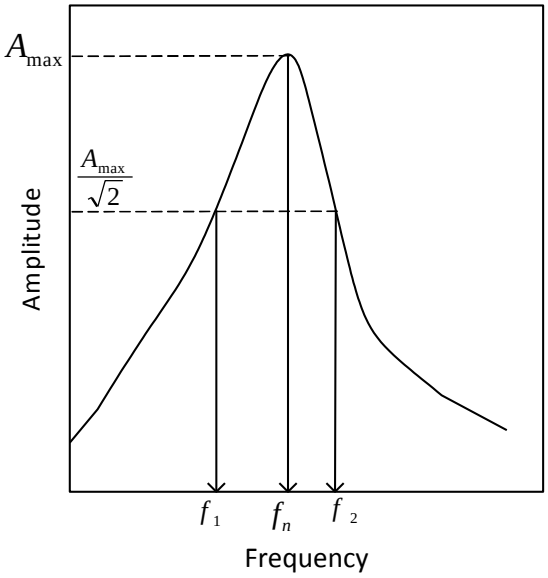

Figure 4.4 Graphical determination of half power bandwidth

4.3.3. Logarithmic Decrement Method

Logarithmic decrement (δ) is obtained from the decay in amplitude (x) of a signal with *n* number of cycles:

$$\delta = \frac{1}{n} log \frac{x_0}{x_n} = \xi \omega_n (t_n - t_0)$$ Equation 4.4

where ω_n is the angular frequency [=2πf_n]. Figure 4.5 shows an example of a signal, and how the damping describes the decay. In the experimental studies, an initial displacement was applied at the free end of the tower and released. The tower was allowed to vibrate freely until it reached static equilibrium.

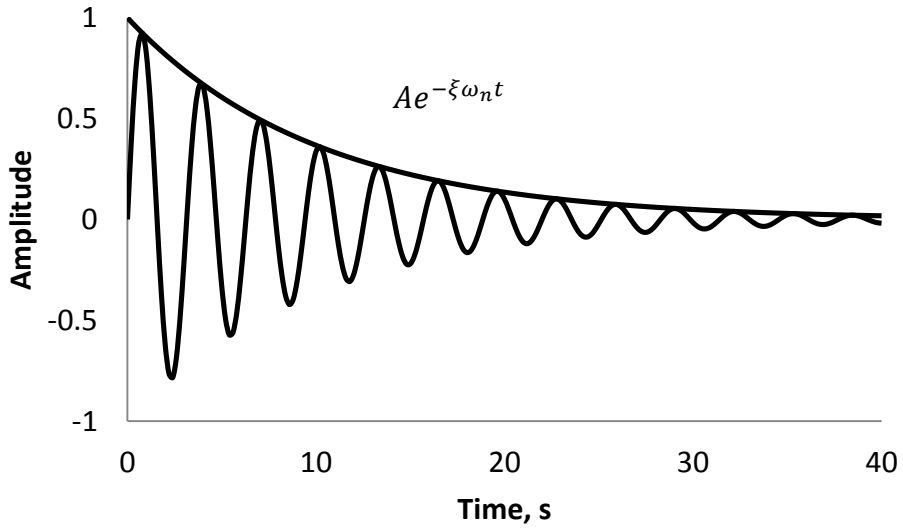

Figure 4.5 Graphical determination of logarithmic decrement

4.3.4. Frequency Response Function

The frequency response function (H) models the behavior of a single degree of freedom system. The H function was calculated using the damping determined by both methods, and compared to the frequency response spectrum.

$$|H(f)| = \frac{1}{\sqrt{\left(1-\frac{f}{fn}^2\right)^2+\left(2\xi\frac{f}{fn}\right)^2}} \qquad \text{Equation 4.5}$$

4.4. Results

Initial lateral deformations were parallel to the direction of measurement of the MEMS accelerometers. Oscillations accumulated with every test and became rotational with time, especially for the tests with the mass in the top of the tower. Failure was observed and recorded. Figure 4.6 shows failures in copper and PVC towers.

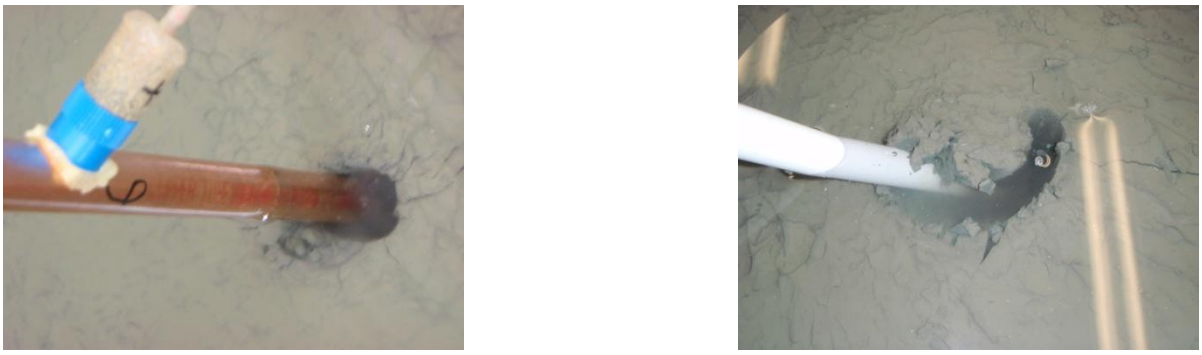

Figure 4.6 Physical model failure in clay for the copper and PVC towers

4.4.1. Natural Frequency

The natural frequency was determined for each test using the peak of the resonance response spectra, see Figure 4.7. The figure shows the frequency response spectra for the copper short tower with the nacelle, embedded in concrete. The natural frequency determined for this test was 1.63 Hz. Table 4.4 shows the results for the entire set of tests performed. As expected, the natural frequency decreased when mass (nacelle and rotor) was added to the tower system, as shown in Figure 4.8. Appendix B shows the graphs of collected signals and response spectra for the entire set of tests performed.

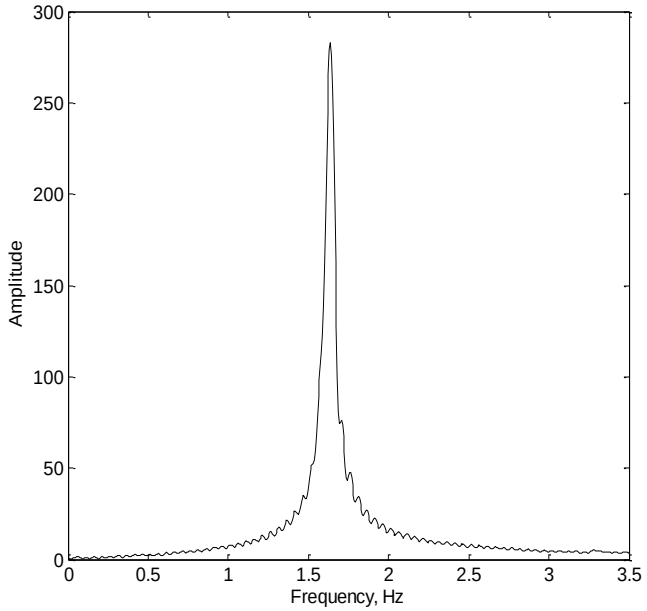

Figure 4.7 Example of the frequency response spectra

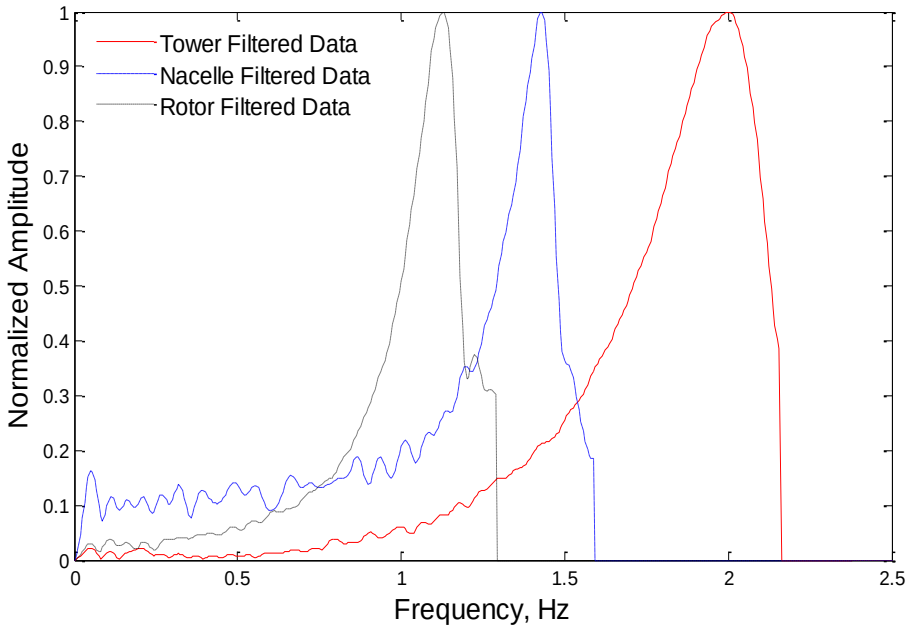

Figure 4.8 Natural frequency comparison for the tower, tower and nacelle, and tower, nacelle and rotor

Table 4.4 Natural frequency results for each of the test performed

Foundation Material	Tower Material	Nacelle	Rotor	f_n calculated, Hz	f_n measured, Hz	Δf_n
Concrete	Copper Long	x	x	1.04	0.96	0.07
		x		1.45	1.39	0.05
				2.14	2.19	-0.05
	Copper Short	x	x	1.21	1.13	0.08
		x		1.71	1.63	0.07
				2.59	2.61	-0.01
	PVC	x	x	0.51	0.41	0.10
		x		0.76	0.76	0.00
				1.34	1.34	0.00
Sand 16D	PVC	x	x	0.55	0.43	0.12
		x		0.82	0.78	0.04
				1.49	1.39	0.10
Sand 8D	PVC	x		0.76	0.76	-0.01
				1.34	1.30	0.04
Soil/Concrete	PVC	x	x	0.55	0.43	0.12
	Copper Short	x	x	1.30	1.12	0.18
	Copper Long	x	x	1.11	0.96	0.15
Clay	Copper Short	x	x	1.32	1.13	0.19
		x		1.87	1.43	0.44
				2.89	2.00	0.89
	PVC	x	x	0.55	0.44	0.11
		x		0.82	0.74	0.08
				1.49	1.33	0.15

Measured and calculated natural frequencies are compared in parity plots, with 0.1 Hz offsets, in Figure 4.9 through Figure 4.11. Dynamic impulse ("flick") and static displacement tests were performed in the tests setups described in Section 4.2, producing equal values of natural frequencies. From the figures is observed that natural frequency of the systems decrease when the mass is increasing, as expected from Equation 4.2.

Measured values of the natural frequency agreed well with the predictions for concrete and sand as the foundation material, being inside the 0.1 Hz offset. Both of these foundation materials, concrete and sand, represent a fixed condition for the copper and PVC towers in agreement with Equation 4.2.

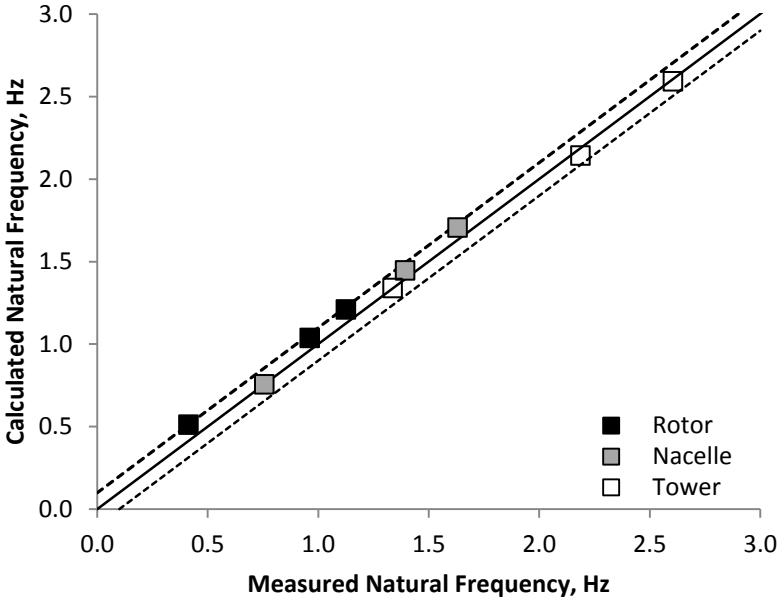

Figure 4.9 Comparison of measured and predicted natural frequency for turbines founded in monopiles in concrete

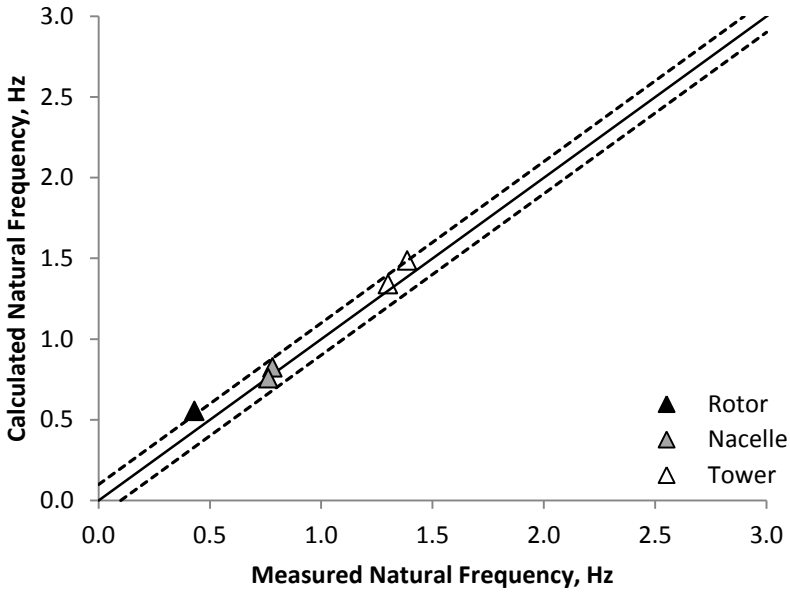

Figure 4.10 Comparison of measured and predicted natural frequency for turbines founded on monopiles in sand

In the case of the soft clay as the foundation material, an overprediction was observed, see Figure 4.11. When the data is separated by the tower material, higher overprediction is observed for the copper short tower. Stiffness of the copper short tower relative to the stiffness of the soft clay is higher, and the fixity assumption at the mudline is no longer applicable. This deviation on the predicted dynamic response becomes important with soft sediments, where the influence of soil nonlinearity is evident.

To explore the influence of pile to soil flexibility, the pile flexibility factor (K_R), as defined in Equation 1.1, was calculated for all the tests setups and compare to the difference between the calculated ($f_{n,c}$) and measured ($f_{n,m}$) natural frequencies. Figure 4.12 show the performance of the natural frequency prediction in relation to variations in K_R. The tower materials embedded in the soft clay plotted in the stiff pile region with $K_R>10^{-2}$.

As K_R increases, or as the pile becomes more rigid, the natural frequency of the system is overestimated. This overestimation is a consequence of the pivot point displacement down the pile, when the pile is loaded repeatedly.

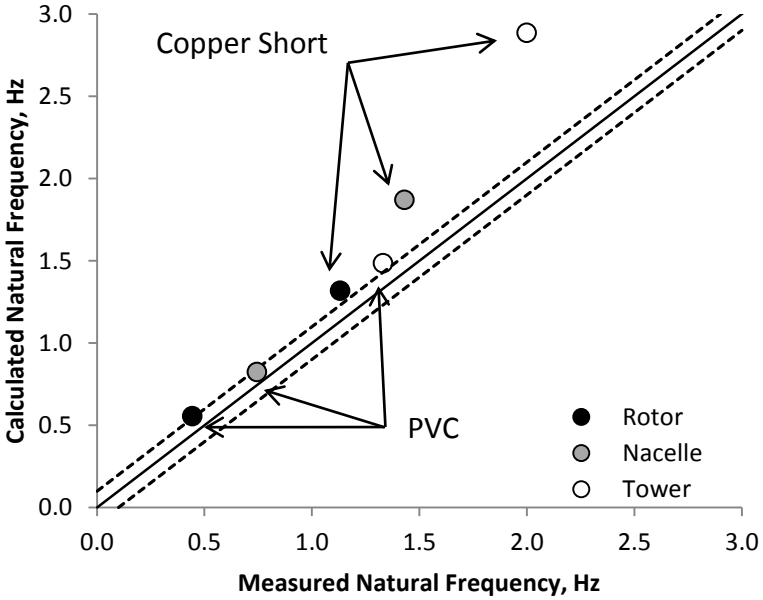

Figure 4.11 Comparison of measured and predicted natural frequency for turbines founded on monopiles in soft clay

These sets of dynamic experiments have proven the sensibility of the natural frequency to stiffness changes in the pile-soil system. Piles that behave in a rigid fashion are more dynamically sensitive to stiffness changes in the system, as stated by Zaaijer (2005).

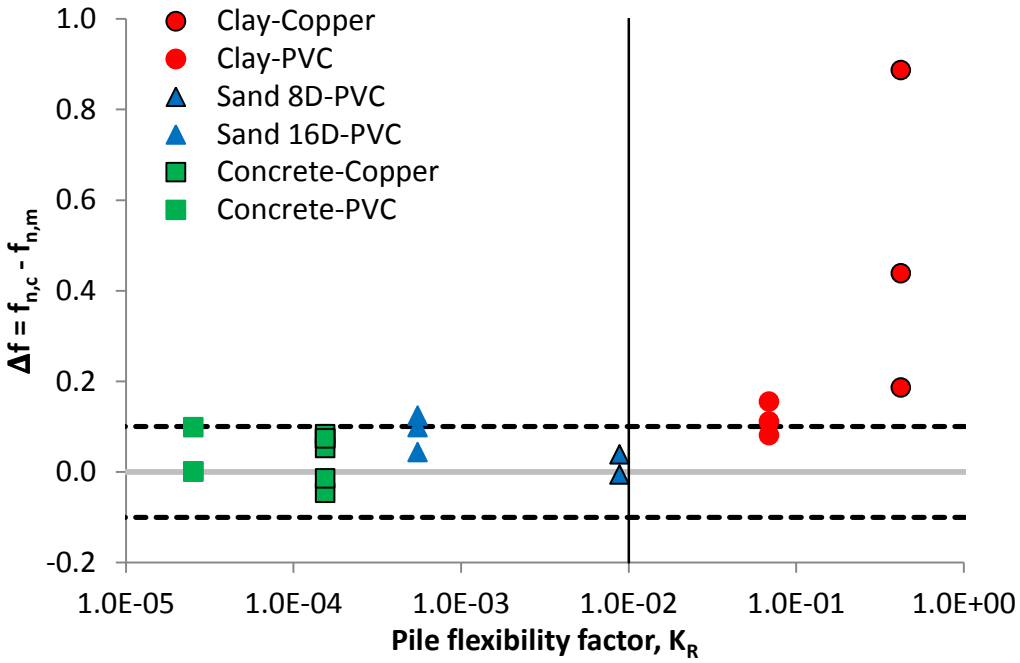

Figure 4.12 Pile flexibility effects on the determination of natural frequency

4.4.2. Damping

The damping in the system was determined as explained in Sections 4.3.2 and 4.3.3. The logarithmic decrement method was a better fit for the data in all cases. The correct algorithm was used to calculate damping. Figure 4.13 shows the comparison between both methods.

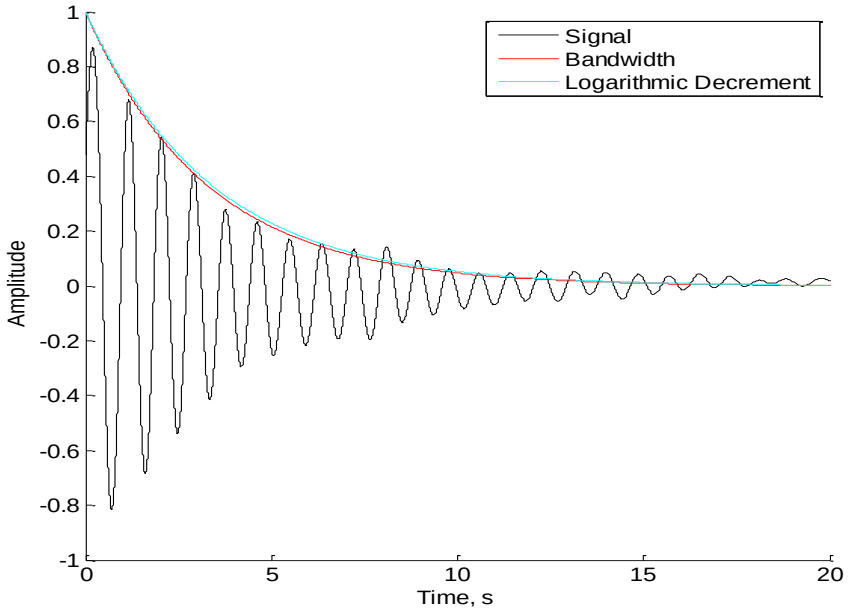

Figure 4.13 Bandwidth and logarithmic decrement method comparison

Table 4.5 shows the damping ratio results for the logarithmic decrement method for each of the tests. Figure 4.14 is presented to evaluate how the damping changes with pile material and pile flexibility factors. To analyze this data, we will look at tower and foundation material separately. First the copper tower, Figure 4.14(a), with a rigid foundation material (concrete) and a K_R=1.5E-4, the calculated damping ratio was 0.01.

When the stiffness of the foundation material was decreased to a soft soil (clay) and the K_R=4.2E-1, the damping increased slightly to 0.04. In the rigid foundation material, no significant changes were observed for the tower with the different masses at the top because the mass is not heavy enough to contribute to the deflection of the foundation material. In the soft material, the tower with the rotor had a higher damping. This can be explained because the added mass at the top of the tower is contributing to the deflection, and if there is higher soil stiffness degradation around the pile we will also have higher damping.

Results for the PVC as the tower material are shown in Figure 4.14(b). For a rigid foundation material, the damping was 0.04 for a K_R of 2.5E-5, and as the foundation material gets softer damping increased from 0.049 to 0.055, for a K_R of 5.5E-4 and 6.9E-2, respectively. This result shows that the pile material had a bigger effect in damping than the pile stiffness. Damping results for the sand as the foundation material shows that the tower with the nacelle embedded 8 diameters (8D) with a K_R=8.8E-3 has a rigid behavior in comparison to the one embedded 16 diameters (16D) with a K_R=5.5E-4. The 8D tower embedment had a damping of 0.041, and the 16D tower embedment had a damping of 0.033. For the same foundation and tower material, but different L/D ratios, the rigid tower had higher damping. In Figure 4.14 is observed that for rigid piles from the same material the damping increases slightly as K_R increases. It was found that tower material had a larger effect in damping than pile flexibility factor, the PVC giving higher damping.

The measured damping was fitted to the theoretical response of a single degree of freedom system using the H function, Equation 4.5. The result is shown in Figure 4.15, where HLD is the H function calculated using damping from the logarithmic decrement and HBW from the bandwidth method. If the bandwidth is overestimating the response this is reflected as an up shift of the frequency response spectra. Appendix B shows signals with the two decay models in the time domain, and the frequency response spectra compared to the single degree of freedom system.

Table 4.5 Damping ratio results

Foundation Material	Tower Material	Nacelle	Rotor	Damping Ratio
Concrete	Copper Long	x	x	0.007
		x		0.008
				0.010
	Copper Short	x	x	0.010
		x		0.010
				0.014
	PVC	x	x	0.040
		x		0.028
				0.024
Sand 16D	PVC	x	x	0.049
		x		0.033
				0.027
Sand 8D	PVC	x		0.041
				0.041
Soil/Concrete	PVC	x	x	0.038
	Copper Short	x	x	0.006
	Copper Long	x	x	0.006
Clay	Copper Short	x	x	0.040
		x		0.030
	PVC	x	x	0.055
		x		0.034
				0.029

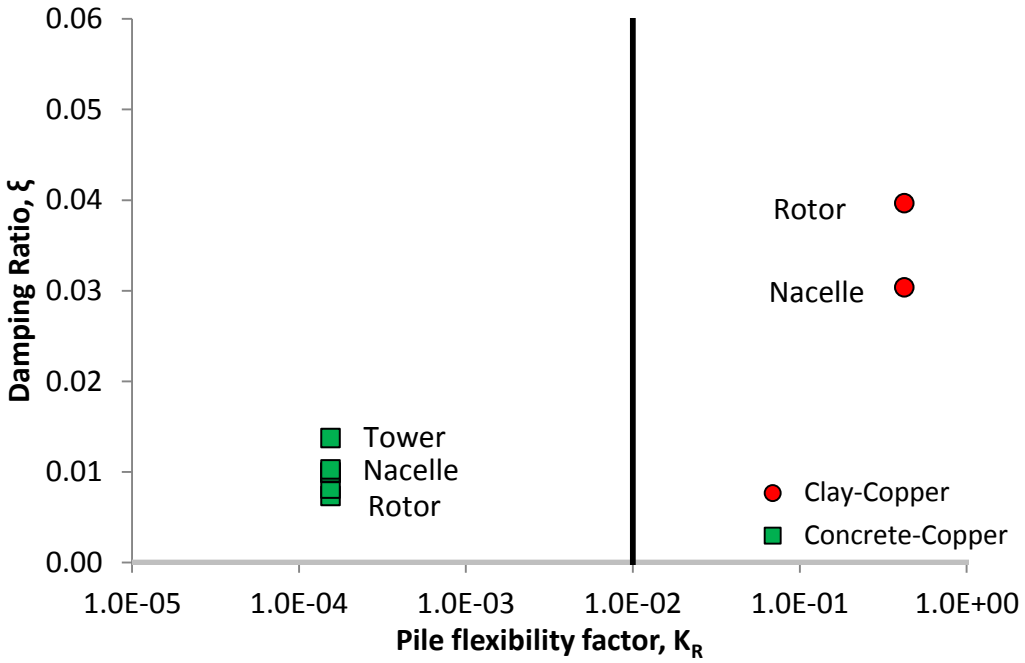

(a) Damping ratio results for the copper tower

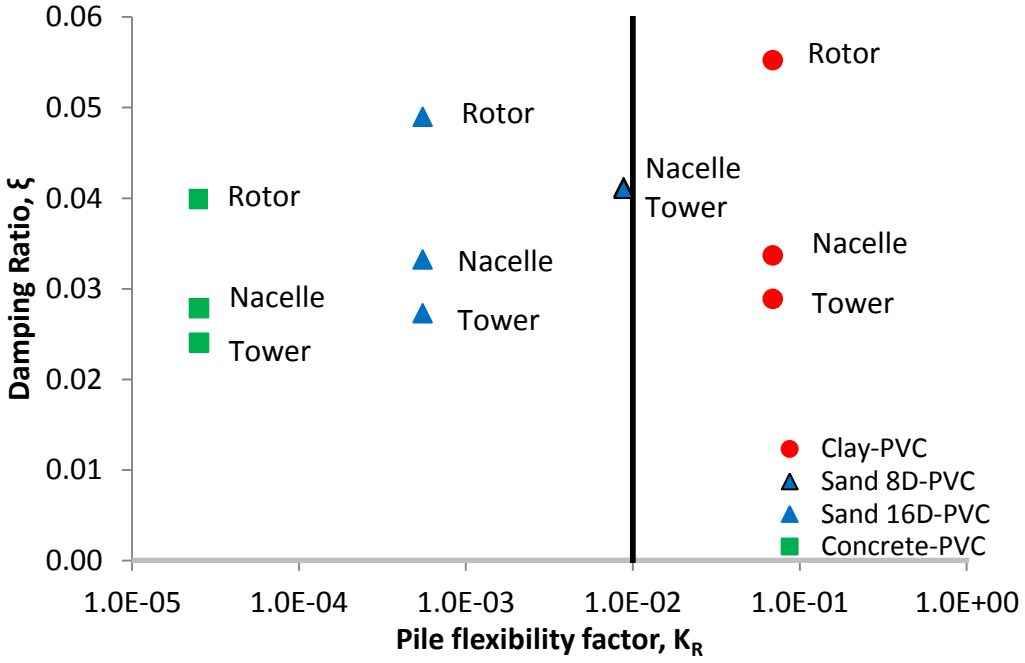

(b) Damping ratio results for the PVC tower

Figure 4.14 Damping ratio for variation in pile flexibility factor

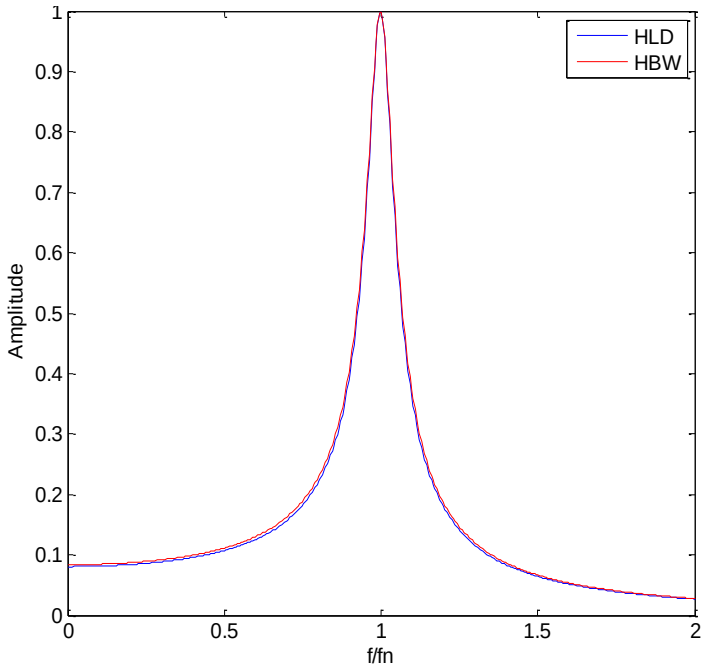

Figure 4.15 Frequency response comparison by fitting the single degree of freedom system response to the data by using Equation 4.5

4.5. Influence of Pile-Soil Relative Stiffness on Dynamic Response

The dynamic response of a system can be characterized by its natural frequency and damping. Good prediction of the natural frequency of the system was achieved for concrete and stiff sandy soil, which maintained a fixed cantilever condition. In the case of the soft clay as the subbottom material there was an overprediction for up to 40% due to the change on the tower length above the fixity point. Figure 4.12 show the difference between the calculated and measured natural frequency as a function of the pile flexibility factor. It was defined before that rigid behavior starts around $K_R=10^{-2}$, for pile-soil systems with higher values of K_R the calculated natural frequency was higher than the measured natural frequency.

Equation 4.2 predicts that an increase in the system mass will decrease the frequency. If the location of the fixity point of the stiff tower is decrease due to soil yielding and plastic deformations in the surrounding soil, the mass of the system will increase, which will reflect as a decrease in the measured natural frequency. The Rayleigh's energy method can be effective to predict natural frequency of a system provided that the assumed boundary conditions are maintained.

Figure 4.14 shows how damping of the system increases as the K_R increases. The soft clay dissipates more energy than the concrete, because induced strain in the soil is higher and there is more stiffness degradation. Soil failure was observed in the surface of the soft clay as cracks, and plastic deformation was observed as a gap between the pile and surrounding soil. This gapping adds a scour component to the system. In Section 2.5, soil hysteretic behavior was presented, results show that concrete behaves as Figure 2.18(a), the stiff sand as Figure 2.18(b), and the soft clay behaves as shown in Figure 2.18(c). Same tower material, PVC, was tested under similar loading conditions, but with different embedment, 8D and 16D. The rigid system displayed slightly higher damping ratios. Pile material showed a larger influence on damping than the foundation material.

The results presented here show that piles with $10^{-2} \leq K_R$ have a slightly higher dynamic sensibility to stiffness changes in the system. Monopiles for offshore wind turbines, will exhibit rigid behavior due to high pile stiffness as compared to soil stiffness. Low tolerances are allowed for the dynamic design of monopiles for offshore wind turbines.

5. Summary and Conclusions

Appropriate engineering design of foundations for offshore wind turbines is crucial for safe, effective, and economic development of offshore wind farms. We have presented a study of design and published recommendations for the prediction of pile displacement and rotations at the mudline. Large scatter and underpredictions up to 90% were observed for the influence factors for the calculation of displacement and rotation for piles that behave in a rigid fashion.

Using finite element analysis, we found good agreement for influence factors published by Randolph (1981) to predict displacement and rotation influence factors for small-diameter piles that exhibit flexible behavior. Our analyses indicate that current methods developed for small-diameter flexible piles may underpredict displacements and rotations for large-diameter flexible piles, as well as for large-diameter and small-diameter rigid piles. Our analyses also suggest that large-diameter monopiles do not follow the same elastic deformation relationships as those developed for small-diameter piles. Large-diameter monopile behavior was demonstrated to be controlled by slenderness (L/D) ratio, as indicated by previous work. Functional design equations were developed to assess displacement and rotations for large-diameter monopiles.

Rayleigh's energy method assumes a cantilever condition at the mudline, but soils do not behave as rigid materials, then we need to look at pile-soil relative stiffness. Rayleigh's energy method overpredicted the natural frequency of rigid monopiles for

offshore wind turbines. In the flexible pile case, Rayleigh's energy method was able to predict the natural frequency with great accuracy.

Dynamic experiments were performed to investigate pile-soil relative stiffness effects on damping ratios. Two tower materials, PVC and copper, founded in three foundation materials were investigated. It was found that for the same tower material, the damping ratios increased as the pile becomes more rigid. This effect seems small, but other effects, such as mass at top of tower and tower material led to similar increases in damping ratio.

Future work is needed to develop functional forms with lower coefficients of variations, especially in the case of moment rotation for stiffness linearly increasing with depth, with a coefficient of 0.79. Coefficient of variation in functional forms should be less than 0.30. Additional analyses are warranted to reduce this coefficient of variation. More research is recommended for assessment of cyclic loading soil degradation and water flow characteristics, as well as plastic deformations due to extreme displacement and rotations at the mudline. Future work recommendations include the assessment of other foundation types, such as hybrid and floating foundations, for deeper waters. For laboratory or large scale experiments, controlled loading and displacement applications are recommended where the loading, displacements and rotations are directly measured.

Bibliography

Achmus, M., Kuo, Y., & Abdel-Rahman, K. (2009). Behavior of monopile foundations under cyclic lateral load. *Computers and Geotechnics, 36*, 725-735.

API RP2A. (2000). *Recommended Practice for Planning, Designing, and Construction Fixed Offshore Platforms-Working Stress Design.* Washington D.C.: American Petroleum Institute.

Burland, J. (1989, November). Ninth Laurits Bjerrum Memorial Lecture: "Small is Beautiful" - the Stiffness of Soil at Small Strains. *Canadian Geotechnical Journal, 26*(4), 499-516.

Burland, J., & Lord, J. (1969). The load deforamtion behaviour of Middle Chalk at Mundford, Norfolk: a comparison between full-scale performance and in-situ and laboratory measurements . *Conference on In-Situ Investigations in Soils and Rock* (pp. 3-15). London: British Geotechnical Society.

Bush, E., & Manuel, L. (2009). Models for Offshore Wind Turbine Foundations and their Influence on Long-Term Loads. *2009 Structures Congress* (pp. 2558-2567). Austin: American Society of Civil Engineers.

Cook, R. (2001). *Concepts and applications of finite element analysis* (4 ed.). John Wiley & Sons, Inc.

DNV. (2007). *Design of offshore wind turbine structures, Offshore Standard DNV-OS-J101.* Det Norske Veritas.

DNV/Risø. (2001). *Guidelines for design of wind turbines.* Technical University of Denmark, National Laboratory for Sustainable Energy. Copenhagen: Det Norske Veritas/Risø.

Doherty, J., & Deeks, A. (2003). Elastic response of circular footings embedded in a non-homogeneous half-space. *Geotechnique, 53*(8), 703-714.

Gerolymos, N., & Gazetas, G. (2006, May). Development of Winkler model for static and dynamic response of caisson foundations with soil and interface nonlinearities. *Soil Dynamics and Earthquake Engineering, 26*(5), 363-376.

Hamre, L., Feizi Khankandi, S., Strom, P., & Athanasiu, C. (2011). Lateral behaviour of large diameter monopiles at Sheringham Shoal Wind Farm. In S. Gourvenec, & D. White

(Ed.), *Frontiers in Offshore Geotechnics II* (pp. 575-580). London: Taylor and Francis Group.

Hetenyi, M. (1946). *Beams on Elastic Foundations.* Ann Arbor: University of Michigan Press.

Holtz, R., & Kovacs, W. (1981). *An Introduction to Geotechnical Engineering.* (N. Newmark, & W. Hall, Eds.) Upper Saddle River, New Jersey: Prentice Hall.

Houlsby, G., & Byrne, B. (2003). Foundations for offshore wind turbines. *Philosophical Transactions of the Royal Society*(361), 2909-2930.

Houlsby, G., Ibsen, L., & Byrne, B. (2005). Suction caissons for wind turbines. In G. a. Cassidy (Ed.), *Frontiers in Offshore Geotechnics: ISFOG 2005* (pp. 75-93). London: Taylor and Francis Group.

Ibsen, L. (2008). Implementation of a new foundations concept for offshore wind farms. *15th Nordic Geotechnical Meeting*, (pp. 19-33). Sandefjord.

Kuhn, M. (1997). Soft or stiff a fundamental question for designers of offshore wind energy converters. *European Wind Energy Conference '97* (p. 4). Dublin: EWEC.

Kuhn, M. (2000). Dynamics of offshore wind energy converters on monopile foundations - experience from the Lely offshore wind farm. *Structure and Foundation Design of Offshore Wind Installations* (pp. 24-25). Chilton: Engineering and Physical Science Research Council.

LeBlanc, C., Houlsby, G., & Byrne, B. (2009, December). Response of stiff piles in sand to long-term cyclic lateral loading. *Géotechnique, 60*(2), 79-90.

Little, R., & Briaud, J. (1988). *Full Scale Cyclic Lateral Load Tests on Six Single Piles in Sand.* Texas A&M University, Civil Engineering Department. St. Louis: U.S. Army Corps of Engineers.

Martinez-Chaluisant, V., Schneider, J., & Fratta, D. (2010). Physical modeling of the dynamic response of offshore wind turbines founded on monopile. *12th International Conference on Engineering, Science, Construction, and Operations in Challenging Environments* (pp. 2079-2086). Honolulu: American Society of Civil Engineers.

Musial, W., & Ram, B. (2010). *Large-Scale Offshore Wind Power in the United States.* National Renewable Energy Laboratory, Department of Energy.

Musial, W., Butterfield, S., & Ram, B. (2006). *Energy from Offshore Wind.* Office of Energy Efficiency and Renewable Energy, U.S. Department of Energy. Golden: National Renewable Energy Laboratory.

Plaxis. (2011). Material Models Manual. *Plaxis 3D Foundation Material Models Manual V2*. Delft, South Holland, Netherlands: Plaxis.

Poulos, H. (1971, May). Behavior of Laterally Loaded Piles: I-Single Piles. *Journal of the Soil Mechanics and Foundation Division, 97*(SM5), 711-731.

Prakash, S. (1981). *Soil Dynamics.* United States of America: McGraw-Hill.

Randolph, M. (1977, December). A theoretical study of the performance of piles. *PhD Dissertation*. Cambridge, England, United Kingdom: University of Cambridge.

Randolph, M. (1981). The response of flexible piles to lateral loading. *Géotechnique, 31*(2), 247-259.

Randolph, M. (2004). Characterisation of soft sediments for offshore applications. *Proc. 2nd Int. Conf. on Site Characterization*, (pp. 209-231). Porto.

Reese, L., & Matlock, H. (1956). Nondimensional solutions for laterally loaded piles with soil modulus assumed proportional to depth. *Proceedings of the 8th Conference on Soil Mechanics and Foundation Engineering*, (pp. 1-41). Austin.

Reese, L., Cox, W., & Koop, F. (1974). Analysis of Laterally Loaded Piles in Sand. *Sixth Annual Offshore Technology Conference* (pp. 473-483). Houston: Offshore Technology Conference.

Reese, L., Wang, S., Isenhower, W., Arrellaga, J., & Hendrix, J. (2004). *LPILE Plus 5.0 User's Manual.* Austin: Ensoft, Inc.

Richart, F., Hall, J., & Woods, R. (1970). *Vibrations of soils and foundations.* Englewood Cliffs: Prentice Hall, Inc.

Santamarina, J., & Fratta, D. (2005). *Discrete Signals and Inverse Problems: An Introduction for Engineers and Scientists.* West Sussex, England: John Wiley and Sons Ltd.

Schneider, J., & Senders, M. (2010, January/February). Foundation design - a comparison of oil and gas platforms with offshore wind turbines. *Journal of the Marine Technology Society, 44*(1), 32-51.

Scira Offshore Energy. (2011). Retrieved September 29, 2011, from Sheringham Shoal: http://www.scira.co.uk/default.htm

Scott, R. (1981). *Foundation Analysis.* (N. Newmark, & W. Hall, Eds.) Englewood Cliffs, New Jersey, United States of America: Prentice-Hall.

Timoshenko, S., Young, D., & Weaver, W. (1974). *Vibration problems in engineering* (Fourth Edition ed.). John Wiley & Sons, Inc.

Zaaijer, M. (2005). *Design Methods for Offshore Wind Turbines at Exposed Sites.* Wind Energy. Delft: Delft University of Technology.

Appendix A Literature Review Additional Graphs

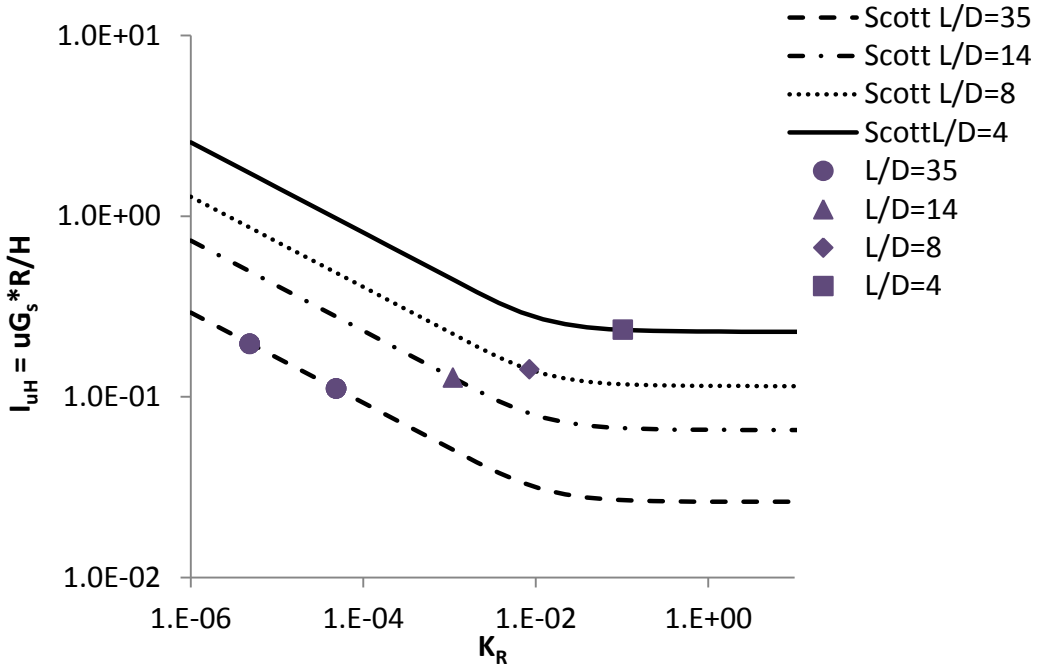

(a) Horizontal Influence Factors

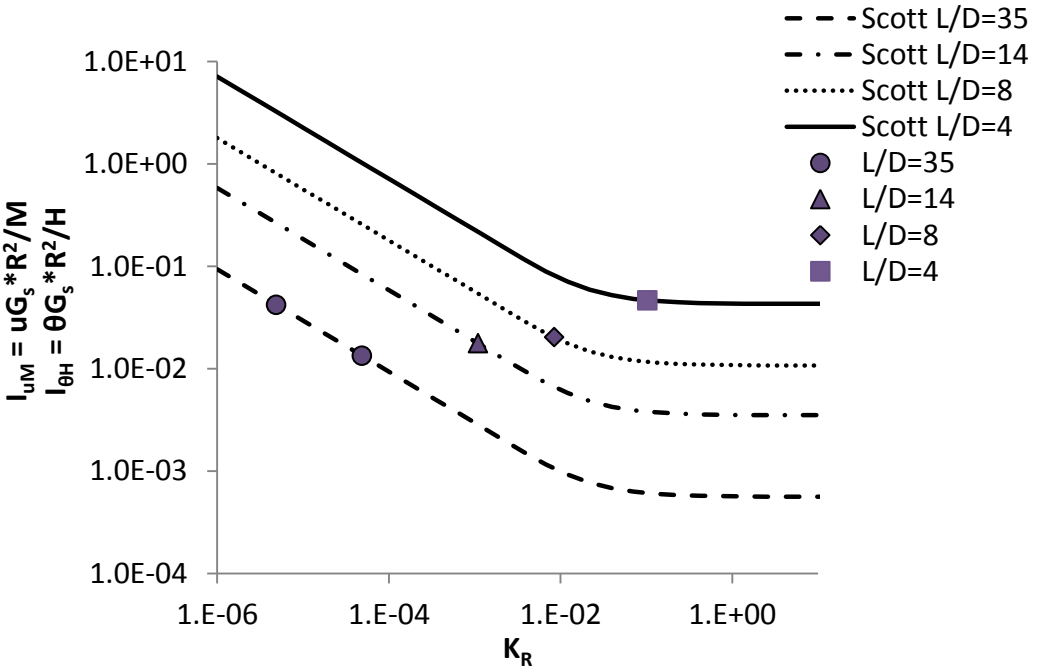

(b) Coupled Influence Factors

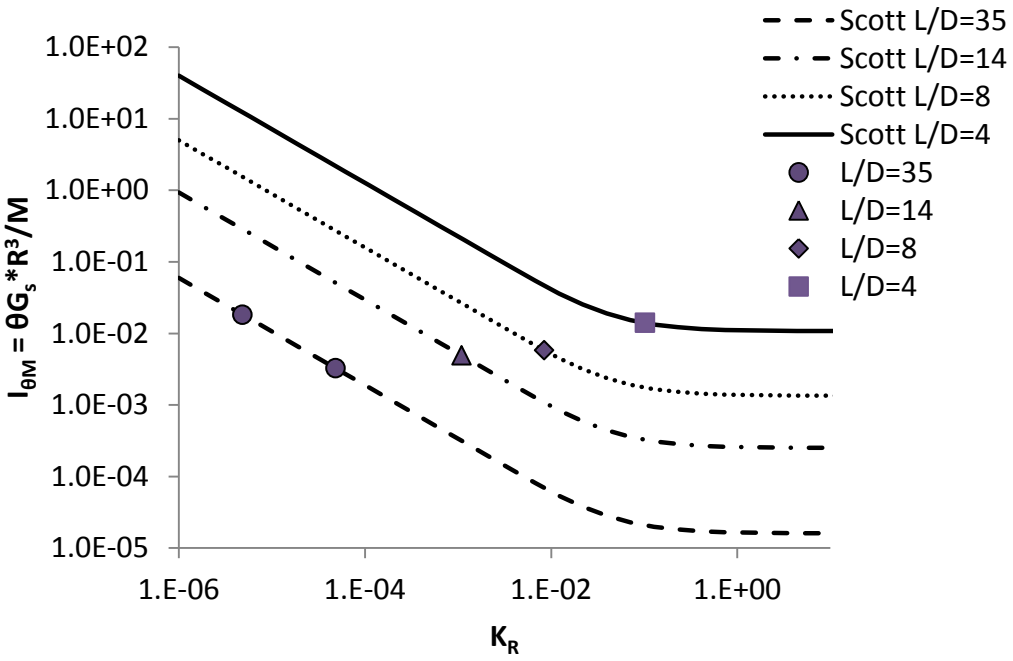

(c) Rocking Influence Factors

Figure A.1 Comparison between Scott (1981) and LPile

Appendix B Natural Frequency and Damping Results

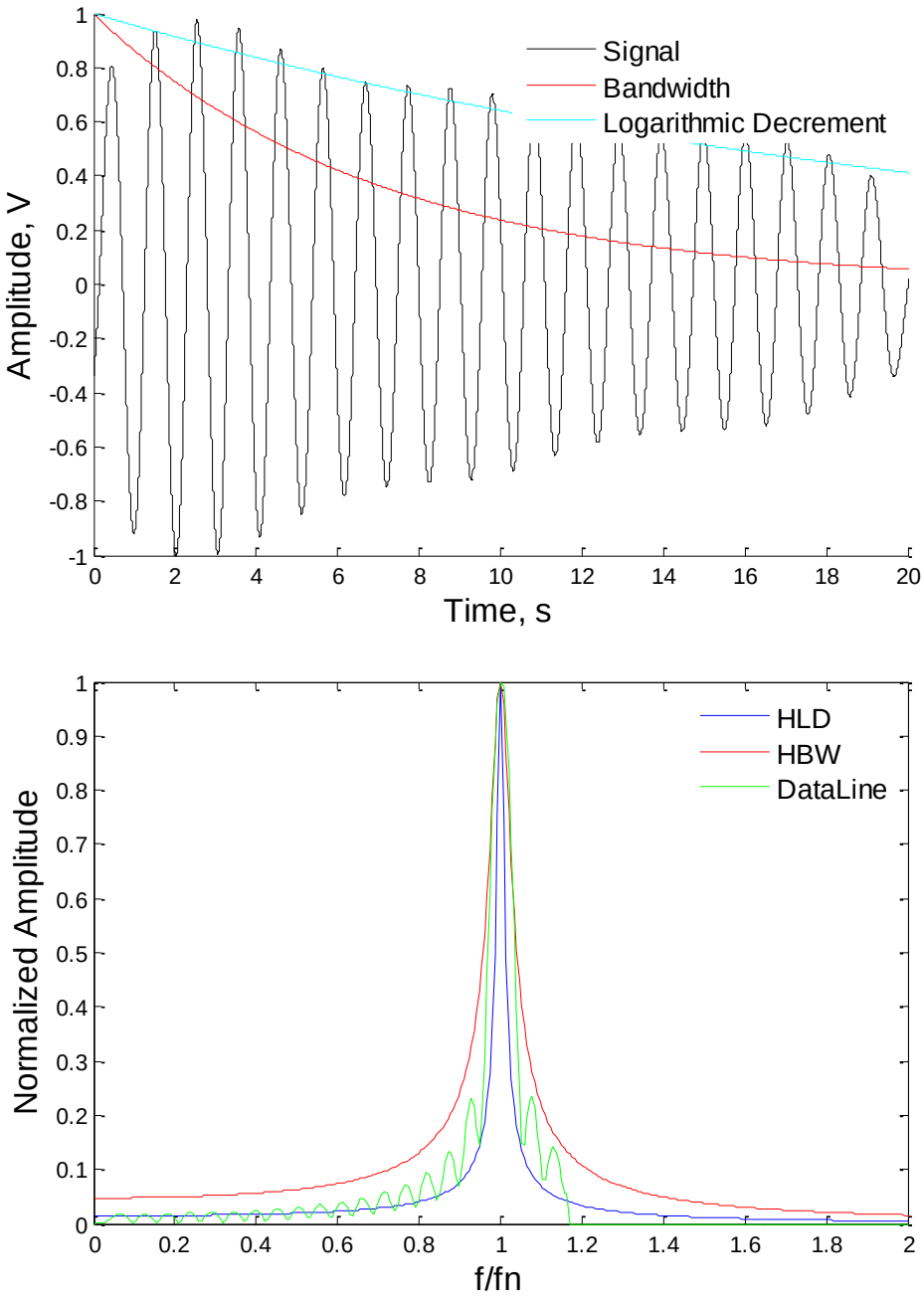

Figure B.1 Copper long tower with rotor and nacelle founded in concrete

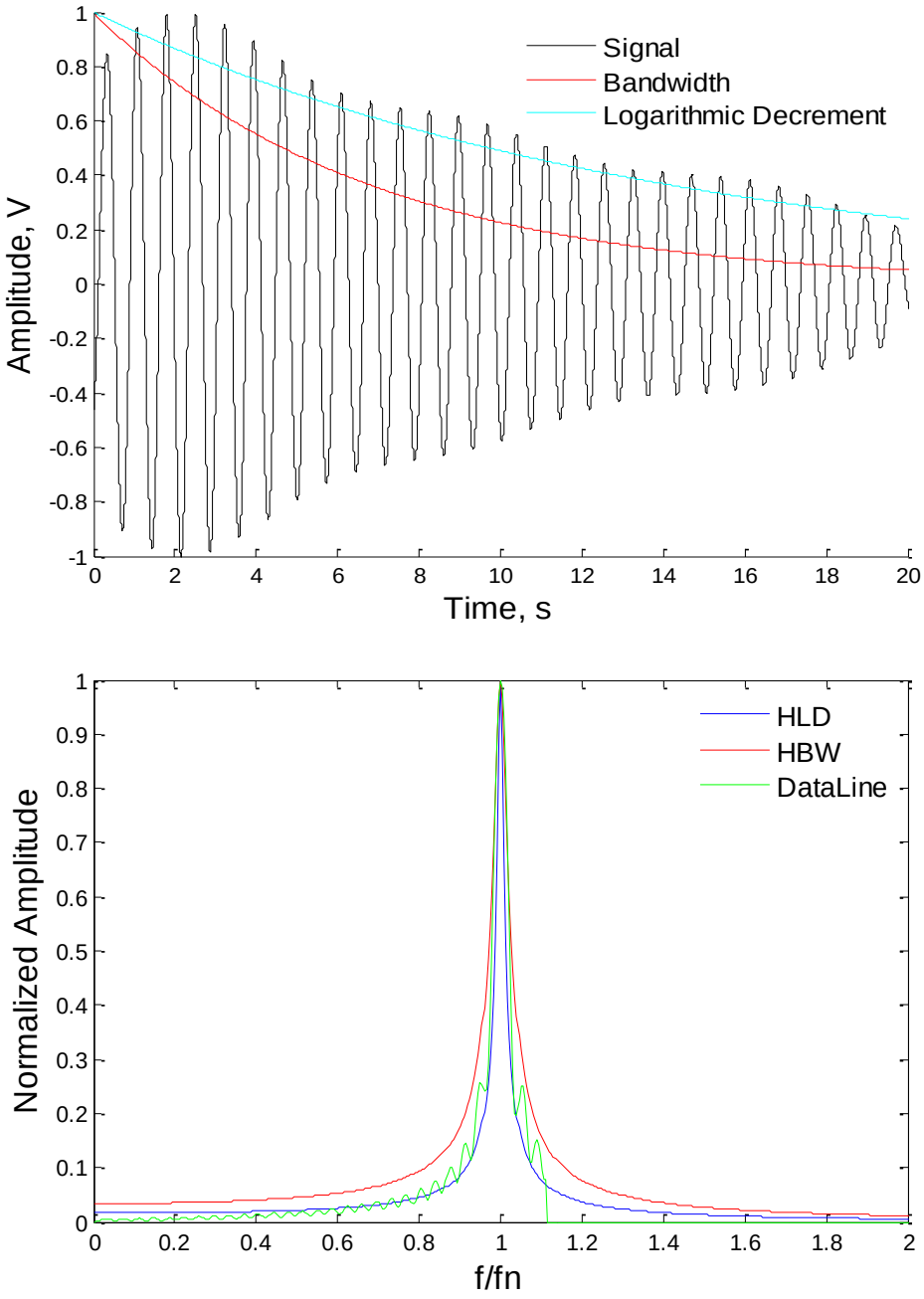

Figure B.2 Copper long tower with nacelle founded in concrete

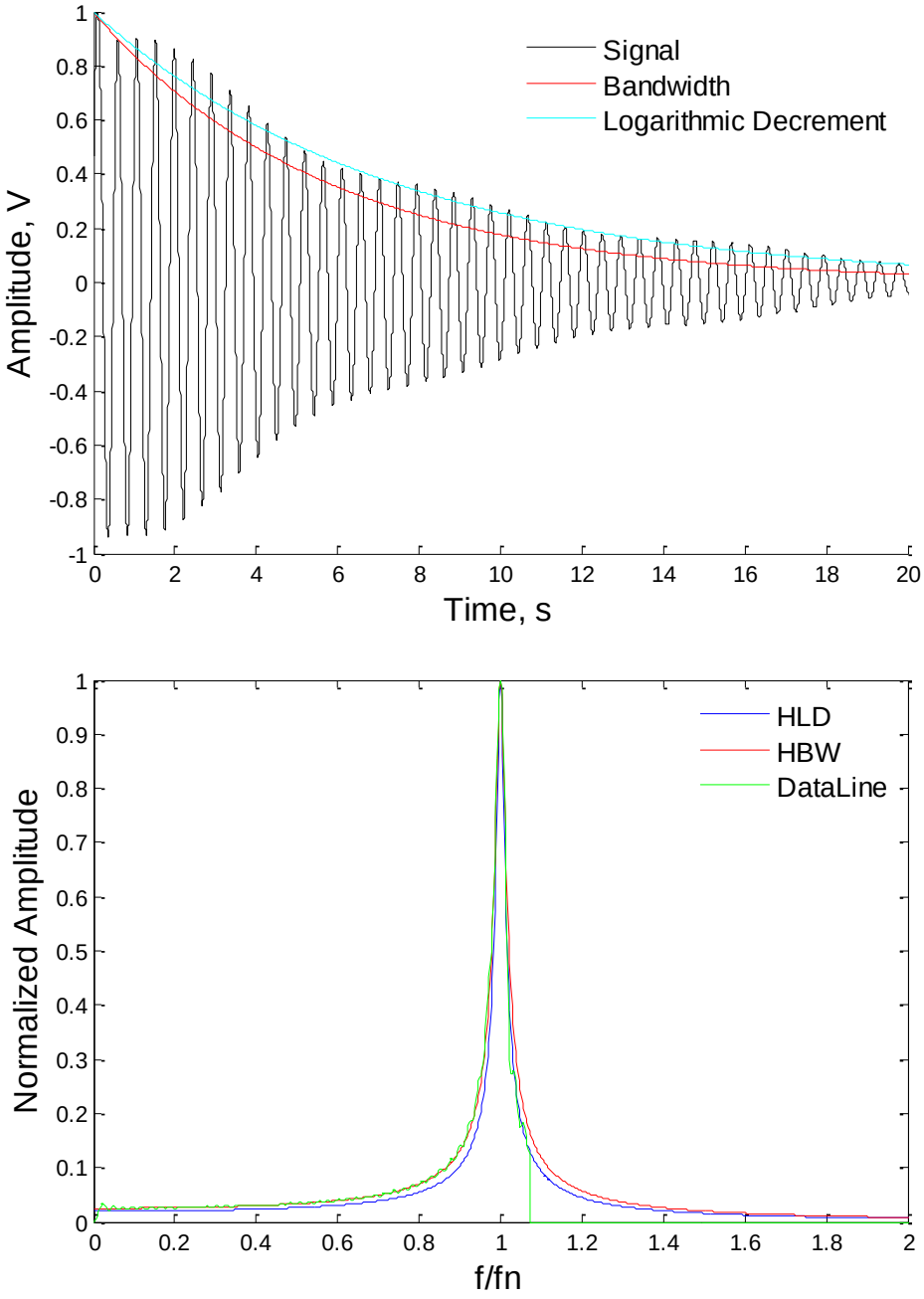

Figure B.3 Copper long tower founded in concrete

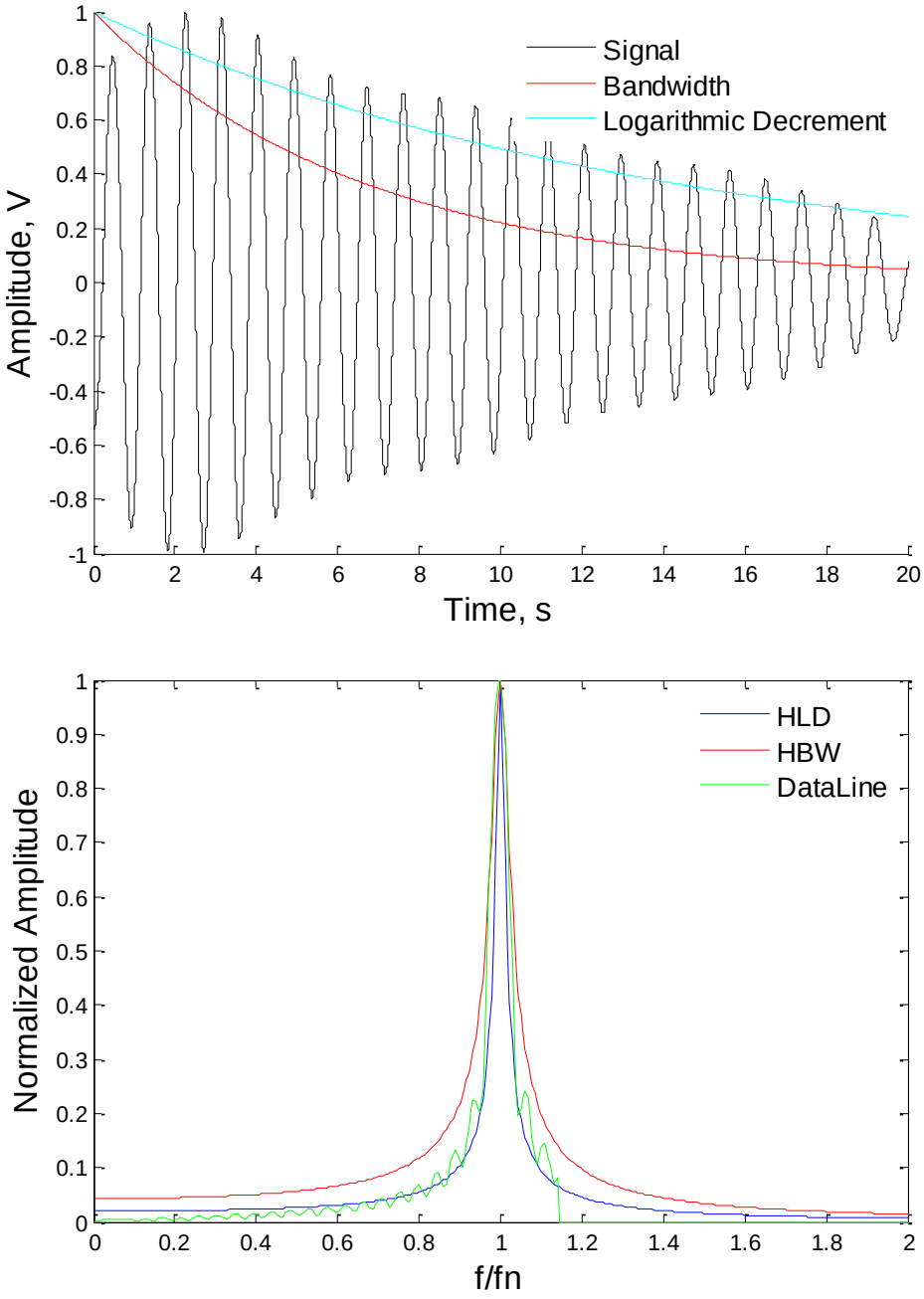

Figure B.4 Copper short tower with rotor and nacelle founded in concrete

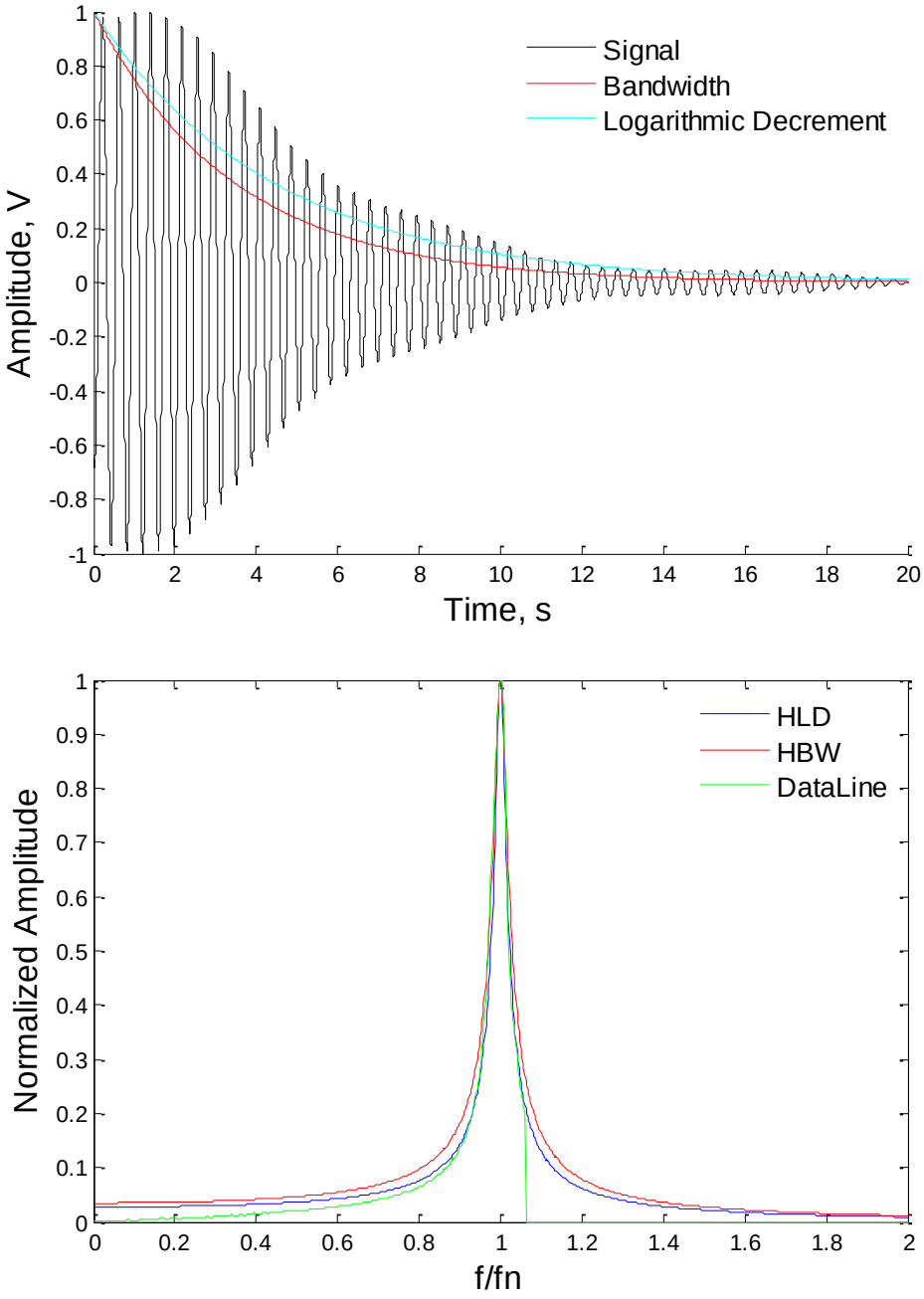

Figure B.5 Copper short tower with nacelle founded in concrete

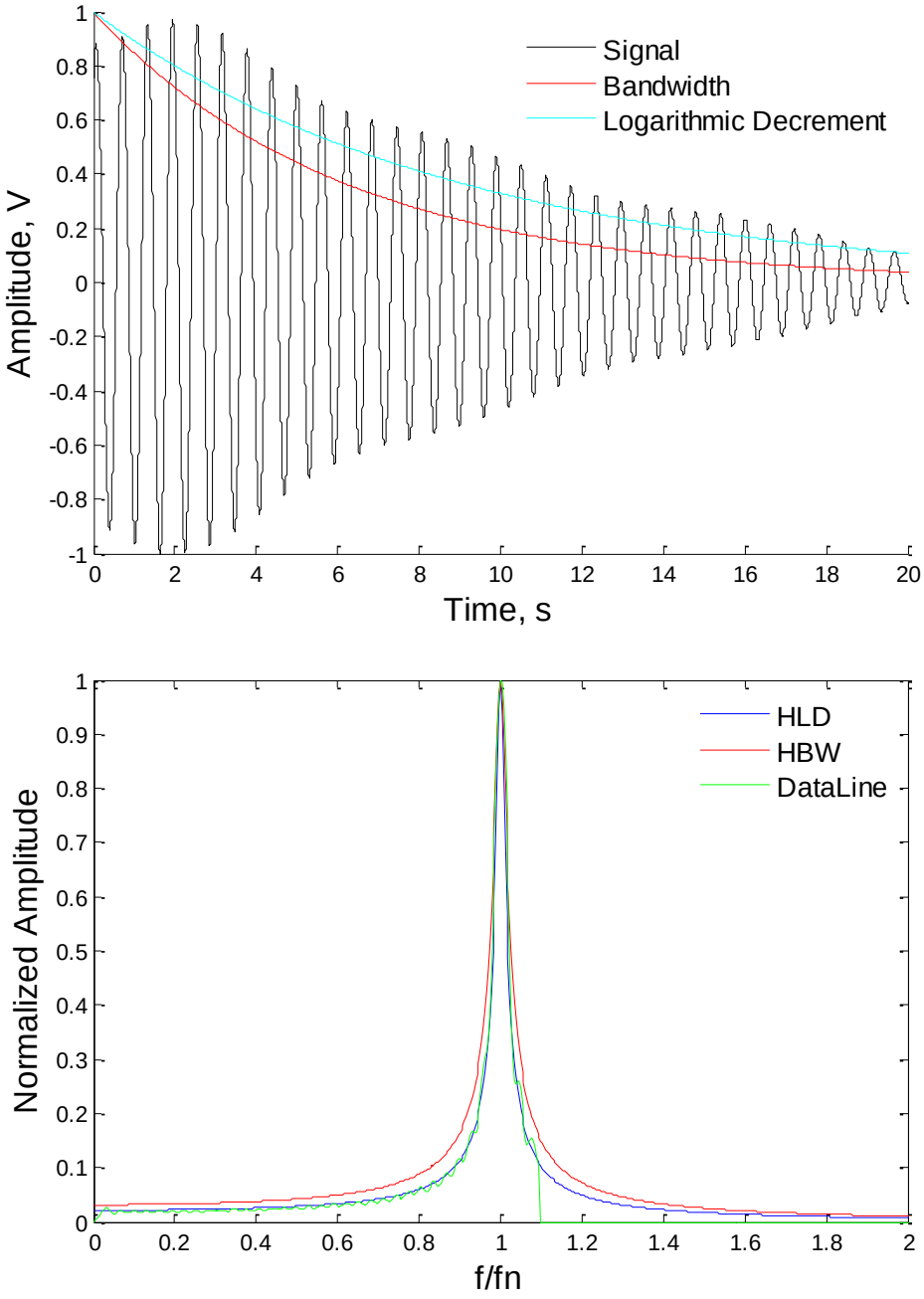

Figure B.6 Copper short tower founded in concrete

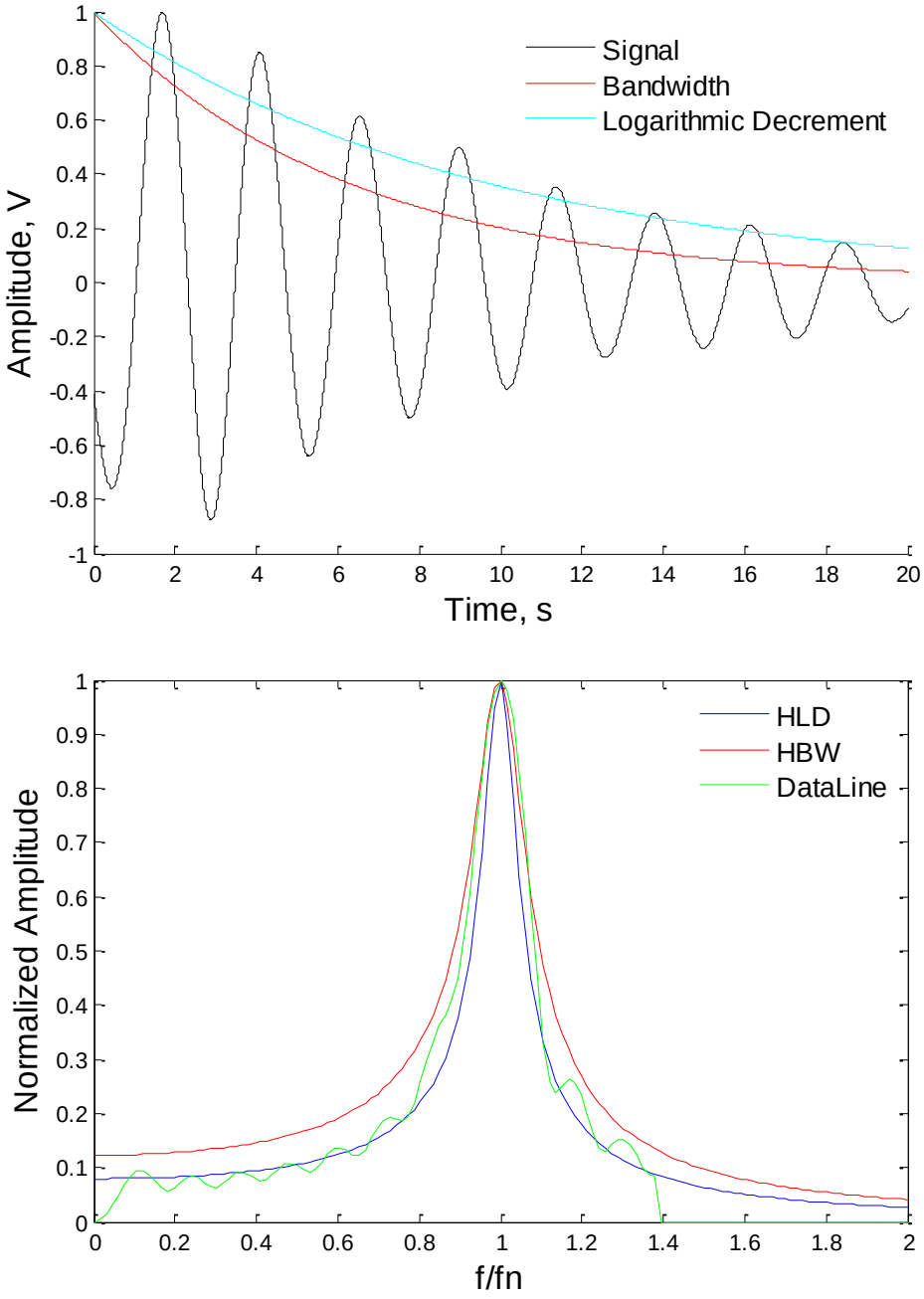

Figure B.7 PVC tower with rotor and nacelle founded in concrete

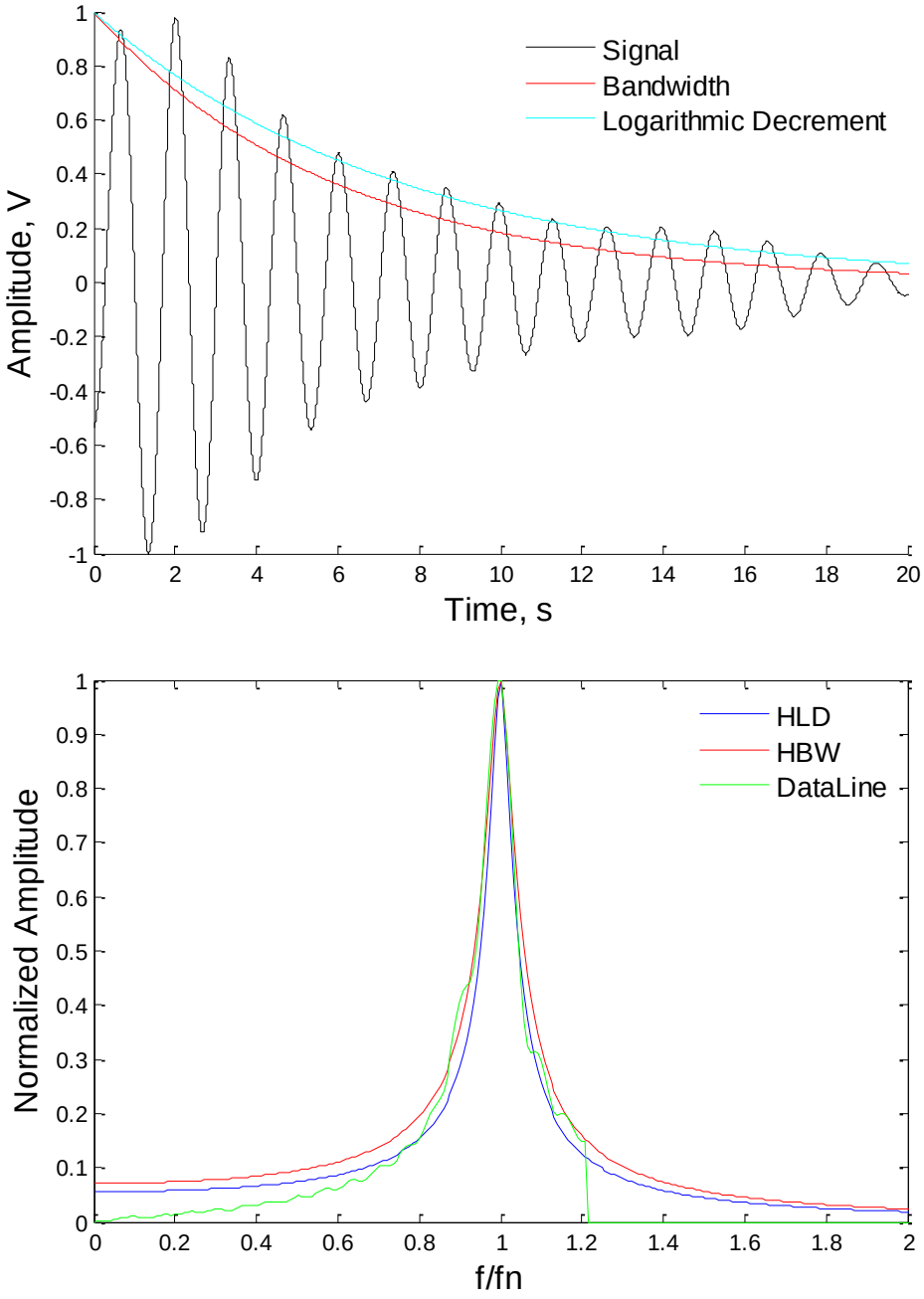

Figure B.8 PVC tower with nacelle founded in concrete

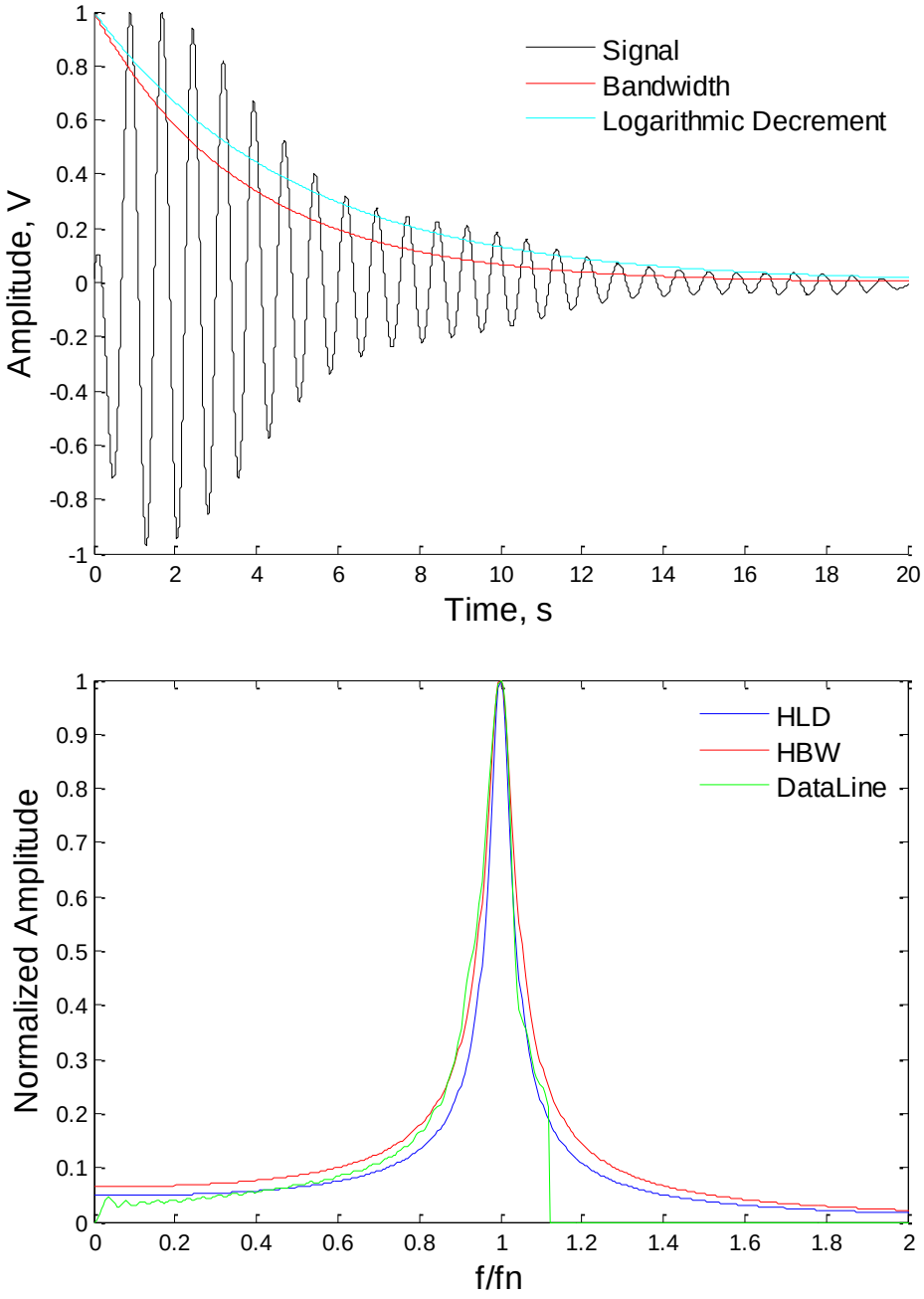

Figure B.9 PVC tower founded in concrete

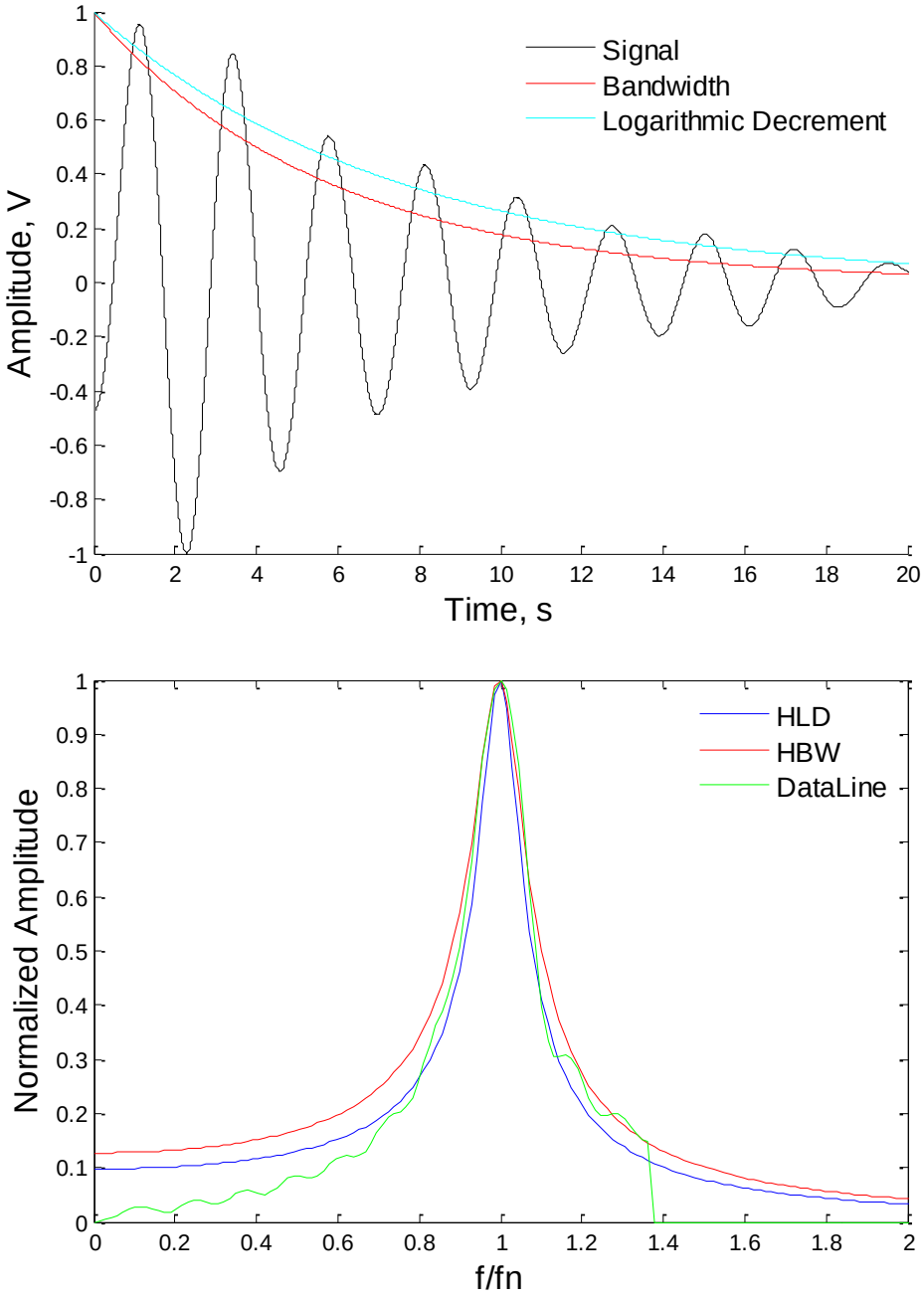

Figure B.10 PVC tower with rotor and nacelle embedded 16D in sand

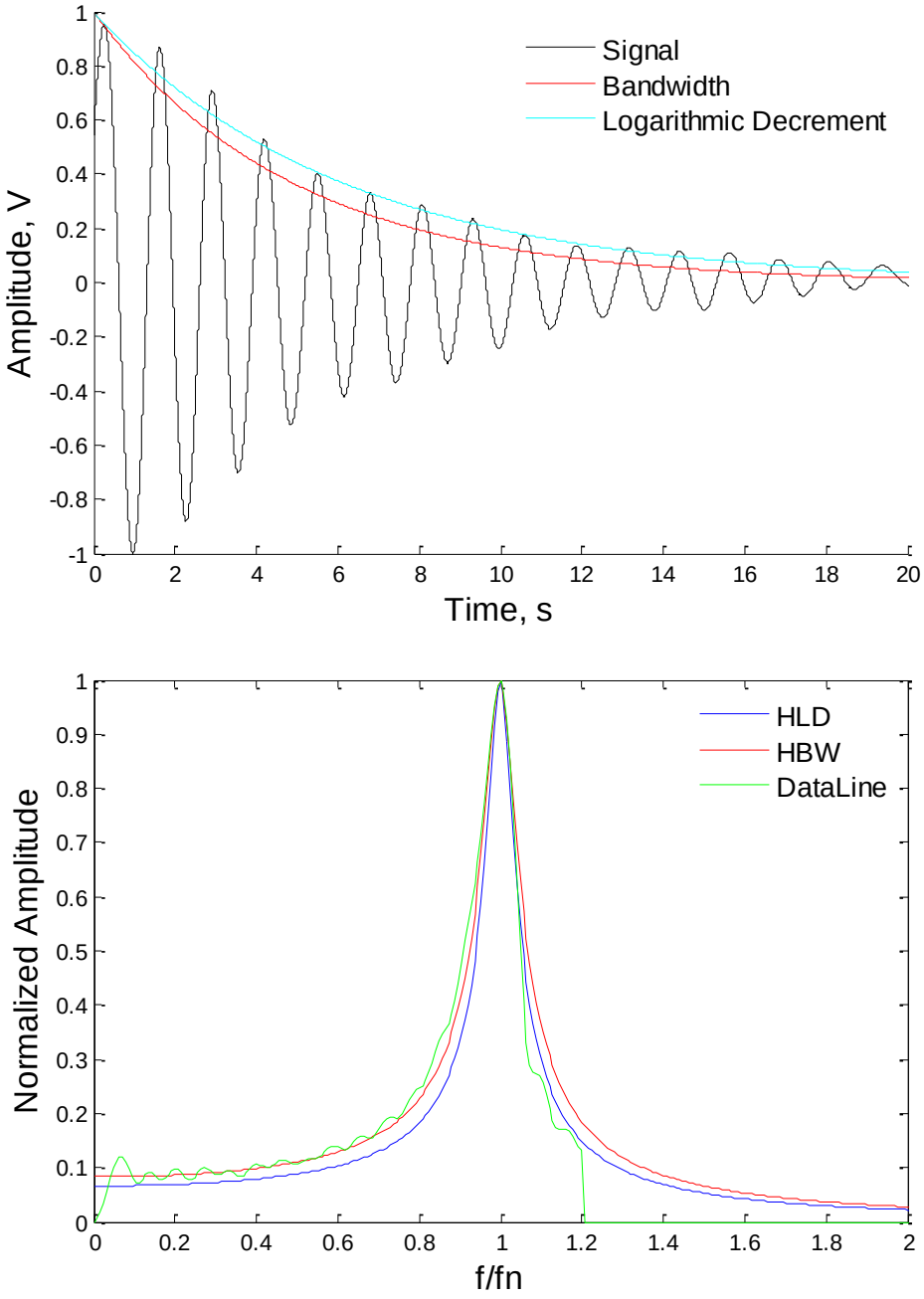

Figure B.11 PVC tower with nacelle embedded 16D in sand

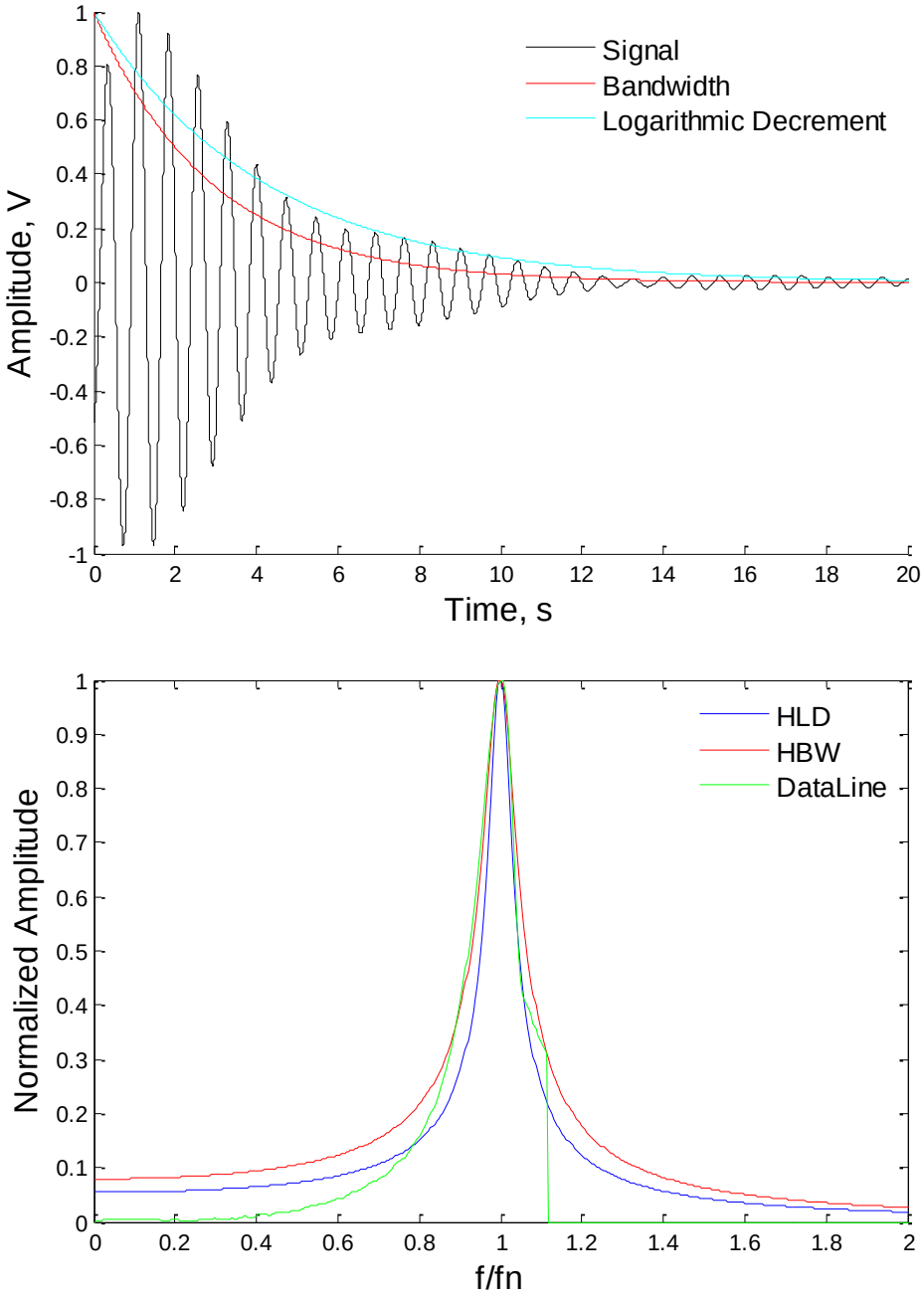

Figure B.12 PVC tower embedded 16D in sand

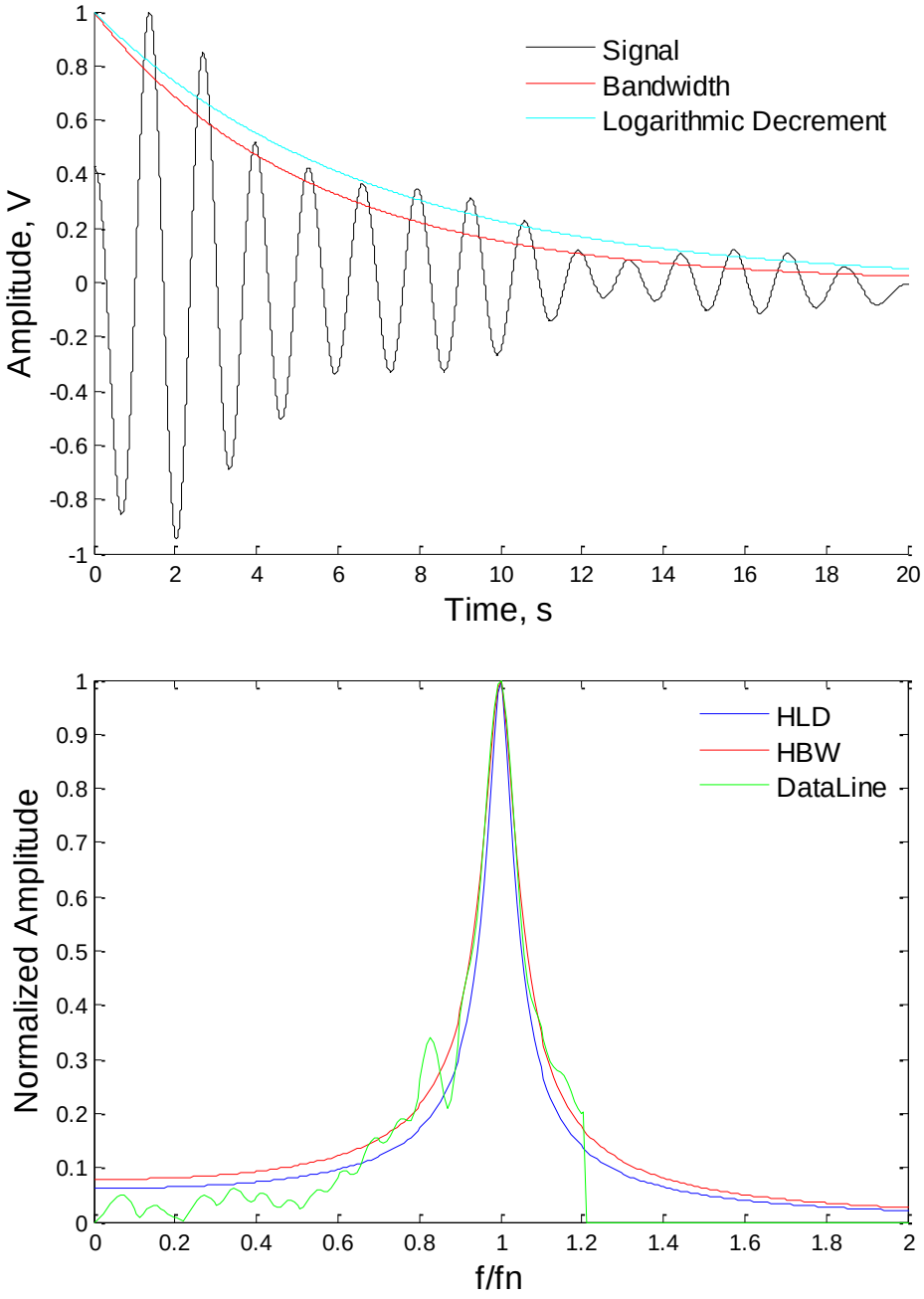

Figure B.13 PVC tower with nacelle embedded 8D in sand

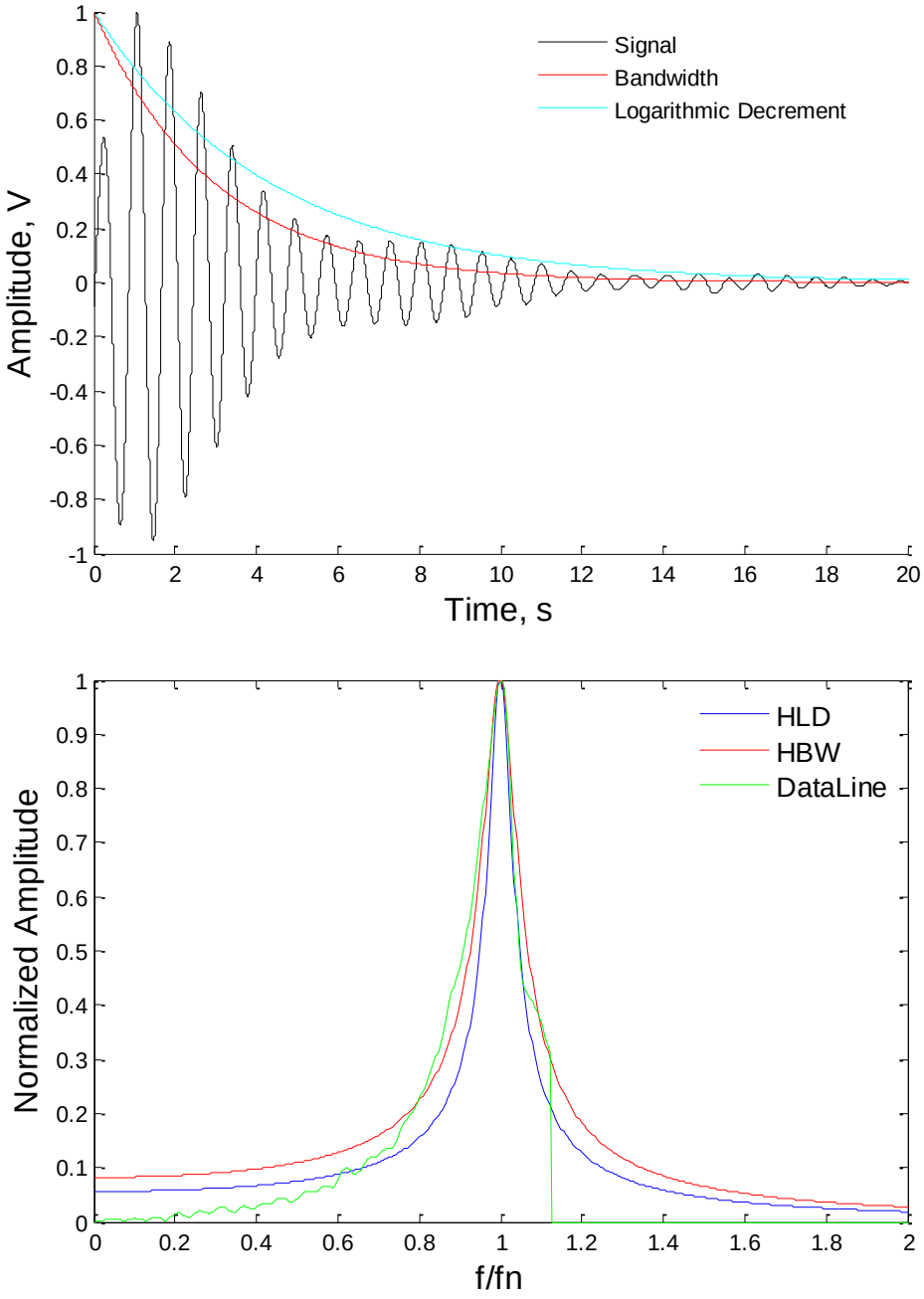

Figure B.14 PVC tower embedded 8D in sand

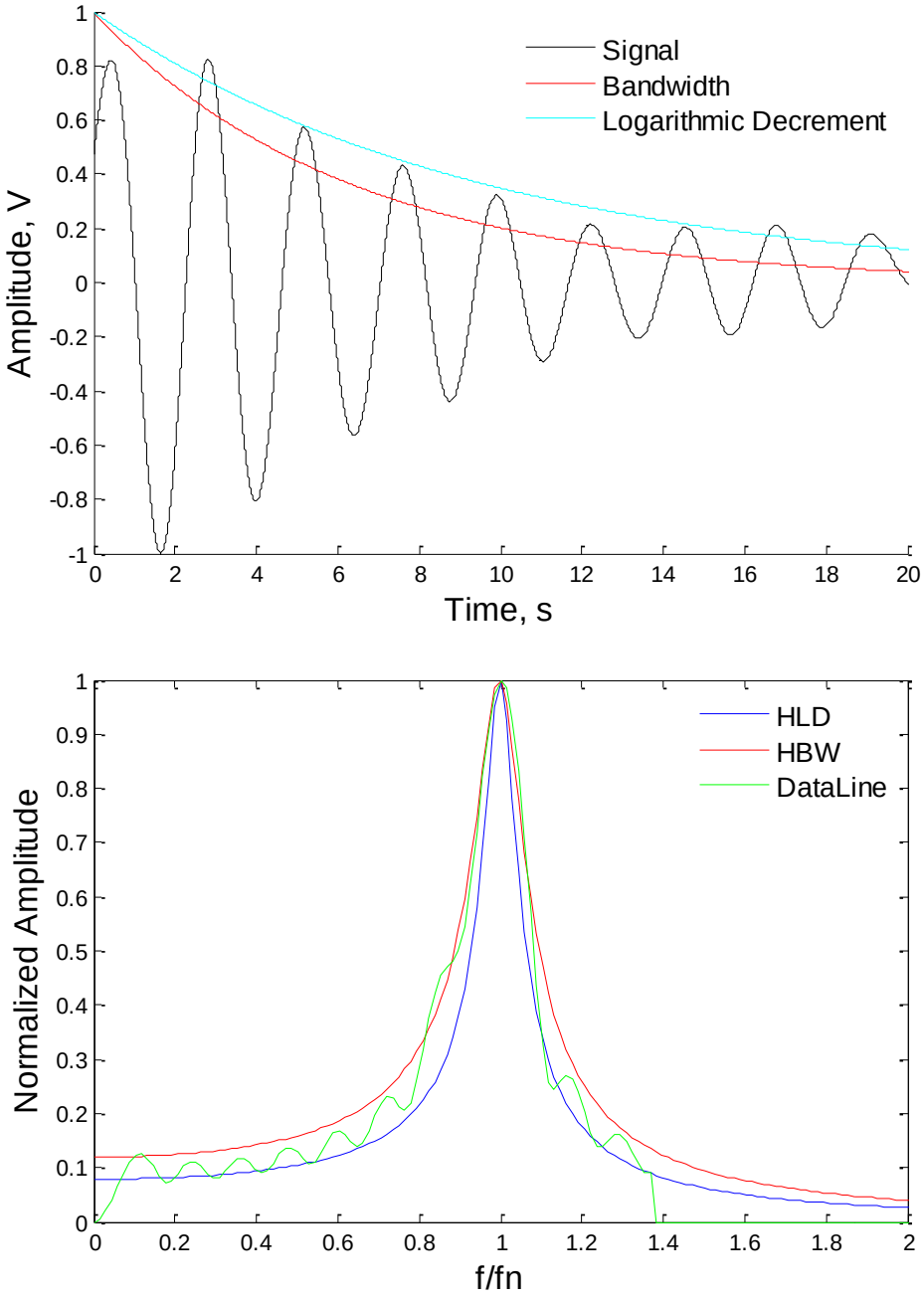

Figure B.15 PVC tower with rotor and nacelle embedded in concrete with a 90 mm clay layer

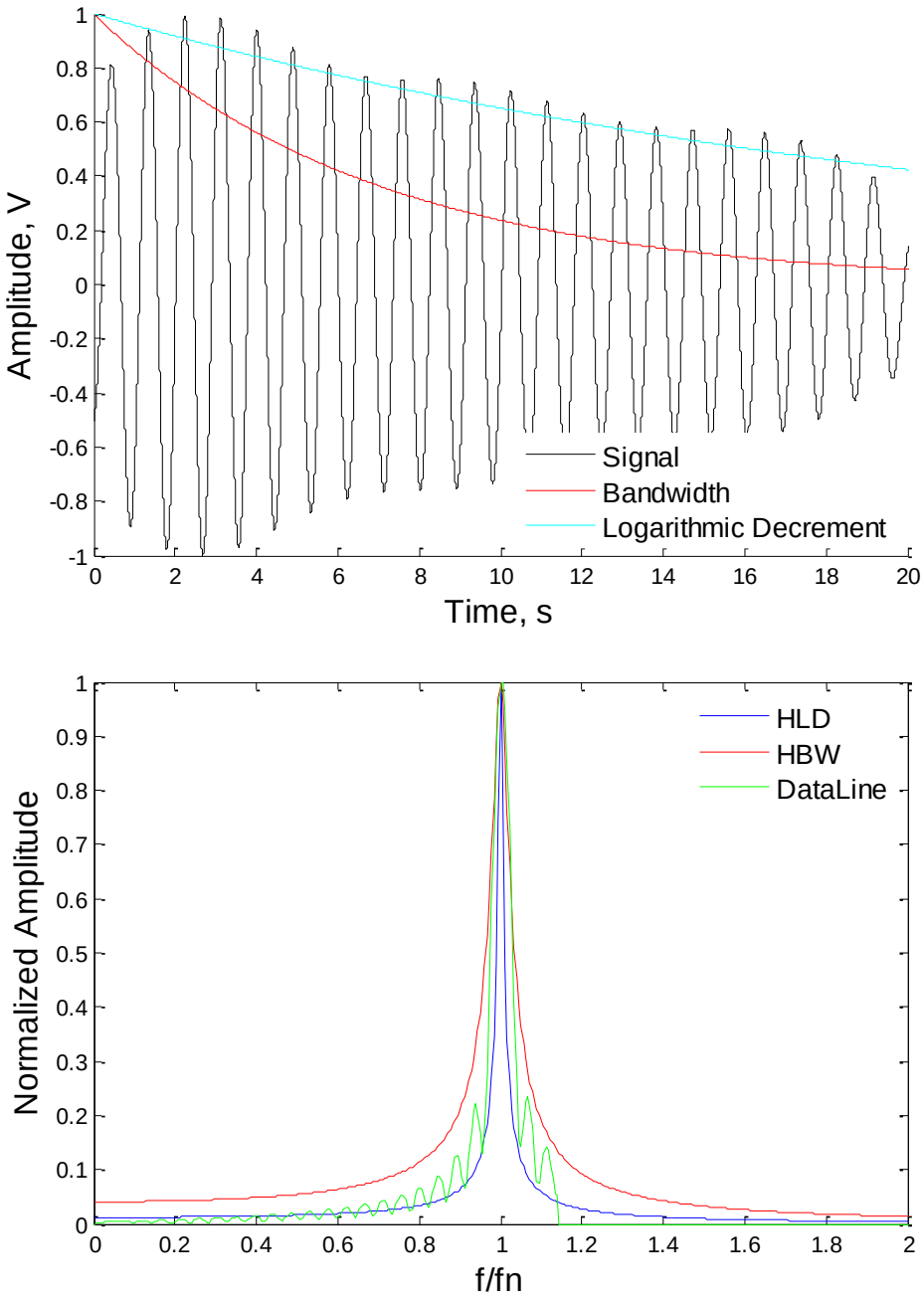

Figure B.16 Copper short tower with rotor and nacelle embedded in concrete with a 90 mm clay layer

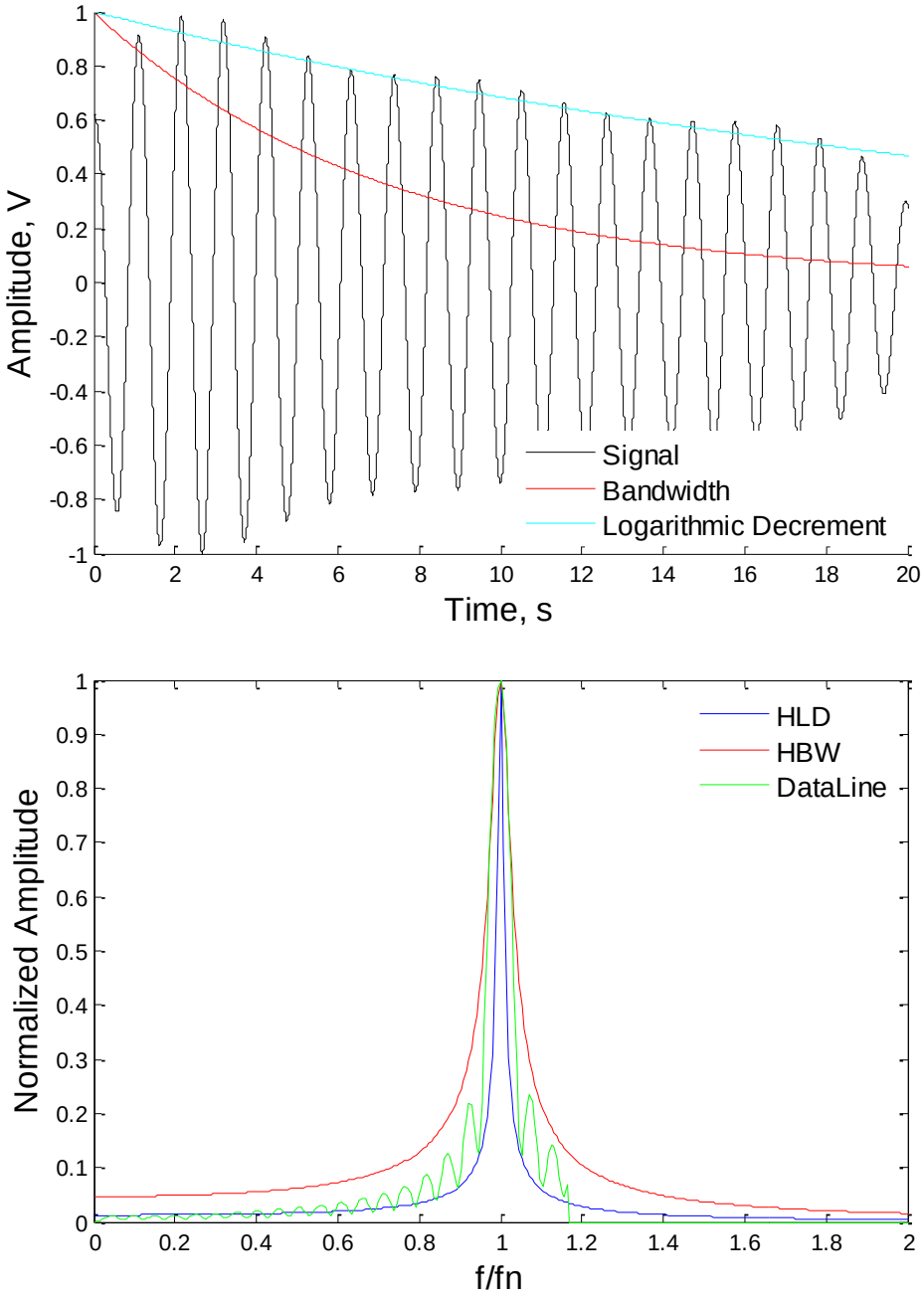

Figure B.17 Copper long tower with rotor and nacelle embedded in concrete with a 90 mm clay layer

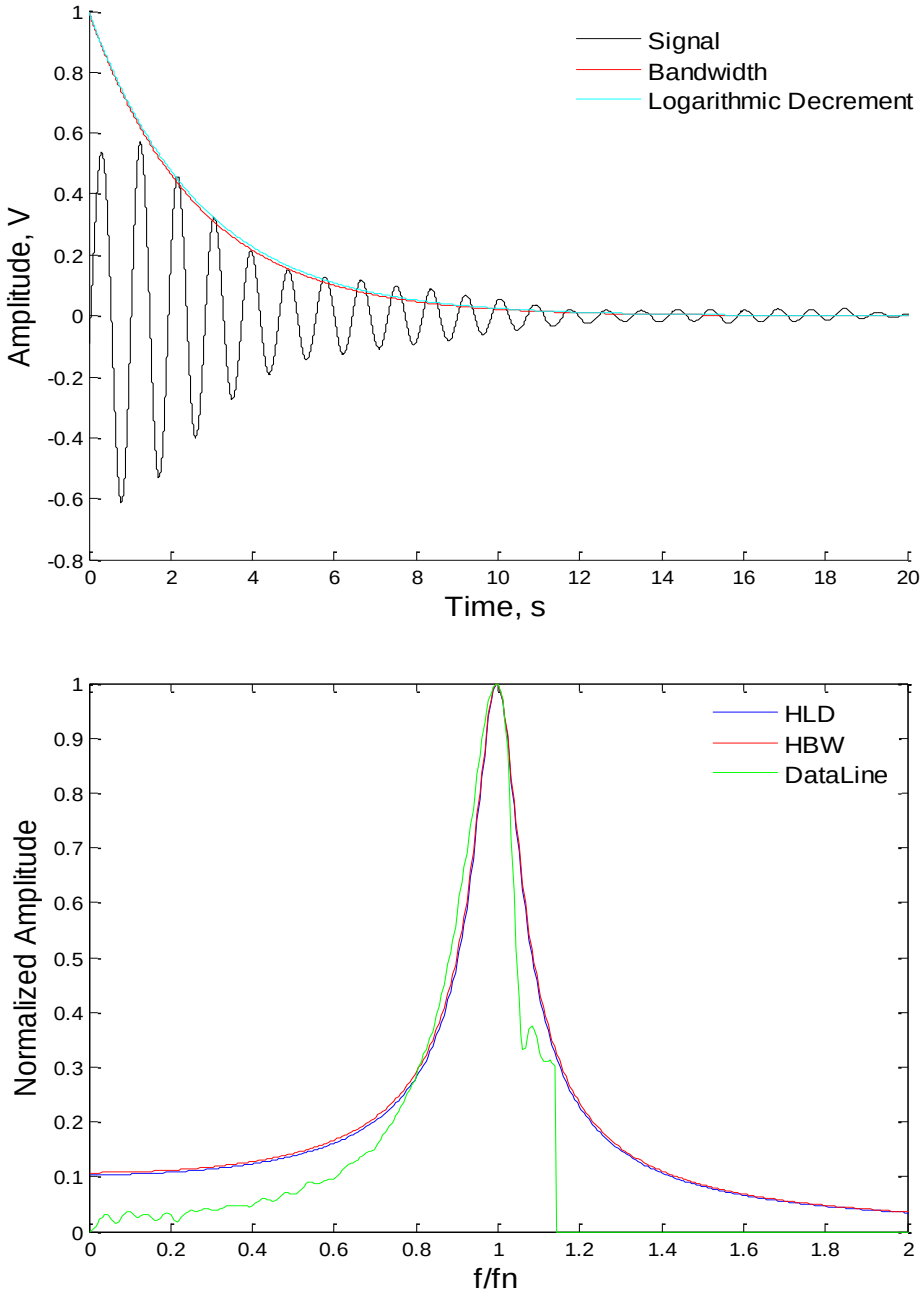

Figure B.18 Copper short tower with rotor and nacelle embedded in clay

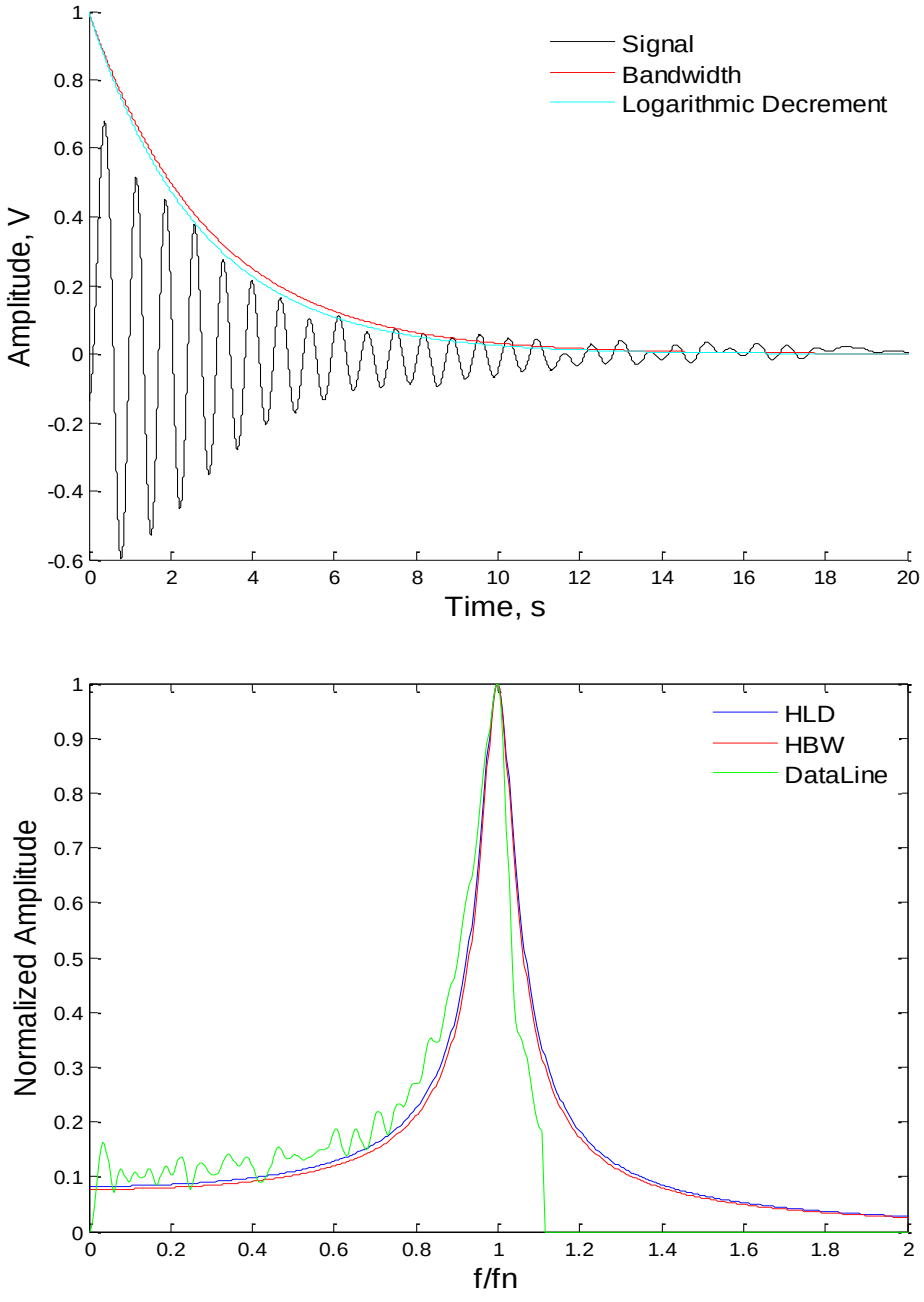

Figure B.19 Copper short tower with nacelle embedded in clay

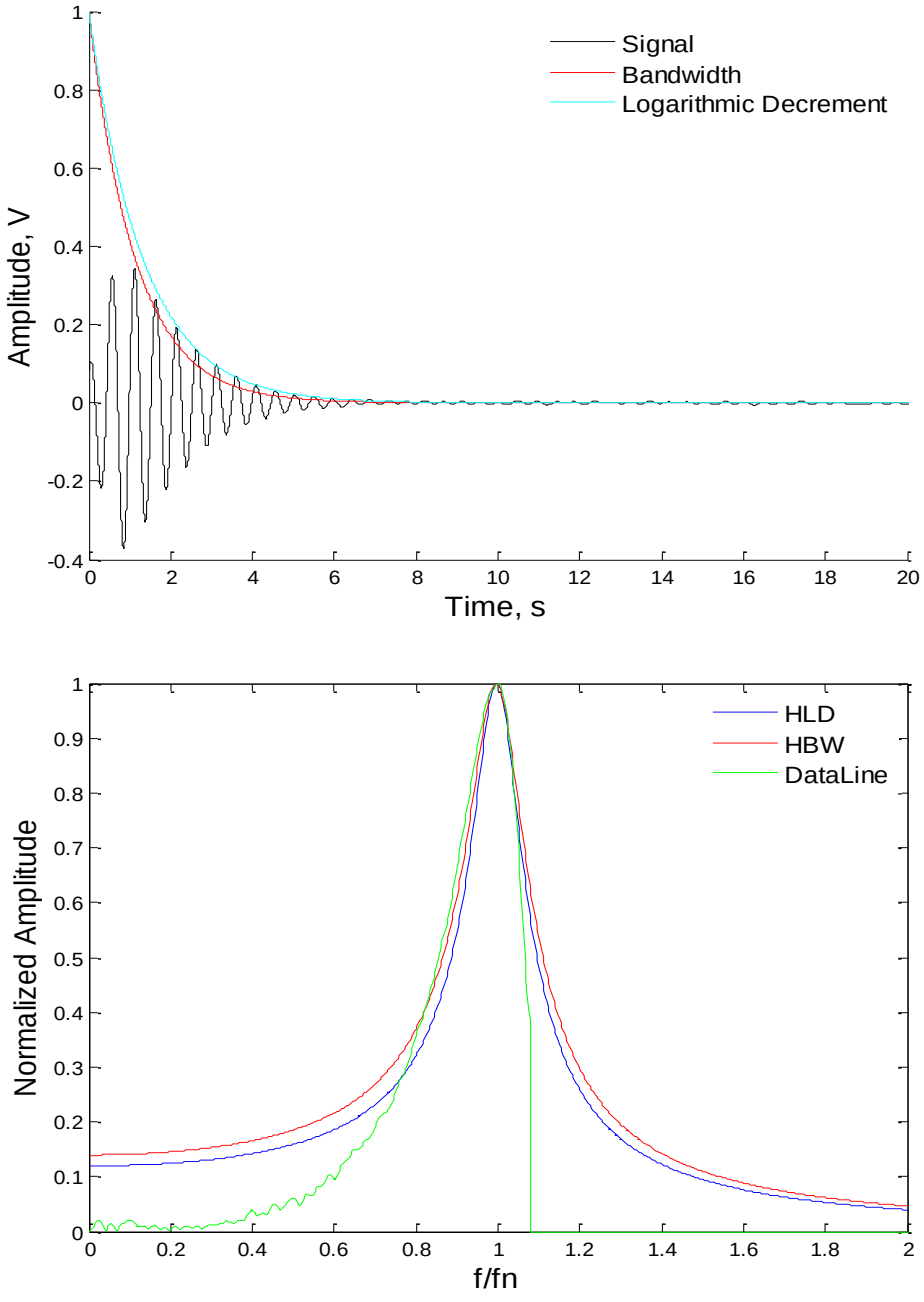

Figure B.20 Copper short tower embedded in clay

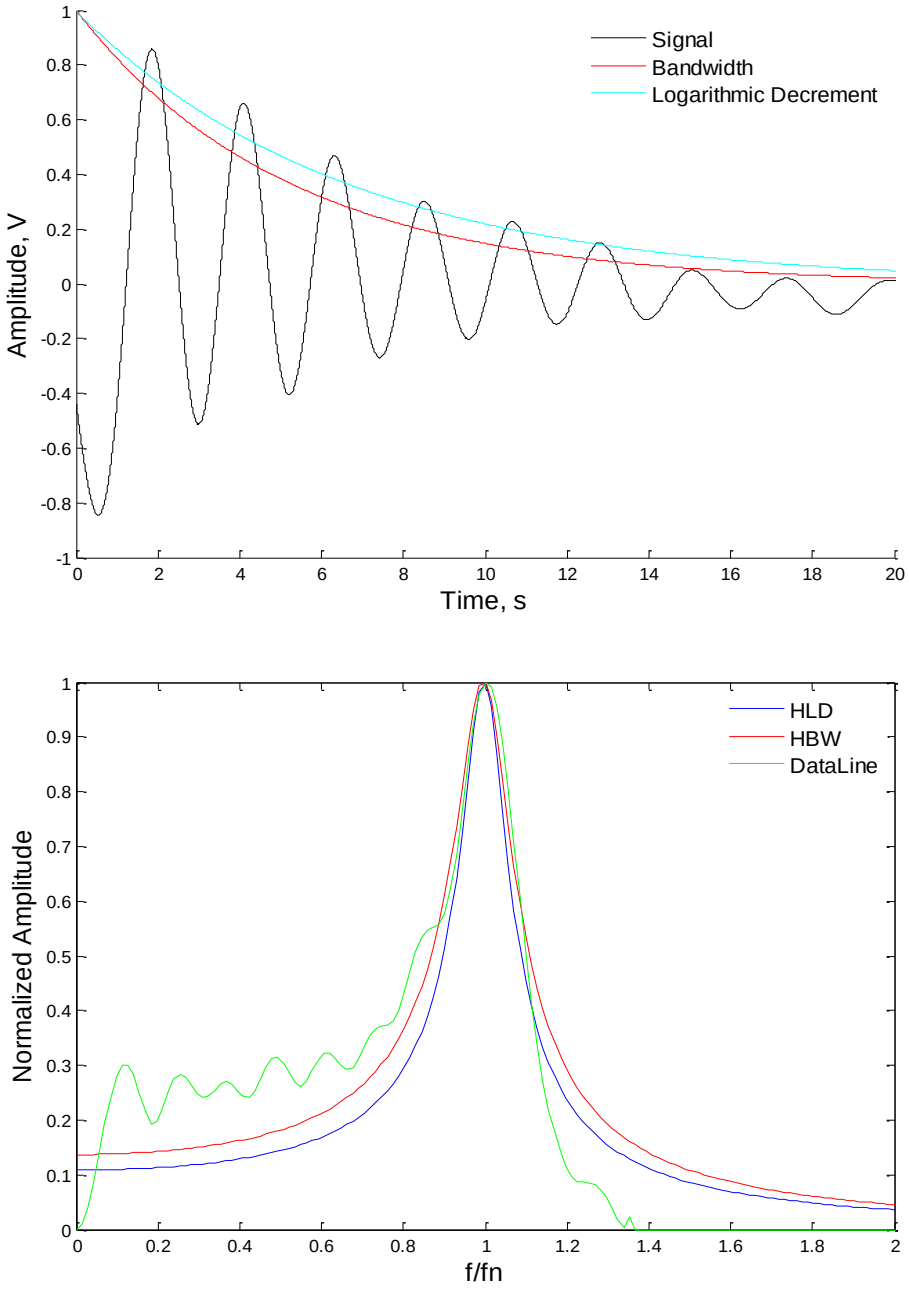

Figure B.21 PVC tower with rotor and nacelle embedded 16D in clay

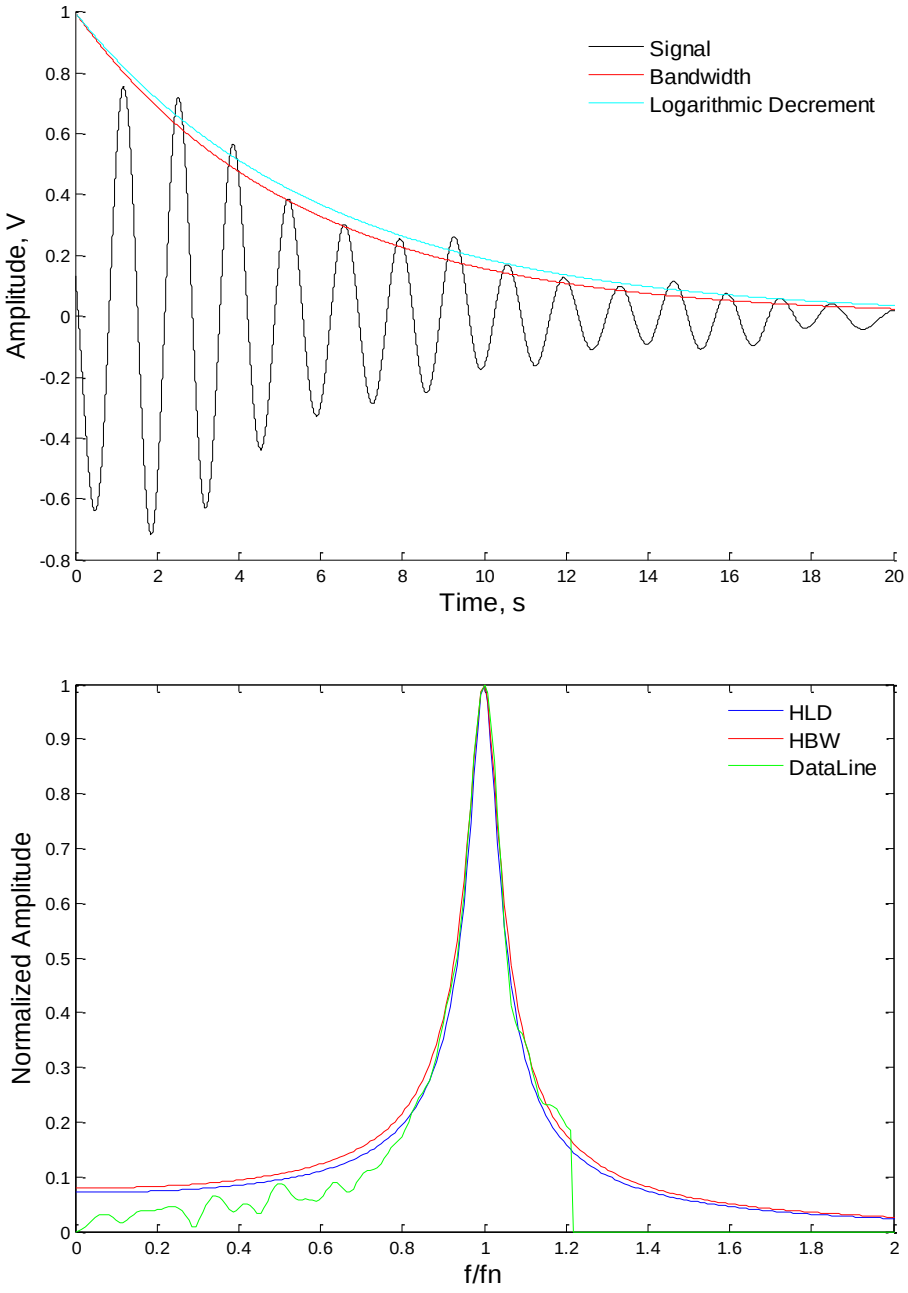

Figure B.22 PVC tower with nacelle embedded 16D in clay

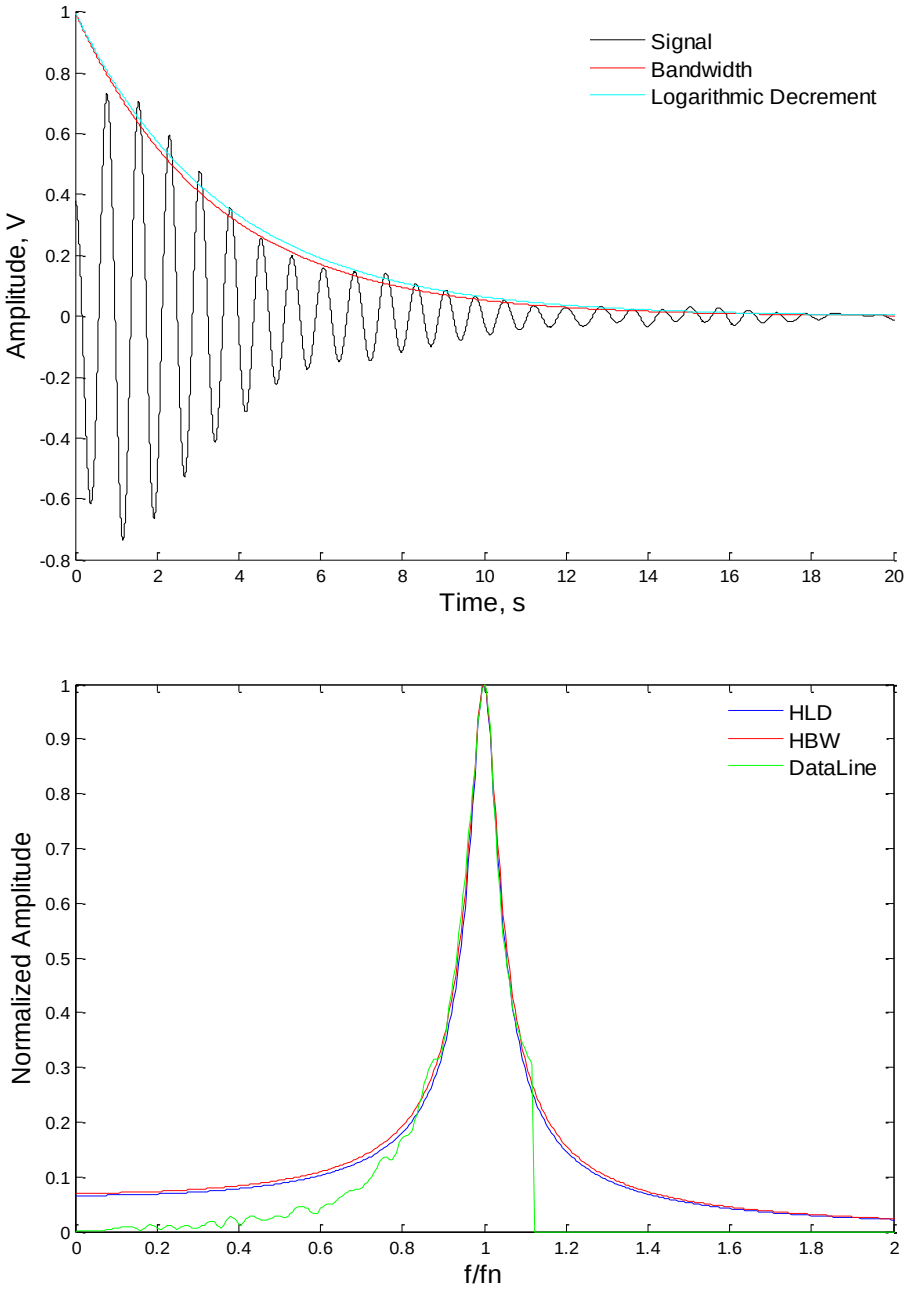

Figure B.23 PVC tower embedded 16D in clay